First International Colloquium on

# Non-linear Dynamics of Deep Drilling Systems

at the Château de Colonster
University of Liège, Belgium

March 12-13, 2009

Proceedings edited by V. Denoël and E. Detournay


Château de Colonster, Liège, Belgium


Organizing committee

V. Denoël
E. Detournay
G. Downton
G. Kerschen



Sponsors

CSIRO

Schlumberger

FNRS

## Foreword

The development of efficient techniques to drill deep boreholes to access the Earth's underground energy resources requires solving formidable technical challenges that do not pale in comparison with complex undertakings in other advanced areas of the Industry such as aerospace. Bits that survive drilling heterogeneous environments for hundreds of meters, downhole robots that automatically steer the drillhead to stay within the hydrocarbon reservoir, downhole instruments that collect data during drilling and send them back to the surface using the circulating mud as the wave transmission medium are examples of creative technologies that have been deployed to meet these challenges. However, scientific challenges as daunting as the technical ones also exist, even though they have not received as much attention and resources. Developments of robust methods to control and mitigate the self-excited vibrations of drilling systems, formulation of comprehensive models for predicting borehole trajectories that can be used to optimize the control of rotary steerable systems, and understanding of efficient means to fragment rocks in the pressure environment of deep holes are examples of such scientific challenges that are not yet resolved. While the solution to these scientific puzzles may not yet be in sight, progress in achieving these goals will most likely accelerate by inviting expertise from disciplines outside of those that have traditionally been brought about to address these problems. We hope that this Colloquium will be a step in that direction, bringing together a small but eclectic group of engineers and scientists willing to share knowledge and expertise on subjects that are relevant to the theme of this Colloquium. With technical sessions including topics as varied as chatters in machining, bouncing balls and impact oscillators, numerical methods for non-smooth dynamics, and borehole propagation models, we hope that lively and open discussions will emerge. The secluded setting offered by the Château de Colonster, located on the Sart-Tilman Campus of the University of Liège, will no doubt offer a superb environment for the working of this Colloquium. Whether this workshop will remain *le* Colloquium on "Nonlinear Dynamics of Deep Drilling Systems" or the first one of a series of such meetings is our challenge to you! We warmly welcome you to Liège!

Vincent Denoël, Emmanuel Detournay and Geoff Downton

## Acknowledgments

The organizers would like to thank CSIRO Petroleum (Australia), Fonds National de la Recherche Scientifique (Belgium) and Schlumberger (USA) for their financial support of this Colloquium, and the University of Liège and the University of Minnesota for providing resources and support to VD and ED.

## Program

THURSDAY MARCH 12TH 2009

### Opening (9:00)

- Vincent Denoël, Emmanuel Detournay and Geoff Dowton
- Presentation of Participants

### Session 1: Non-Linear Dynamics of Mechanical Systems

- 9:15 Bernard Brogliato: *An Introduction to Numerical Methods for Non-smooth Mechanical Systems with Impacts and Friction*
- 10:00 Gabor Stepan: *Bi-Stable Region Estimations for Cutting*
- COFFEE BREAK (10:45)
- 11:00 Tamas Insperger: *State-Dependent Delay Models for Metal cutting processes*
- 11:45 Thomas Erneux: *Delay Induced Canard Explosion in High Speed Machining*

LUNCH AT THE CHATEAU DE COLONSTER (12:30)

### Session 2: Dynamics of Impact Oscillators

- 13:30 Marian Wiercigroch: *Global and Local Dynamics of Drifting Oscillator for Different Contact Models*
- 14:15 Luiz Franca: *A Novel Approach to Evaluate Rotary-Percussive Drilling With Roller-Cone Bits*
- COFFEE BREAK (15:00)
- 15:15 Stéphane Dorbolo: *The Dynamics of the Bouncing Trimer*

## Session 3: Self-Excited Vibrations of Drilling Systems with Drag Bits

- 16:00 Christophe Germay: *Self-Excited Oscillations of Drag Bits*
- 16:30 Bart Besselink: *Modeling and Experimental Validation of Axial Drillstring Dynamics*
- 17:15 Emmanuel Detournay: *Apparent Coexistence of Multiple Regimes of Self-Excited Vibrations in Drilling Systems*
- 17:45 Discussion (Moderator: Stepan Gabor)

Dinner at the Maison du Pèket (19:30)

---

Friday March 13th 2009

## Session 4: Non-Linear Drillstring Response

- 9:00 Gaetan Kerschen: *Using Passive Nonlinear Targeted Energy Transfer to Stabilize Drillstring Systems*
- 9:45 Marian Wiercigroch: *Influence of Friction Characteristics on Stick-slip Vibration of Drillstrings*
- Coffee break (10:30)
- 10:45 Nathaniel Wicks: *Modeling Transient Vibrations while Drilling using a Finite Rigid Body Approach*
- 11:30 Vincent Denoël: *The Problem of a Drillstring Inside a Curved Borehole: a Perturbed Eulerian Approach*

Lunch at the Chateau de Colonster (12:15)

### Session 5: Borehole Propagation

- 13:30 Geoff Downton: *A Quasi-Polynomial Expression for Borehole Propagation Incorporating both Spatial and Temporal Effects*
- 14:15 Emmanuel Detournay: *Mathematical Model of the Near-Bit Region of an Advancing Drilling System*
- Coffee break *(*15:00)
- 15:15 Luc Perneder: *Theoretical Determination of the Bit-Rock Interaction Coefficients*
- 15:45 Thomas Richard: *Experimental Determination of the Bit-Rock Interaction Coefficients*
- Drinks (16:30)

### Round Table & Closing Session (Moderator: Nathan van de Wouw)

# Table of Contents

# An introduction to numerical methods for nonsmooth mechanical systems with impacts and friction

Bernard Brogliato

INRIA, BIPOP team-project, ZIRST Montbonnot, 655 avenue de l'Europe, 38334 Saint Ismier, France

## 1 Introduction

Non-smooth dynamical systems (NSDS) usually embed systems whose trajectories are not at least continuously differentiable everywhere, and for which powerful tools like tangential linearization at a point, or the (classical) implicit function theorem, do not apply because of the lack of differentiability of their right-hand-side. There are many types of NSDS. Here we shall focus on two particular, yet important because they represent common physical systems, classes of NSDS: systems with Coulomb friction (discontinuous acceleration), and systems with impacts or, better said, complementarity lagrangian systems (discontinuous velocities). Our aim is to introduce on two very simple examples a class of *implicit* time-discretizations: the Euler backward scheme and Moreau's catching-up scheme. We shall deal with *time-stepping* (or *event-capturing*) algorithms only. For *event-driven* schemes see [1] and references therein. The SICONOS platform for the simulation of NSDS is briefly presented.

## 2 A simple variable structure system

The simplest variable-structure system one may imagine is given by the differential inclusion

$$\dot{x}(t) \in -\mathrm{sgn}(x(t)) = \begin{cases} -1 & \text{if} \quad x > 0 \\ 1 & \text{if} \quad x < 0 \\ [-1,1] & \text{if} \quad x = 0 \end{cases} \tag{1}$$

As shown recently in [6] in a more general setting than (1), the *explicit* Euler discretization of (1), i.e. $x_{k+1} \in x_k - h\ \mathrm{sgn}(x_k)$, $h > 0$ the time-step, yields oscillations in the neighbordhood of the sliding surface (in this simple example the origin) $x = 0$, despite the algorithm converges. This is because the switches of

the vector field are led in the implicit method, by the state $x_k$. Such oscillations (or limit cycles) are a pure numerical artefact that should be avoided. If one considers for instance that (1) is a Filippov's differential inclusion, then after a finite time $t^*$ and whatever $x(0)$, the solution is $x(t) = 0$ for all $t \geq t^*$. Also all the derivatives $x^{(i)}(t) = 0$ on $(t^*, +\infty)$. Clearly the Filippov's solution is not well approximated by the explicit method on the sliding surface because its derivatives will not be zero at all. This is quite disturbing in many cases where one would like a smooth stabilization on the sliding surface. From a contact mechanics perspective, this means that the explicit numerical method is not able to correctly simulate the *sticking mode*, i.e. when the reaction force lies in the interior of the friction cone (see simulated examples in the survey [5] for systems of the form $\ddot{x}(t) \in -\text{sgn}(\dot{x}(t))$). In other words, the *multivalued* part of the $\text{sgn}(\cdot)$ multifunction is not correctly handled by the explicit Euler method.

Let us investigate now the backward Euler discretization of (1), i.e.

$$x_{k+1} \in x_k - h\ \text{sgn}(x_{k+1}) \tag{2}$$

The interpretation of (2) is that $x_{k+1}$ is the solution of a generalized equation. Using for instance maximal monotonicity arguments, it can be shown that this GE possesses a unique solution for any $x_k$ and any $h > 0$. To advance from step $k$ to step $k+1$, one has to find $x_{k+1}$ as the intersection between the graph of the multifunction $x_{k+1} \mapsto -h\ \text{sgn}(x_{k+1})$ and the graph of the function $x_{k+1} \mapsto x_{k+1} - x_k$. As shown on figure 1, the intersection is indeed always unique, and the method always converges in a finite number of steps $k^*$ to $x_{k^*+n} = 0$ (at the machine precision) for all $n \geq 1$ (on the figure one has $x_{k-2} = x_{k-3} - h$, $x_{k-1} = x_{k-2} - h$, $x_k = x_{k-1} - h$, $x_{k+1} = 0$). The numerical solution smoothly stabilizes on the sliding surface, without any spurious oscillations.

This is in fact a generic property of implicit Euler schemes, which can be shown to hold true in more general differential inclusions involving the sign multifunction. In more general cases, the GE for $x_{k+1}$ (which is a *one-step nonsmooth problem* (OSNSP) to be solved iteratively at each step $k$) is rewritten after a Newton's linearization as a mixed complementarity problem (MCP), that may be solved by many existing linear complementarity solvers. The main features of the implicit Euler method are:

- The switches are monitored by a multiplier $\lambda_{k+1}$ computed as the solution of a MCP, not by the state $x_k$: this is a kind of *dual* method.

- It extends to multiple switching surfaces (or multiple contact points in mechanics with Coulomb friction).

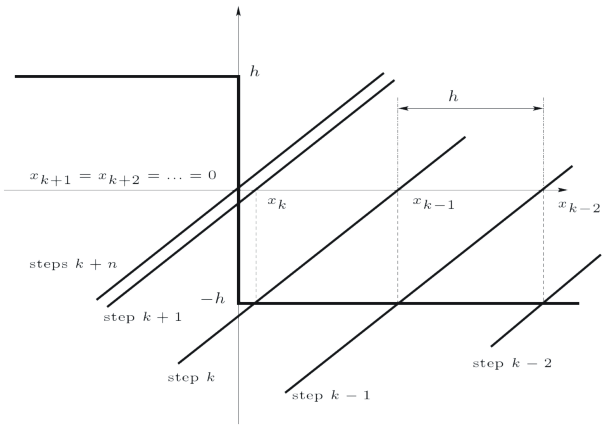


Figure 1: Iterations of the backward Euler method.

- It can handle accumulations of events (stick/slip transitions). A single time-step may even contain an infinity of events!
- It converges and is or maximal order 1 (not very accurate if few events and long smooth motion periods, then prefer an event-driven method).
- It does not need an accurate detection of the events and an accurate computation of the events times.
- It encapsulates the multivalued part of the characteristic. This is fundamental when the system reaches its equilibrium right inside the multivalued part !

As a general remark, higher order schemes (Runge-Kutta, multistep, Newmark) may be used, however they do not improve the accuracy of the method because non-smoothness decreases the order.

# 3 The bouncing-ball system

We now turn our attention to the simplest non-smooth mechanical system with impacts: the bouncing-ball, whose dynamics is given by

$$\begin{cases} m\ddot{q}(t) + mg = \lambda \\ 0 \leq \lambda \perp q \geq 0 \\ \dot{q}(t^+) = -e\dot{q}(t^-) \text{ if } q(t) = 0 \text{ and } \dot{q}(t^-) \leq 0 \end{cases} \tag{3}$$

One may first try a direct implicit discretization of this dynamics, like this is done for some classes of linear complementarity systems [4]. However this

doesn't work for mechanical systems, because the velocity may jump and the restitution law (third line of (3)) has to be taken into account. One way to solve this problem has been proposed by J.J. Moreau [8, 9, 10] (see also [1, 3] for non-mathematical introduction to the sweeping process), who introduced so-called *measure differential inclusions* in the framework of the second-order *sweeping process*. It consists in a first step in rewriting the dynamics as

$$-\,dv - g\,dt \in N_{T_\Phi(q(t))}\left(\frac{v(t^+) + ev(t^-)}{1+e}\right) \tag{4}$$

with $e \in [0,1]$, $\Phi = \mathbb{R}^+$, $dv$ is the differential measure of the velocity $\dot{q}(\cdot)$ (a sort of generalized derivative equal to $\dot{q}(t^+)dt$ outside impacts, and to a Dirac measure at impact times), $dt$ is the Lebesgue measure, $T_\Phi(q)$ is the tangent cone to $\Phi$ at $q$, $N_K$ is the normal cone to a convex set $K$. The main features of this differential inclusions are:

- It is an inclusion of *measures*. The normal cone in the right-hand-side[1] contains impulses of the contact force, denoted as $d\lambda$, which are measures. Therefore one may read (4) as $-\,dv - g\,dt = d\lambda$, $d\lambda \in N_{T_\Phi(q(t))}(\frac{v(t^+)+ev(t^-)}{1+e})$.
- It is a velocity/impulse formulation of the dynamics. At impact times $d\lambda(\{t\})$ is a positive bounded quantity.
- It is very well suited for the development of a time-stepping method, since it encapsulates in one-shot all the motions of the system.
- It may be seen as a kind of pre-conditionning of the contact force (that is a Dirac measure at the impact times), similarly to what is done for the simulation of differential-algebraic equations (DAE) to reduce the index.
- It extends to $n-$degree of freedom systems with very large number of unilateral contacts with multivalued friction (*e.g.* granular material).

The implicit time-discretization of the inclusion (4) is:

$$-v_{k+1} + v_k - hg \in N_{T_\Phi(q_k)}\left(\frac{v_{k+1} + ev_k}{1+e}\right), \quad t \in [kh, (k+1)h] \tag{5}$$

and $q_{k+1} = q_k + hv_{k+1}$, where $v_k$ plays the role of $v(t^-)$, $v_{k+1}$ plays the role of $v(t^+)$, $h > 0$. Similarly to (2) one has to solve a generalized equation in $v_{k+1}$. Using some basic result of convex analysis it may be shown that (5) is *equivalent* to

[1] The mass $m$ has been dropped since multiplying a cone by a positive constant does not change the cone.

$$v_{k+1} = -ev_k + (1+e)\ \mathrm{proj}\left[T_\Phi(q_k); v_k - \frac{hg}{1+e}\right] \tag{6}$$

When $v_k < 0$ and $q_k = 0 \in \partial\Phi$, one gets $v_{k+1} = -ev_k$: this is known as Newton's impact law [3]. Therefore the OSNSP to be iteratively solved at each step $k$ is a *projection onto a convex set*. This generalizes to $n-$degree of freedom systems with multiple contacts with friction (see [1, Chapters 12 and 14] for a thorough review on OSNSPs and solvers). The major features of the discrete inclusion (5) are:

- the element in the normal cone of the right-hand-side is $d\lambda([hk, h(k+1)]) = \int_{[hk,h(k+1)]} d\lambda$, that is the measure of the interval $[hk, h(k+1)]$ by the contact force impulse. This is always a **bounded** quantity. Therefore, this time-stepping algorithm does not try at approximating a Dirac measure at the impacts.
- Convergence results as $h \to 0$ have been proved [7].
- It handles accumulations of events (impacts, stick/slip transitions) without slowing down the computations.
- It has low accuracy on smooth portions of the motion.
- It allows for phenomena like Painlevé paradoxes (frictional paroxisms).
- In the $n-$-dimensional case with very large number of unilateral contacts with friction (possibly several thousands in granular matter), the method still performs very well.

See [1, §10.2] for a summary of the existing applications of this numerical method.

# 4 The SICONOS platform

The SICONOS Platform is a scientific computing software dedicated to the simulation of non-smooth dynamical systems (NSDS). Especially, the following classes of NSDS are addressed: Mechanical systems with contact, impact and friction, electrical circuits with ideal and piecewise linear components, differential inclusions and complementarity systems. This is written in C++ with an API in Python, and GPL licensed. The platform can be downloaded at http://siconos.gforge.inria.fr/ .

Both Moreau's time-stepping scheme, and an event-driven method are implemented in SICONOS. The OSNSP solvers that are implemented are QP, LCP,

MLCP and NCP solvers: splitting based methods, Lemke's method, various non-smooth Newton's methods, PATH; and frictional contact solvers (projection-type, Alart-Curnier's algorithm, NSGS splitting method). 2D and 3D unilateral frictional contacts are implemented, without faceting the friction cone (a procedure that should be avoided, see [1, §13.3.7]). For more details and examples see [2] and [1, Chapter 14].

# 5 Conclusions

The numerical simulation of non-smooth mechanical system requires specific methods, which are able to handle phenomena like events accumulation, sliding modes on codimension $m \geq 1$ surfaces, impulsive contact forces. Above all the numerical method should be able to well approximate the multivalued parts of the piecewise smooth laws entering the dynamics. The implicit Euler method and the implicit Moreau's method are an example of such algorithms.

# References


[1] V. Acary, B. Brogliato, *Numerical Methods for Nonsmooth Dynamical Systems. Applications in Mechanics and Electronics*, Springer Verlag, Lecture Notes in Applied and Computational Mechanics vol.35, Heidelberg, 2008.

[2] V. Acary, F. Pérignon, An introduction to SICONOS. INRIA technical report 3040, July 2007. Available at http://siconos.gforge.inria.fr/

[3] B. Brogliato, *Nonsmooth Mechanics*, 2nd Edition, Springer London, 1999.

[4] M.K. Camlibel, W.P.M.H. Heemels, J.M. Schumacher, Consistency of a time-stepping method for a class of piecewise-linear networks. IEEE Transactions on Cicuits and Systems – I, vol.49, pp.349-357, 2002.

[5] A.L. Dontchev, F. Lempio, Difference methods for differential inclusions: A survey. SIAM Reviews, vol.34, no 2, pp.263-294, 1992.

[6] Z. Galias, X. Yu, Euler's discretization of single input sliding mode control systems. IEEE Transactions on Automatic Control, vol.52, no 9, pp.1726-1730, September 2007.

[7] M.D.P. Monteiro Marques, *Differential Inclusions in Nonsmooth Mechanical Problems. Shocks and Dry Friction* , Birkauser, PNLDE 9, 1993.

[8] J.J. Moreau, Liaisons unilatérales sans frottement et chocs inélastiques. Comptes Rendus de l'Académie des Sciences, 296 série II, pp.1473-1476, 1983.

[9] J.J. Moreau, Standard inelastic shocks and the dynamics of unilateral constraints. in *Unilateral Problems in Structural Analysis*, no 288 CISM Courses and Lectures, Springer (Del Piero and Maceri, Editors), pp.173-221, 1985.

[10] J.J. Moreau, Unilateral contact and dry friction in finite freedom dynamics. In *Nonsmooth Mechanics and Applications*, no 302 CISM Courses and Lectures, Springer (Moreau and Panagiotopoulos, Editors), pp.1-82, 1988.

Gábor Stépán[1], Zoltán Dombóvári[1,2], Eddie R. Wilson[3]

[1] Department of Applied Mechanics, Budapest University of Technology and Economics, Hungary

[2] IDEKO Technological Centre

[3] Department of Engineering Mathematics, University of Bristol, United Kingdom

# 1 Introduction and mechanical modelling

One of the important goals of the optimisation of cutting processes is to maximise the volume of the chip cut within a certain time. There are several boundaries identified in the operational space of the cutting parameters, namely, the chip width, the chip thickness and the cutting speed. These boundaries are related to the maximum power, maximum cutting force, feed rate, depth of cut, etc. The most difficult boundary to handle is signposted by the harmful relative vibrations between the tool and the work-piece. The so-called regenerative effect is considered as one of the main reasons of these vibrations, which cause poor surface quality or, in extreme cases, damage the machine tool structure. The central idea of this regenerative effect is that the motion of the tool depends on its past motion, that is, a large time delay occurs in the slightly damped oscillator model of the machine tool. This delay is inversely proportional to the cutting speed. The first thorough and detailed experiments on the nonlinear regenerative vibrations [1] often showed small domains of attraction around the stable stationary cutting. A rigorous analytical investigation on the nature of the loss of stability of stationary cutting was performed only much later only by means of Centre Manifold reduction and Normal Form calculation [2]. The local unstable vibration separates two independent attractors, the stationary cutting and a large amplitude nonlinear oscillation that is also stable in dynamical systems sense. Still, this latter vibration is often mentioned as 'instability' by engineering terminology referring to its harmful nature. The region where this co-existence can occur will be called the region of bi-stability, while the terminology unsafe zone is also used for the same idea in production technology. Despite of the fact that these large-amplitude vibrations are of little interest from a technological view-point, the location and the size of the bi-stable domain are important, since they define the parameter region where the cutting process is more or less

sensitive to perturbations caused by, e.g., non-homogeneous work-piece material. Figure 1(b) shows a 1 DOF damped oscillator subjected to the nonlinear cutting force. The corresponding governing equation has the form

$$\ddot{q}(t) + 2\kappa\omega_n\dot{q}(t) + \omega_n^2 q(t) = \frac{1}{m}F_q(t) \tag{1}$$

where $\omega_n$ and $\kappa$ are the natural angular frequency and the damping ratio of the essential vibration mode described by the general coordinate $q$ that refers to the tool position. $F_q(t)$ is the corresponding component of the resultant cutting force $F(t)$. Stationary cutting force measurements indicate that the nonlinear cutting force characteristics often involve an inflection point on the otherwise monotonous increasing function against the chip thickness as shown in Fig. 1(c). The conventional power-law approximation of the empirical cutting force is not able to describe this inflection point. The effect of this possible inflection point is analysed from a nonlinear dynamics view-point when a cubic polynomial approximation of the cutting force characteristics is used.

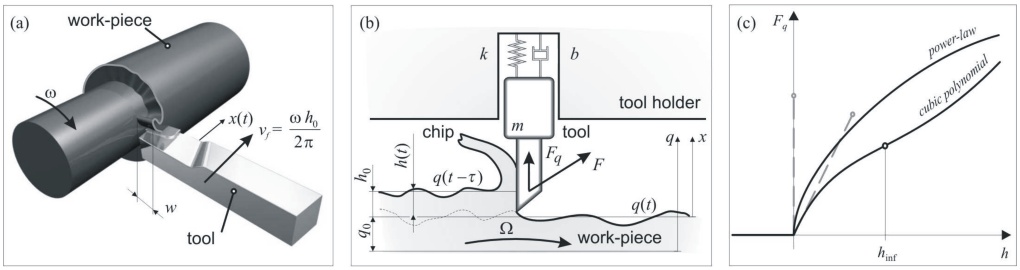


Figure 1: Panels (a) and (b) show the arrangement of the machine tool-work-piece system in case of orthogonal cutting. Panel (b) illustrates a planar mechanical model. Panel (c) shows the differences between the power and the cubic expressions of the empirical nonlinear cutting force characteristics.

## 2 Nonlinear regenerative effect and bi-stable zone

Figure 1(b) presents the variation of the instantaneous chip thickness $h(t)$ as a function of the present position $q(t)$ and the delayed position $q(t-\tau)$ of the tool:

$$h(t) = q(t-\tau) - q(t) + h_0, \tag{2}$$

where $h_0$ is the prescribed chip thickness, $\tau = 2\pi/\Omega$ is the period of the rotating work-piece, $\Omega$ is its angular velocity. If a cubic polynomial expression of the cutting force depends on the actual chip thickness (see Fig. 1(c)) and this actual

chip thickness is expressed as above, the equation of motion has the form of a delay-differential equation:

$$\ddot{q}(t) + 2\kappa\omega_n\dot{q}(t) + \omega_n^2 q(t) = \frac{w}{m}\left[\rho_1 h(t) + \rho_2 h^2(t) + \rho_3 h^3(t)\right]. \qquad (3)$$

The cutting force characteristics must be always increasing, which means for the 3 parameters $\rho_{1,2,3}$ of the cubic polynomial cutting fore component $F_q$ that

$$\frac{\partial F_q}{\partial h}(h) \geq \frac{\partial F_q}{\partial h}(h_{inf}) = w\left(\rho_1 - \frac{1}{3}\frac{\rho_2^2}{\rho_3}\right) > 0 \quad \Leftrightarrow \quad 3\rho_1\rho_3 - \rho_2^2 > 0. \qquad (4)$$

Figure 2(b) shows the size of the bi-stable region in % as a function of the chip thickness $h_0$ where the nonlinear cutting force parameters $\rho_{1,2,3}$ are fixed at the values taken from [1]. The experimental results taken form the same report [1], are denoted by dots and they follow the analytical prediction well. This is remarkable since the conventional power-law characteristics provide a constant $\sim 4\%$ width for the bi-stable region. The most critical theoretical chip thickness $h_{cr}$ , where the size of the bi-stable region is maximal, can be calculated analytically: $h_{cr} = -\rho_1/\rho_2$. In the meantime, the quantitatively more accurate path-following method determined the switching points more precisely, and the real size of the maximal bi-stable zone is shown to be about half the size of the analytical estimation (see Figure 2(b)) – but this value is still at about 50%, which is about 12 times larger than the one predicted by the power-law formulation.

# 3 Conclusion

The classical model of regenerative vibration was investigated with new kinds of nonlinearities; based on some experimental results, the proposed model includes an essential inflection point in the force characteristics. In case of orthogonal cutting, the existence condition of unstable self-excited vibrations is given along the stability limits, which is related to the force characteristic at its inflection point. An analytical estimation is derived for the chip width where the co-existence of stable stationary cutting and a strange stable self-excited vibration 'outside' the unstable periodic motion is expected. It was shown how this domain of bi-stability depends on the theoretical chip thickness. The comparison of these results to the experimental observations and also to the bifurcation results obtained for standard nonlinear cutting force characteristics provides relevant information on the nature of the nonlinearity of the cutting force.

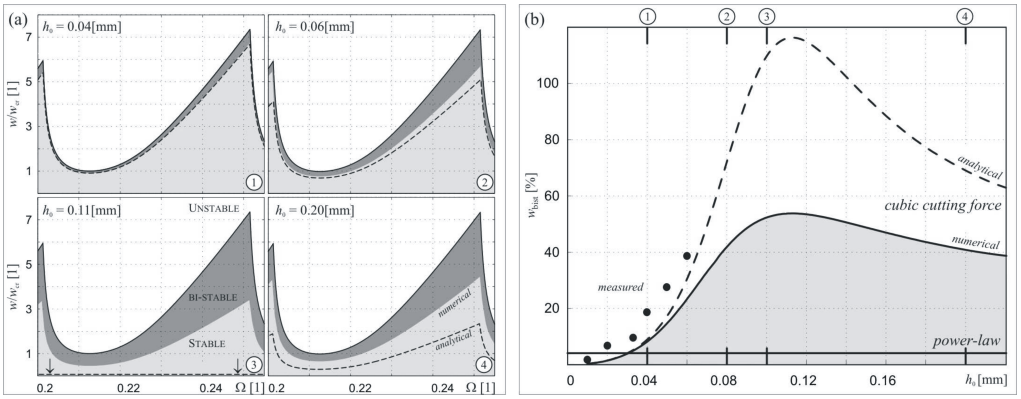


Figure 2: In panel (a) several intersections are shown with respect to the desired chip thickness h0 of the $4^{th}$ lobe and its unsafe zone (grey area). In panel (b) the relative widening of the bi-stable region are presented in case of cubic and power-law cutting force characteristics. (dashed: analytical solution, continuous: computed by DDE-BIFTOOL [3], points: results of Tobias' measurements ($\kappa = 0.01$) [1].

## Acknowledgement

This research was supported by the Hungarian National Science Foundation under grant no. K68910.

## References

[1] Shi, H.M., Tobias, S.A., Theory of finite amplitude machine tool instability, Int. J. Machine Tool Design and Research, 24, pp. 45-69, 1984.

[2] Stepan, G., Kalmar-Nagy, T., Nonlinear Regenerative Machine Tool Vibrations, ASME Design Engineering Technical Conferences, 1997, Sacramento, California, DETC97/VIB-4021, pp. 1-11.

[3] Engelborghs, K., Luzyanina, T., and Roose, D., Numerical Bifurcation Analysis of Delay Differential Equations Using DDE BIFTOOL, ACM Trans. on Math. Software, 28, pp. 1–21, 2002.

# State-dependent delay models for metal cutting processes

Gábor Stépán, Tamas Insperger

Department of Applied Mechanics, Budapest University of Technology and Economics, Hungary

## 1 Introduction

An important phenomenon that limits the productivity of machining is the onset of self-excited vibrations, also known as machine tool chatter. One reason for such vibrations is the so-called regeneration effect: the tool cuts a surface that was modulated during the previous revolution of the workpiece (in case of turning) or by the previous tooth of the tool (in case of milling). This phenomenon can be modeled by delay-differential equations (DDEs). In models with constant regenerative delay, the arising vibrations are associated with subcritical Hopf bifurcations [1, 2]. The locations of these Hopf bifurcations of machining processes are usually shown in the form of stability lobe diagrams. These diagrams plot the stable axial cutting depth as function of the spindle speed.

If the regenerative process is to be modeled accurately, then the vibrations of the tool should also be included in the time delay. In turning processes, the time delay is basically determined by the rotation of the workpiece but it is also affected by the current and the delayed position of the tool as it was shown in [3, 4]. This results in a DDE with state-dependent delay (SD-DDE) where the delay depends on the present state and also on a delayed one, thus giving an implicitly defined delay. The effect of state-dependent delay is also important in rotary cutting processes like in drilling or in milling. One application is deep drilling with drag bits [5], where state-dependent regenerative delay typically arises due to the torsional vibrations of the tool. State-dependent delay also appears in milling models even when only the bending oscillations of the tool is considered and its torsional compliance is neglected [6].

The theory of SD-DDEs is an actively developing research area in mathematics, and results, like linearization techniques and stability analysis, are not used in engineering problems yet. A good overview about the properties of SD-DDEs was recently provided in [7]. SD-DDEs are always nonlinear, since the state itself arises in its own argument through the delay. Linearization of SD-DDEs is complicated by the fact that the solution of the system is not differentiable

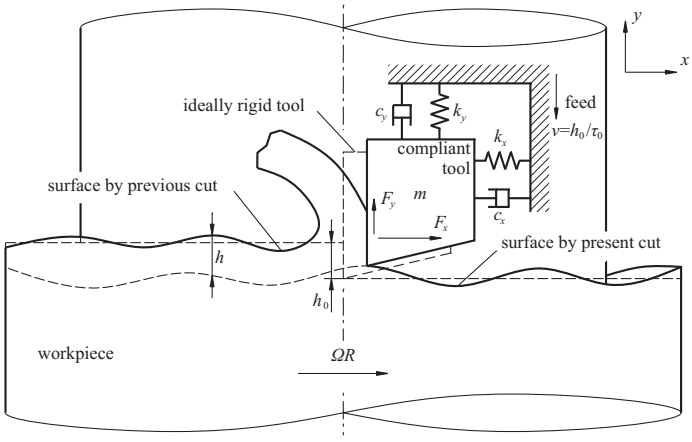


Figure 1: Model of regeneration in turning process.

with respect to the state-dependent delay. Consequently, "true" linearization is not possible, rather we are looking for a linear DDE, which is associated to the original system in the sense that they have the same local stability properties. The linearization technique for general autonomous SD-DDEs was given in [8] and for time-periodic SD-DDEs in [9].

In this paper, the results about the state-dependent delay model of turning and milling processes presented in [3], [4] and in [6] are summarized.

## 2 State-dependent delay model for turning

The mechanical model of the turning process can be seen in Fig. 1. The tool is assumed to be compliant and experiences vibrations in directions $x$ and $y$, while the workpiece is assumed to be rigid. The system can be modeled as a 2 DOF oscillator excited by the cutting force. As in standard models of regenerative machine tool chatter, the chip thickness and, consequently, the cutting force depend on the current and a delayed position of the tool. In the current model, the regenerative delay $\tau$ is not constant due to the compliance of the tool in the direction $x$, but it can be given in the implicit form

$$R\Omega\tau = 2R\pi + x(t) - x(t-\tau), \tag{1}$$

where $R$ is the radius of the workpiece and $\Omega$ is the spindle speed in [rad/s]. This equation shows that the time delay $\tau$ depends on the current position $x(t)$ and on the delayed position $x(t-\tau)$ of the tool, that is, the time delay is state-dependent: $\tau = \tau(x_t)$, where $x_t(s) = x(t+s)$, $s \in [-r, 0]$, $r \in \mathbb{R}^+$.

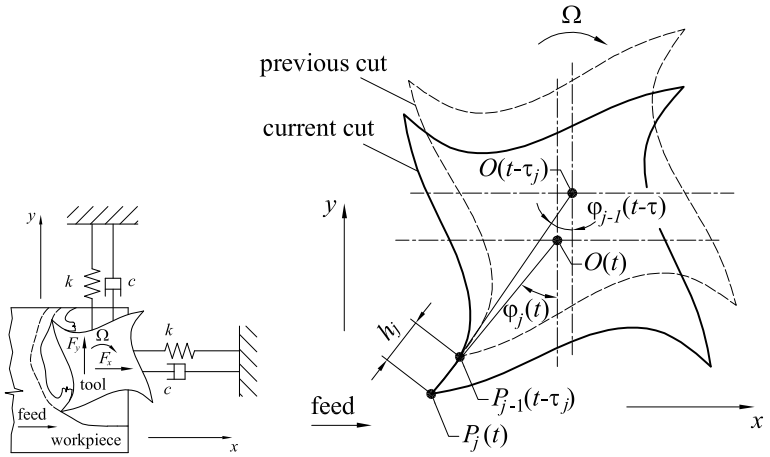


Figure 2: Model of regeneration in milling process.

The equations of motion of the system can be given as

$$m\ddot{x}(t) + c_x\dot{x}(t) + k_x x(t) = K_x w\left(v\tau(x_t) + y(t-\tau(x_t)) - y(t)\right)^q, \qquad (2)$$

$$m\ddot{y}(t) + c_x\dot{y}(t) + k_x y(t) = K_y w v\left(\tau(x_t) + y(t-\tau(x_t)) - y(t)\right)^q, \qquad (3)$$

where the state-dependent delay $\tau(x_t)$ is defined implicitly by Eq. (1). The left hand side of Eqs. (2) and (3) describe the tool as a 2 DOF oscillator with modal mass $m$, damping $c_x$, $c_y$ and stiffness $k_x$, $k_y$. The right hand side corresponds to the cutting force, where $K_x$ and $K_y$ are the cutting coefficients, $w$ is the depth of cut, $v$ is the speed of the feed and $q$ is an exponent ($q = 0.75$ is a typical empirical value for this parameter). For more details on the modeling, see [3].

## 3 State-dependent delay model for milling

The state-dependent delay model of milling processes is more complicated than that of the turning process. The corresponding mechanical model can be seen in Fig. 2. The tool is assumed to be compliant in directions $x$ and $y$, and the workpiece is assumed to be rigid, thus, the system can be modeled as a 2 DOF oscillator excited by the cutting force. The time delay $\tau_j$ between the $(j-1)^{\text{th}}$ and $j^{\text{th}}$ teeth can be derived in a purely geometric way. The exact condition for the delay is that point $P_{j-1}(t-\tau_j)$ is located in the section determined by points $P_j(t)$ and $O(t)$. This consideration leads to the equation

$$\begin{aligned}&\left(v\tau_j + x(t-\tau_j) - x(t)\right)\cos\left(-\Omega t + (j-1)\vartheta\right)\\ &\quad - \left(y(t-\tau_j) - y(t)\right)\sin\left(-\Omega t + (j-1)\vartheta\right) = R\sin\left(\Omega\tau_j - \vartheta\right), \qquad (4)\end{aligned}$$

which is an implicit equation for the time delay. This equation shows that the time delay $\tau_j$ of the $j^{\text{th}}$ tooth depends on time $t$, on the current position $x(t)$ and $y(t)$ and on the delayed position $x(t-\tau_j)$ and $y(t-\tau_j)$ of the tool, that is, the time delay is time and state dependent: $\tau_j = \tau_j(t, x_t, y_t)$. The equations of motion of the system can be given as

$$\begin{aligned} m\ddot{x}(t) + c\dot{x}(t) + kx(t) = \sum_{j=1}^{N} \alpha_{x,j}(t) \Big( & R(1 - \cos(\Omega\tau_j(t, x_t, y_t) - \vartheta)) \\ & + (v\tau_j(t, x_t, y_t) + x(t - \tau_j(t, x_t, y_t)) \\ & - x(t)) \sin\varphi_j(t) + (y(t - \tau_j(t, x_t, y_t)) - y(t)) \cos\varphi_j(t) \Big)^q, \end{aligned} \tag{5}$$

$$\begin{aligned} m\ddot{y}(t) + c\dot{y}(t) + ky(t) = \sum_{j=1}^{N} \alpha_{y,j}(t) \Big( & R(1 - \cos(\Omega\tau_j(t, x_t, y_t) - \vartheta)) \\ & + (v\tau_j(t, x_t, y_t) + x(t - \tau_j(t, x_t, y_t)) \\ & - x(t)) \sin\varphi_j(t) + (y(t - \tau_j(t, x_t, y_t)) - y(t)) \cos\varphi_j(t) \Big)^q, \end{aligned} \tag{6}$$

where

$$\alpha_{x,j}(t) = wg(\varphi_j(t)) \left( K_{\text{t}} \cos(\varphi_j(t)) + K_{\text{n}} \sin(\varphi_j(t)) \right), \tag{7}$$

$$\alpha_{y,j}(t) = wg(\varphi_j(t)) \left( K_{\text{n}} \cos(\varphi_j(t)) - K_{\text{t}} \sin(\varphi_j(t)) \right), \tag{8}$$

and the time delay is given by the implicit equation (4). The left hand side of Eqs. (5) and (6) describe the symmetric tool as a 2 DOF oscillator with modal mass $m$, damping $c$ and stiffness $k$. The right hand side corresponds to the cutting force, where $R$ is the radius of the tool, $\vartheta = 2\pi/N$ is the pitch angle of the tool with $N$ being the number of teeth, $\Omega$ is the spindle speed in [rad/s], $w$ is the depth of cut, $K_{\text{t}}$ and $K_{\text{n}}$ are the tangential and the normal cutting coefficients and $q = 0.75$. The function $g$ is a screen function, it is equal to 1, if the $j^{\text{th}}$ tooth is active, and it is 0 if not. For more details on the modeling, see [6].

# 4 Stability properties and conclusions

Linearization and stability analysis for the SD-DDE model of turning processes can be performed in a nice analytical way, and numerical techniques can be used to compute the corresponding bifurcations. For milling processes, however, this analysis is more complicated, since the model is a time-periodic SD-DDE. Here,

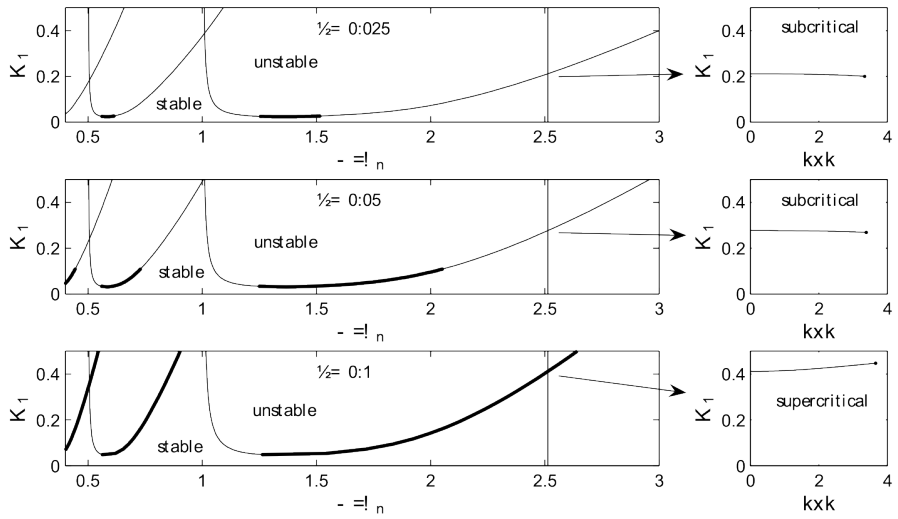


Figure 3: Change of criticality along the lobes. Thick lines - supercritical, thin lines - subcritical.

the results presented in [3, 4] about SD-DDE model of turning are summarized briefly.

Fig. 3 shows stability lobe diagrams in the plane of the dimensionless spindle speed $\Omega/\omega_n$ (with $\omega_n$ being the natural angular frequency) and dimensionless depth of cut $K_1 = K_y w (2\pi R)^{q-1}/(m\omega_{\mathrm{n}}^2)$. Numerical analysis of the periodic orbits arising during the linear loss of stability showed that both sub- and supercritical Hopf bifurcations may appear for different values of the dimensionless feed $\rho = v\tau_0/(2\pi R)$. Here, $\tau_0 = 2\pi/\Omega$ is the mean time delay and $R$ is the radius of the workpiece.

It was found that if $\rho < 0.0209$ then the Hopf bifurcation is always subcritical similarly to the constant delay models. However, if $\rho$ is increased, then the Hopf bifurcation at the right hand side of the lobes becomes supercritical, while the left hand side remains mostly subcritical. The state-dependent delay in the turning model has a kind of stabilizing effect. It increases the linear stability limits and it turns the subcritical bifurcations to supercritical ones.

## Acknowledgement

The authors acknowledge the support from the Hungarian National Science Foundation (OTKA) under grant no. K72911 (T.I.) and T068910 (G.S.).

## References


[1] Shi, H.M., Tobias, S.A., Theory of finite amplitude machine tool instability. *International Journal of Machine Tool Design and Research* **24**, 45–69 (1984).

[2] Stépán, G., Kalmár-Nagy, T., Nonlinear regenerative machine tool vibration. *Proceedings of the 1997 ASME Design Engineering Technical Conferences*, Sacramento, California, DETC97/VIB-4021 (1997).

[3] Insperger, T., Stépán, G., Turi, J., State-dependent delay in regenerative turning processes. *Nonlinear Dynamics*, **47**(1–3), 275–283 (2007).

[4] Insperger, T., Barton, D.A.W, Stépán, G., Criticality of Hopf bifurcation in state-dependent delay model of turning processes, *International Journal of Non-Linear Mechanics*, **43**(2) (2008), pp. 140-149.

[5] T. Richard, C. Germay and E. Detournay, E., A simplified model to explore the root cause of stick-slip vibrations in drilling systems with drag bits. *Journal of Sound and Vibration*, **305**, 432–456 (2007).

[6] T. Insperger, G. Stépán, F. Hartung and J. Turi, State-dependent regenerative delay in milling processes. *Proceedings of ASME International Design Engineering Technical Conferences*, Long Beach CA, paper no. DETC2005-85282 (2005).

[7] F. Hartung, T. Krisztin, H.-O. Walther and J. Wu, Functional differential equations with state-dependent delay: theory and applications. In *Handbook of Differential Equations: Ordinary Differential Equations*, volume 3, Elsevier, North-Holand, 435–545 (2006).

[8] Hartung, F., Turi, J., Linearized stability in functional-differential equations with state-dependent delays. *Proceedings of the conference Dynamical Systems and Differential Equations*, added volume of *Discrete and Continuous Dynamical Systems*, 416–425 (2000).

[9] F. Hartung, Linearized stability in periodic functional differential equations with state-dependent delays. *Journal of Computational and Applied Mathematics* **174**, 201–211 (2005).

# Delay induced canard explosion in high speed machining

Sue Ann Campbell[1], Emily Stone[2], Thomas Erneux[3]

[1] Department of Applied Mathematics, University of Waterloo, Waterloo, Ontario, Canada

[2] Department of Mathematical Sciences, The University of Montana, Missoula, U.S.A.

[3] Université Libre de Bruxelles, Optique Nonlinéaire Théorique, Campus Plaine, Bruxelles, Belgium

## 1 Introduction

We consider a delay differential equation describing high-speed machining. By using singular perturbation techniques, we analyze the emergence of periodic solutions in the limit of small delays. In dimensionless form, this equation is given by

$$x'' + \gamma x' + x = F(x - x(t-\tau), x') \tag{1}$$

where $t$ is time scaled by the natural frequency of a specific vibrational mode. $x(t)$ is the amplitude of the vibration normalized by the nominal chip thickness $t_1$, $\gamma$ is the dimensionless damping rate, and the forcing function $F$ is the projection of the cutting force onto the vibration direction which occurs at an angle $\theta$ with respect to the vertical from the tool path. See Figure 1. $F$ is proportional to the chip thickness (i.e., $x - x(t-\tau)$, the difference between the position at time $t$ and at the time one revolution $\tau$ ago). From the Merchant-Oxley [1, 2] model of steady orthogonal cutting and in the case of a vertical vibration ($\theta = 0$), the forcing function $F$ takes the simple form

$$F = \beta\left[1 - (x - x(t-\tau))\right](1 + ax' + bx'^2). \tag{2}$$

$F$ depends on the instantaneous chip thickness given by the expression in the square brackets. The polynomial in $x'$ is a truncation of an asymptotic expansion for a nonlinear stick-slip type friction force. The parameter $\beta$ combines several physical parameters such as the chip width and the strength of the material. $\beta$ is our bifurcation parameter and Eqs. (1)-(2) have been studied numerically and analytically [4, 5].

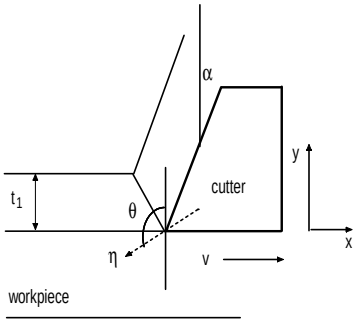


Figure 1: Diagram of cutting tool and workpiece in an orthogonal cutting operation. $t_1$ is the chip thickness, $v$ is the cutting speed, $\alpha$ is the rake angle of the tool, $\theta$ is the vibration angle, and $\eta$ is the vibration amplitude. For a vertical vibration, $\theta = 0$.

## 2 High speed limit

Our objective is to investigate the high speed limit ($\tau \to 0$) of Eqs. (1)-(2). Introducing the deviation $y = x - \beta$, Eqs. (1)-(2) can be rewritten as

$$\begin{aligned} y'' + \gamma y' + y &= \beta(ay' + by'^2) \\ &\quad -\beta(y - y(t-\tau))(1 + ay' + by'^2). \end{aligned} \tag{3}$$

We next expand the bifurcation parameter as

$$\beta = \beta_0 + \tau\beta_1 + ... \tag{4}$$

where $\beta_0 = \gamma/a$ is the Hopf bifurcation point of the basic solution $y = 0$ if $\tau = 0$ and $\beta_1$ is our new control parameter. Inserting (4) into Eq. (3) and expanding $y(t-\tau)$ for small $\tau$, we obtain

$$y'' + y - \beta_0 by'^2 = \tau\left[\beta_1(ay' + by'^2) - y'\beta_0(1 + ay' + by'^2)\right] + O(\tau^2). \tag{5}$$

Figure 2 shows the long-time limit-cycle solutions of Eq. (5) for two different but close values of $\beta_1$. The Z-shaped broken line is the nullcline

$$y = \beta_0 by'^2 + \tau\left[\beta_1(ay' + by'^2) - y'\beta_0(1 + ay' + by'^2)\right]. \tag{6}$$

The transition from a small amplitude limit-cycle to a large amplitude relaxation cycle close to $\beta_1 = \beta_{1c} \simeq 34$ is called a canard explosion and it happens within an exponentially small range of the control parameter (i.e., $\beta_1 - \beta_{1c} =$

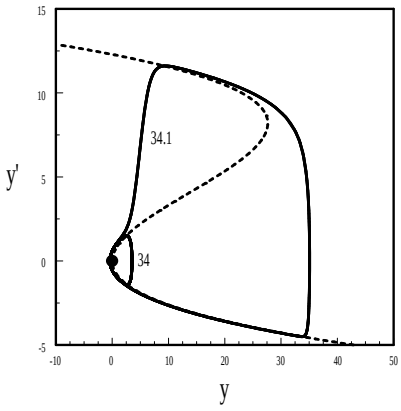


Figure 2: Canard explosion in the phase plane $(y, y')$. The values of the fixed parameters are $\gamma = 2$, $a = 0.25$, $b = 0.125$, and $\tau = 0.1$. $\beta_0 = \gamma/a = 8$ and the values of $\beta_1$ for the two limit-cycles is indicated in the figure. The broken line is the nullcline (6).

$O(\exp(-1/\tau))$. Because this phenomenon is hard to detect, it was nicknamed a canard, after the French newspaper slang word for hoax [6, 7]. The canard explosion can be investigated mathematically by studying the singular limit $\tau \to 0$. In this limit, the leading order solution satisfies the left hand side of Eq. (5) which is an equation for a conservative oscillator. It admits a one parameter family of periodic solution. In order to determine how each periodic solution depends on the bifurcation parameter $\beta_1$, the right hand side of Eq. (5) needs to satisfy a solvability condition. This condition leads to the bifurcation equation for the amplitude of $y$ as a function of $\beta_1$ and describes the progressive change of the periodic solution from its Hopf bifurcation to the canard explosion [5].

## 3 Discussion

It is important to realize that if $\tau = 0$, the solution of Eq. (3) is unbounded in time as soon as $\beta > \beta_0$. A small delay $\tau$ is therefore enough to stabilize time-periodic solutions. The expression of the nullcline (6) indicates that the relaxation oscillations grow in amplitude like $y \sim \tau^{-2}$ and $y' \sim \tau^{-1}$ as $\tau \to 0$. Our singular perturbation analysis is based on the limit of small delays and small damping rates. It could be used for all mechanical models described by nearly conservative equations and subject to a delayed feedback or a delayed feedback control [8]. Such problems appear for the delayed control of container cranes [9] and for lasers subject to a delayed opto-electronic feedback [10].

## Acknowledgments

E.S. and S.A.C. would like to thank the University of Montana-Missoula PArtnership for Comprehensive Equity (PACE) for travel support. S.A.C. also acknowledges the support of NSERC. The research of T.E. was supported by the Fonds National de la Recherche Scientifique (Belgium).

## References

[1] M. Merchant, Mechanics of the cutting process, J. Appl. Phys. 16 (1945), p. 267.

[2] P. Oxley The mechanics of machining, Ellis Horwood Ltd., Chincester, 1989.

[3] E. Stone and A. Askari, Nonlinear models of chatter in drilling processes, Dynamical Systems **17**, 65-85 (2002)

[4] E. Stone and S. Campbell, Stability and bifurcation analysis of a nonlinear DDE model for drilling, Journal of Nonlinear Science **14**, 27-57 (2004)

[5] S.A. Campbell, E. Stone, and T. Erneux, Delay induced canards in a model of high speed machining, to appear in Dynamical Systems (2009)

[6] E. Benoît, J. Callot, F. Diener, and M. Diener, Chasse au canard, Collectanea Mathematica **31**, 37-119 (1981)

[7] W. Eckhaus, Relaxation oscillations including a standard chase on French ducks, Asymptotic Analysis II, Springer Lecture Notes Math **985**, 449-494 (1983)

[8] E. Schöll and H. Schuster, Handbook of Chaos Control, 2nd Rev. Enl. Edition, Wiley-VCH, Weinheim, 2007.

[9] T. Erneux and T. Kalmár-Nagy, Nonlinear Stability of a Delayed Feedback Controlled Container Crane, J. of Vib.and Cont. **13,** 603-616 (2007)

[10] D. Pieroux and T. Erneux, Strongly pulsating lasers with delay, Phys. Rev. A **53**, 2765-2771 (1996)

# Contact force models and the dynamics of drifting impact oscillator

O.K. Ajibose , M. Wiercigroch, E. Pavlovskaia, A.R. Akisanya

Centre for Applied Dynamics Research, School of Engineering, King's College, Aberdeen University, Aberdeen, UK

## 1 Introduction

Vibration enhanced drilling modules have been modelled as drifting oscillators. The successful application and design of this module requires the understanding of the interaction between the drill-bit inserts and the rock during impact. Therefore, an accurate description of the contact force between these two impacting bodies is important. This work describes the effects of contact force models on the global and local dynamics of a drifting oscillator.

Three contact force models are considered, namely: the Kelvin-Voigt (KV), the Hertz stiffness (HS) and the nonlinear contact stiffness and damping (NSD) models. The Kelvin-Voigt model was studied extensively in our previous work (e.g. [1-3]) and is a reference for the current two models. In the HS model, the contact force is a sum of spring force obeying the Hertz's law and a linear damping force [4]. The NSD model presents the contact forces as a combined effect of Hertz's spring and a nonlinear hysteresis damping element [4, 5].

This abstract compares the influence of the contact force models proposed by [4] and [5], with the KV model used in our earlier studies [1-3] on the dynamics of the drifting impact oscillator. The similarities and differences in the results obtained from the analysis of local and global dynamics for each model for various parameter values are stated.

## 2 Modelling

The physical model of a drifting oscillator can be described as follows. A mass, $m = 1$ is subjected to an external force, $f$ which consists of a harmonic component of amplitude $a$, frequency $\omega$ and phase shift $\varphi$, and a static component $b$ . The mass impacts intermittently with a slider which has massless top and bottom plates connected to each other by a spring and a damper. The spring has a

stiffness, $k = 1$, which is a function of the relative displacement of both plates, while the damping coeffcient, $c = 2\xi$, is a function of the relative velocity of the plates. This is similar to the stick-slip phenomenon reported in [6,7] in which progressive motion of the mass occurs when the threshold of the dry friction force, $d = 1$, is exceeded by the contact force. The displacement of the mass is defined as $x$, while the displacements of top and bottom plates of the slider are $z$ and $v$ respectively.

There are three phases of motion for this system, namely: no contact, contact without progression, and contact with progression. There is no interaction between the mass and the slider during the no contact phase, while during the contact without progression phase, the mass and the top plate of the slider are in contact but the bottom plate experiences no motion. In the contact with progression phase, the mass contacts the top plate and there is a simultaneous motion of the mass, the top and the bottom plates of the slider. The Kelvin-Voigt model was studied extensively in our previous work (e.g. [1-3]) and forms a reference in this study for the other two models. In the HS model, the contact force is a sum of a spring force obeying the Hertz's law and a linear damping force. The NSD model presents the contact forces as a combined effect of Hertz's spring and a nonlinear hysteresis damping element. The contact force $F_c$ for the three models are related to the displacements and velocities according to

$$F_c = \begin{cases} (z-v) + 2\xi_1(z'-v') & KV \\ (z-v)\sqrt{|z-v|} + 2\xi_2(z'-v') & HS \\ (z-v)\sqrt{|z-v|} + (1+2\xi_3(z'-v')) & NSD \end{cases} \tag{1}$$

where $\xi_i\,(i = 1, 2, 3)$ are defined as the damping coeffcient for the three models. We note that although the displacement $z$, of the slider top plate during the contact with progression is in phase with the displacement of the mass $x$, the magnitude of $x$ is greater than that of $z$ by the gap $g_0$, between the initial position of the slider top plate and the mass, i.e. $x = z + g_0$.

The equations of motion given above for the different phases of motion can be written concisely as

$$\begin{aligned} x' &= y, \\ y' &= a\cos(\omega\tau + \varphi) + b - \mathcal{P}_1\mathcal{P}_2(1-\mathcal{P}_3)\mathcal{L}_1\left(z, v, z'\right) - \mathcal{P}_1\mathcal{P}_3, \\ z' &= \mathcal{P}_1 y - (1-\mathcal{P}_1)\mathcal{L}_2(z,v)/2\xi, \\ v' &= \mathcal{P}_1\mathcal{P}_3\mathcal{P}_4\left(\mathcal{L}_3(z,v)/2\xi + y\right). \end{aligned} \tag{2}$$

where $\mathcal{P}_1$, $\mathcal{P}_2$, $\mathcal{P}_3$ and $\mathcal{P}_4$ are Heaviside functions defined as:

$$\begin{aligned} \mathcal{P}_1 = H(x-z-g), \quad \mathcal{P}_2 = H(\mathcal{L}_2(z,v)) \\ \mathcal{P}_3 = H(\mathcal{L}_2(z,v)-1), \qquad \mathcal{P}_4 = H(v'). \end{aligned} \tag{3}$$

Functions $\mathcal{L}_1(z, v, z')$, $\mathcal{L}_2(z, v)$, and $\mathcal{L}_3(z, v)$ are defined in Table 1 for each contact force model.

| | KV | HS | NSD |
|---|---|---|---|
| $L_1(z, v, z')$ | $2\xi z' + z - v$ | $2\xi z' + (z - v)^{3/2}$ | $(2\xi z' + 1)(z - v)^{3/2}$ |
| $L_2(z, v)$ | $z - v$ | $(z - v)^{3/2}$ | 1 |
| $L_3(z, v)$ | $z - v - 1$ | $(z - v)^{3/2} - 1$ | $1 - (z - v)^{-3/2}$ |

Table 2: Definition of functions $\mathcal{L}_1$, $\mathcal{L}_2$ and $\mathcal{L}_3$.

# 3 Global and Local Dynamics

A comparison of the influences of the contact models on the local and global dynamics of drifting impact oscillators was carried out by performing the numerical integration of the differential equations using the same parameters for these models. The efficiency of the system is mainly dependent on the frequency of the dynamic force and the damping factor, since both parameters play major roles in the energy consumption of the system. For this reason, the dynamics of the system is compared at moderate and high values of both parameters. In this section, we first consider the dynamics at low values of frequency ($\omega \leq 0.1$) and damping coeffcient ($\xi \leq 0.1$) and then consider same at higher values of the same parameter ($\omega \geq 0.1$ and $\xi \geq 0.1$).

The time histories of this system are shown in Fig. 1 for $a = 0, 3$; $\xi = 0.05$; $\omega = 0.1$ and $g = 0.02$ for three different static loads $b_1 = 0.1$, $b_2 = 0.125$ and $b_3 = 0.15$. The results reveal that the short term (local) local dynamic response of the three models are almost identical. It can also be observed that the average progression rate for each of the static loads is approximately the same.

In Fig. 2-a, the bifurcation diagrams showing the variation of the velocity $y$, with the static load $b$ for parameters $a = 0.3$, $\omega = 0.1$, $g = 0.02$, and $\xi = 0.05$ reveal that although the dynamic response of the system may be similar for each force model, their points of bifurcation differ slightly. Beyond the static load, $b \approx 0 : 165$, it can be observed from Fig.2-a that the response of the system is characterised by intermittent regions of chaotic and periodic motion. These results suggest that in practical terms, the KV model suffciently predicts the long term behaviour of a drifting oscillator with low forcing frequency and low damping coefficient.

For high values of the frequency and damping coefficient, the bifurcation diagrams (Fig.2-b) showing the variation of the velocity $y$ with the static load $b$ for parameters $a = 0.3$, $\omega = 1.0$, $g = 0.02$ and $\xi = 0.1$ reveal that the force models

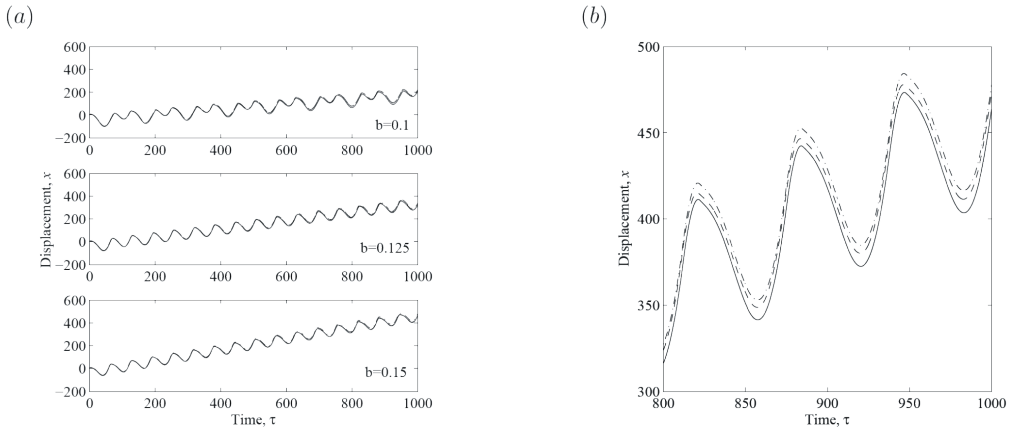


Figure 1: Time histories computed for the three models: HS, NSD and KV; using the parameters $a = 0.3$, $\xi = 0.05$, $\omega = 0.1$, $g = 0.02$, $\varphi = \frac{\pi}{2}$ and HS (dash-dash), NSD (dash-dot), and KV (solid). (a) at $b = 0.1$, $b = 0.125$ and $b = 0.15$, (b) Time histories between $\tau = 800$ and $\tau = 1000$ at $b = 0.15$.

generally give different results for long-term dynamical behaviour. The three models exhibit chaotic motion for static force ranging from $b = 0$ to $b = 0.01$. However, between the region $b = 0.01$ and $b = 0.02$, the HS model exhibits periodic motion while the KV and NSD models continue to be chaotic. Another region of major difference is between regions $b = 0.19$ to $b \approx 0.21$ where although all three models exhibit periodic motion the period number is not the same. The KV model exhibits period two motion, while the HS and NSD models exhibit period four motion

# 4 Conclusions

The influence of different force contact models on the global and local dynamics of drifting oscillators has been investigated for three different models of the contact force: Kelvin Voigt, Hertz stiffness and nonlinear stiffness and damping. The nonlinear dynamic analysis of the system was carried out for the three contact force models. The results of this analysis show that the local dynamics of the system for the three dynamic models are almost identical. Hence, the simpler KV model adequately describes the dynamic behaviour. However, the global dynamics is dependent on the model applied. It is also noted that the HS model gives global results that are topologically similar to the KV model while the behaviour of the NSD model differs in structure.

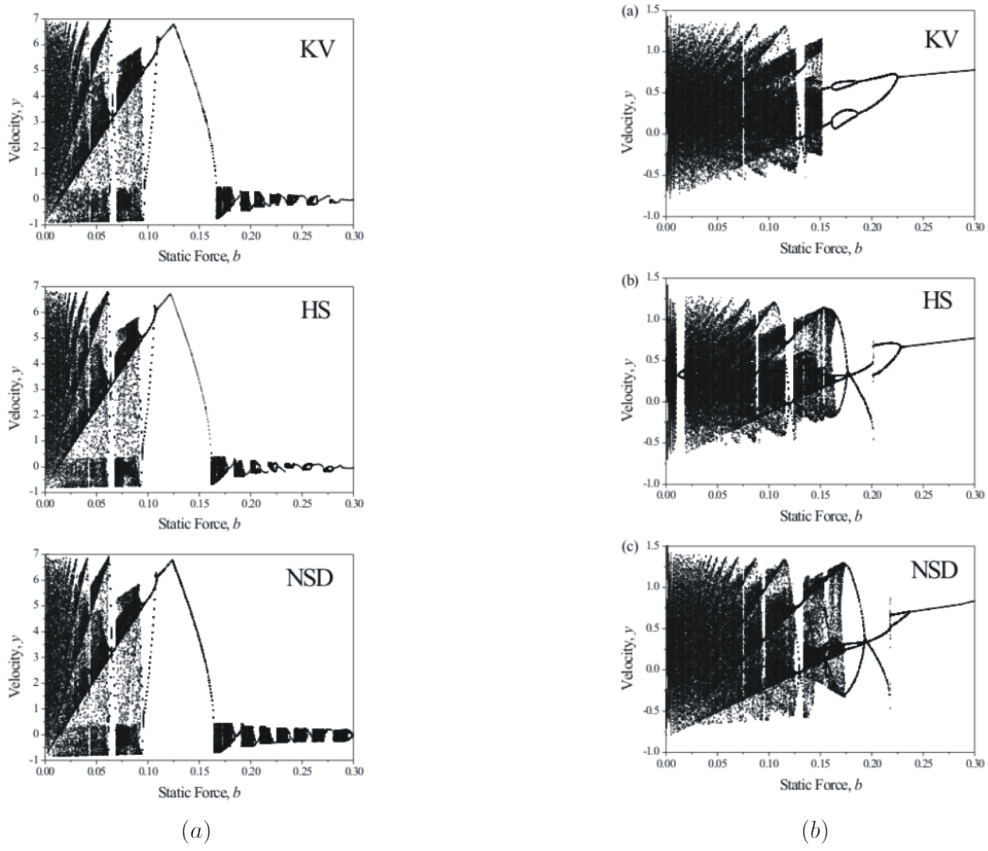


Figure 2: Bifurcation diagram $y = f(b)$ for the three models at $a = 0.3$, $g = 0.02$, $\varphi = \frac{\pi}{2}$ and (a) $\omega = 0.1$, $\xi = 0.05$ or (b) $\omega = 1.0$, $\xi = 0.1$.

## References


[1] E. Pavlovskaia,M. Wiercigroch and C. Grebogi. Modeling of an impact system with a drift. Phys. Rev. E, 64, 0562244(2001).

[2] E. Pavlovskaia and M. Wiercigroch, Analytical drift reconstruction for visco-elastic impact oscil- lators operating in periodic and chaotic regimes. Chaos Solitons & Fractals, 19, 151-161(2004).

[3] E. Pavlovskaia and M. Wiercigroch Low dimensional maps for piecewise smooth oscillators. Journal of Sound and Vibration, 305, 750-771(2007).

[4] L. Pust and F. Peterka. Impact oscillator with Hertz's model of contact. Meccanica, 38, 99-114 (2003).

[5] S. Muthukumar and R. DesRoches. A Hertz contact model with nonlinear damping for pounding simulation. Earthquate. Engng Struct. Dyn., 35, 811-828, 2006.

[6] M. Wiercigroch. A note on the switch function for the stick-slip phenomenon, Journal of Sound and Vibration, 175, 700-704(1994).

[7] U. Galvanetto and S.R. Bishop. Stick-slip vibrations of a two degree-of-freedom geophysical fault model, Int. J. Mech. Sci, 36, 683-698(1994).

# A Novel Approach to Evaluate Rotary-Percussive Drilling With Roller-Cone Bits

Luiz Franca

Drilling Mechanics Group, CSRIO Petroleum, Perth, Australia

## 1 Introduction

Resonance Hammer Drilling (RHD) is a new rotary-percussive technology, which is being studied at CSIRO as an alternative method to improve drilling performance in deep wells. This drilling method consists of a small downhole hammer mounted onto a conventional rotary drilling assembly with a roller-cone bit. Different from percussive drilling [5], RHD is a hybrid form of drilling, since the normal operating parameters, namely the weight-on-bit $W$ and the angular velocity $\Omega$ are still acting as in conventional rotary drilling.

This paper proposes a new methodology to evaluate the efficiency of the RHD technique. First, a complete model of the drilling response of roller-cone bits under impulsive loading is established, i.e. a set of relations between the weight-on-bit $W$, the torque-on-bit $T$, the energy per blow $I$, number of blows per revolution $f$, the rate of penetration $V$, and the angular velocity $\Omega$. The derivation of the bit-rock interface laws presented here follows the phenomenological approach used for PDC bits [1, 2], while taking into consideration the energy transfer in percussive drilling proposed by Hustrulid & Fairhust [3].

## 2 Bit-Rock Interaction Model for Resonance Hammer Drilling

In the case of the RHD method, we postulate that the penetration per revolution $d$ is composed by two distinct parts: a penetration caused by rotary drilling $d_r$ and a penetration generated by percussive drilling $d_p$,

$$d = d_r + d_p. \tag{1}$$

Additionally, we assume that the interface laws are rate-independent and that there is a linear relationship between $W$, $T$, and $d_r$ (after taking into account the

existence of a threshold) and between $If$ and $d_p$. Combining both rotary and percussive processes, a complete model of the drilling response is explicity given by

$$\begin{aligned} \tau + \lambda\kappa &= \varepsilon d + \mu\sigma^* al \\ \varpi + \zeta\lambda\kappa &= \zeta\varepsilon d + \sigma^* al \end{aligned} \tag{2}$$

where $\tau = 2T/a^2$ represents a scaled torque-on-bit, $\varpi = W/a$ a scaled weight-on-bit, $\kappa = 2Ifc/a^2$ a scaled impulsive load, $\lambda = \varepsilon/\psi$ is the intrinsic specific energy ratio, $\zeta$ is a number, $\mu$ is a coefficient of friction, $\sigma^*$ is the threshold or normal stress, $c$ is the energy transfer coefficient, $a$ is the bit radius and $l$ represents the total contact length. Therefore, another representation of Eq (2) can be obtained, scaling $\tau$, $\varpi$ and $\kappa$ by $d$

$$E + \lambda(1 - \mu\zeta)P = E_0 + \mu S \tag{3}$$

where $E_0 = (1 - \mu\zeta)\varepsilon$, $E = \tau/d$ is the specific energy, $P = \kappa/d$ is the hammering strength and $S = \varpi/d$ is the drilling strength. Figure 1a illustrates graphically the bit-rock interaction laws (Eq. 2) in the $E$-$P$-$S$ diagram. Notice that the proposed model accounts for the two components of the intrinsic specific energy, namely, $\varepsilon$ the component associated with rotary drilling and $\psi$ the component associated with percussive drilling. The ability to independently evaluate $\varepsilon$ and $\psi$ allows us to objectively measure the relative efficiency of both the rotary-percussive and the conventional rotary drilling methods.

## 3 Experimental Results

The proposed model has been benchmarked against experimental data conducted with an in-house designed laboratory drilling rig, see Figure 1b. This rig consists of four main components: upper assembly, hammer system, bit assembly and core drive mechanism. The upper assembly is designed to perform tests under kinematic control. The impulsive loading is introduced into the drilling process through the hammer system, which consists of a free-mass elastically suspended and excited by a motor. A roller-cone bit mounted on a sophisticated anvil represents the bit assembly. The core drive mechanism drives the rock sample at a controlled angular velocity.

A series of tests at atmospheric pressure under kinematic control have been carried out in Castlegate sandstone. Experiments have first been conducted with conventional rotary drilling, and the corresponding bit-rock interaction parameters identified. The observed response is in agreement with the proposed model

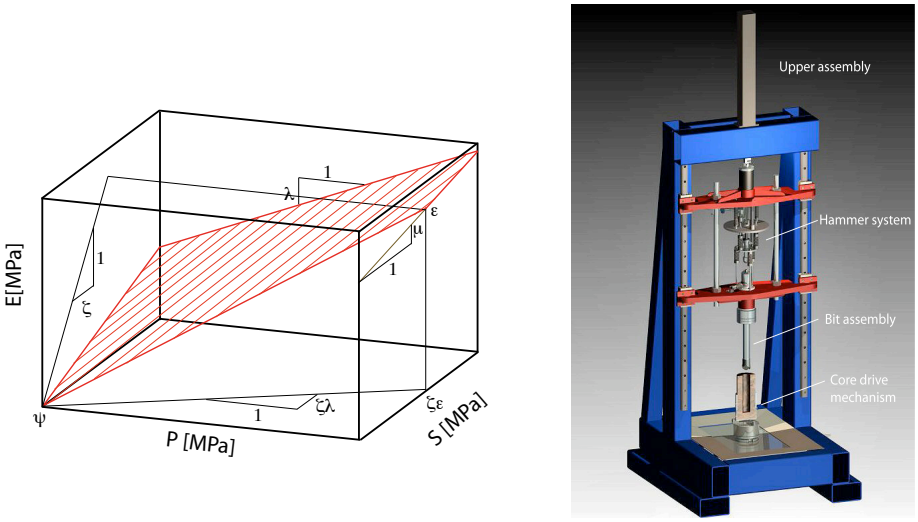


(a) (b)

Figura 1: (a) Schematic *E-P-S* diagram; (b)Drilling rig used to investigate the RHD technique.

and the intrinsic specific energy associated with rotary drilling $\varepsilon$ appears to be well correlated to the uniaxial compressive strength of the rock $q$. This result suggests therefore that there is a correlation between $\varepsilon$ and $q$ in tests conducted at atmospheric pressure. Pessier & Fear [4] reported similar correlation between the minimum specific energy $E_{sm}$ and $q$ in tests performed with roller-cone bits and Richard et al. [6] between $\varepsilon$ and $q$ in scratch tests.

Next, experiments conducted in Castlegate sandstone at atmospheric pressure using the RHD are investigated. Results have shown that a smaller weight-on-bit $W$ (resulting in a smaller $T$) is required when the hammer is activated in tests performed with a constant penetration per revolution $d$. However, the identified ratio of intrinsic specific energy rates $\lambda$ is a small number, suggesting that most of the energy provided to the bit by hammering is dissipated in the form of plastic deformation in these experiments. Figure 2 shows a typical result performed in Castlegate sandstone in the *E-P-S* diagram for four different penetration per revolution: $d$ = 0.5, 1.0, 1.5 and 2.0 mm/rev. Here we can notice that all the responses are indeed contained in the drilling plane (Eq. 2), the drilling efficiency increases with $d$ and the response is practically on the drilling line (100% of efficiency) for $d$ = 2.0 mm/rev.

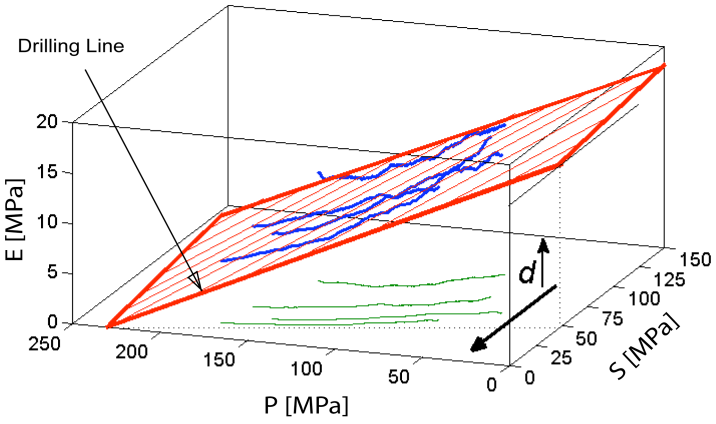


Figure 2: Experimental results performed with Castelgate sandstone for $d = 0.5$, 1.0, 1.5 and 2.0: $E$–$P$–$S$ diagram.

# 4 Conclusions

This work investigates a new rotary-percussive drilling technique, called Resonance Hammer Drilling (RHD). Firstly, a complete model of the drilling response of roller-cone bits with and without precussive action is established. Next, a series of tests conducted in Castlegate sandstone at atmospheric pressure under kinematic control are analysed within the framework of the proposed model. All results are in agreement with the proposed phenomenological model, suggesting that this model can be used to investigate drilling response of roller-cone bits with and without impact loading. Also, the intrinsic specific energy associated with rotary drilling $\varepsilon$ appears to be correlated to the uniaxial compressive strength of the rock $q$. Considering the RHD technique, the intrinsic specific energy ratio $\lambda$ is identified as a small number, $\lambda << 1$. This observation points out that more energy is necessary with the RHD method as compared to conventional rotary drilling. However, we believe that $\lambda$ and, consequently, the usefulness of impulsive loads, will increase in brittle materials, since in this case the energy dissipation is generally in the form of micro- and macro-cracks. Although more energy is required to drill ductile rocks, much less $W$ and $T$ are required when impulsive loads are added to the system. Hence, the RHD technique has potential application as an alternative method for drilling highly deviated wells or horizontal wells and to explore deep reserves, where the limitations of $W$ can be compensated by percussive action.

## Acknowledgements

The author would like to thank Emmanuel Detournay and Thomas Richard for their valuable advices.

## References

[1] Detournay E. and Defourny P. (1992), A Phenomenological Model for the Drilling Action of Drag Bits, Int. J. Rock Mech. Min. Sci. & Geomech. Abstr., 29 (1), 12-23.

[2] Detournay E., Richard T. and Shepherd M. (2008), Drilling response of drag bits: Theory and experiment, Int. J. Rock Mech. Min. Sci., 45 (8), 1347–1360.

[3] Hustrulid W.A. and Fairhust C. (1971) A Theoretical and Experimental Study of The Percussive Drilling of Rock, Int. J. Rock Mech. Min. Sci., Vol 8, 311-333.

[4] Pessier R. C. and Fear M. J. (1992), Quantifying common drilling problems with mechanical specific energy and a bit-specific coefficient of sliding friction, In SPE Annual Technical Conference and Exhibition, SPE 24584, 373–388.

[5] Melamed Y., Kiselev A., Gelfgat M., Dreesen D., Blacic J. (2000), Hydraulic Hammer Drilling Technology: Developments and Capabilities, J. of Energy and Resources Technology, 122, 1-7.

[6] Richard T., Detournay E., Drescher A., Nicodème P. and Fourmaintraux D. (1998), The scratch test as a means to measure strength of sedimentary rocks, SPE/ISRM 47196, Proc. EuRock'98 (Rock Mechanics in Petroleum Engineering), The Norwegian University of Science and Technology, Trondheim, published by the Society of Petroleum Engineers, Vol. 2, pp. 15-22.

# Dynamics of a bouncing trimer

Stéphane Dorbolo, François Ludewig, Nicolas Vandewalle

GRASP, Physics Department, University of Liège, Belgium

## 1 Introduction

The bouncing ball is a well known problem and is often given as the typical non-linear system that exhibits the period doubling route to chaos [1, 2]. Recently, the interest in this subject has been renewed through granular shaken systems [3]. When a large assembly of grains is shaken, compaction, convection, or even gas-like behaviours may be observed according to the number of grains and to the acceleration of the plate that vibrates the packing. The packing may be considered as inelastic bouncing ball [3].

The shape of an object is rarely as simple as an ideal sphere. The increase of complexity is obtained by increasing the number of contacts between the object and the plate. The first step, coined dimer, is a object formed by two beads linked by a rigid rod. The bouncing of that object on a vertically shaken plate has been studied in 2004 [4]. Here, we analyze the motion of a trimer on a vibrating plate [5]. The trimer is composed by three metallic beads equally distant. The motivation is twice: (i) to evidence a new self-propelled particle and (ii) to show periodical modes.

## 2 Experimental set-up

The plate is vertically and sinusoidally shaken by an electromagnetic shaker (G&W V55) via a linear bearing in order to ensure the unidirectionnal vibration. The forcing parameters are the frequency $f$ and the reduced acceleration $\Gamma$ given by the ratio between the maximal acceleration of the plate $4\pi^2 A f^2$ where $A$ is the amplitude and the gravity $g$. The frequency is fixed between 25 Hz and 100 Hz while the amplitude allows to reach accelerations up to $\Gamma = 10$. By studying the accelerometer signal, it is possible to measure the time delay between successive contacts of the trimer and the plate. From the sets of time delays, the statistic distributions are

deduced for each considered acceleration. The beads composing the trimer have a diameter of 10 mm. Two trimers have been considered a small one (the side of the trimer $c$ equals 35 mm) and a large one ($c$ =56 mm).

## 3 Phase diagram

When the small trimer is placed on a vibrated plate, several modes can be observed: (i) the trimer moves horizontally (self-propelled mode, SFP), (ii) the trimer rotates (R), (iii) the three beads bounce once every two periods at the same phase (PER-2) and (iv) the three beads bounce once every three periods at the same period (PER-3). In order to understand when the modes occurs a phase diagram has been built in the parameter space: $f - \Gamma$. The trimer is first place on the plate at rest. The frequency is fixed, then the amplitude is increased until the trimer can tumble. The phase diagram is reported in Fig.1 (top). The modes R, PER-2 and PER-3 are found in narrow regions around particular accelerations $\Gamma_R \approx 3$, $\Gamma_{PER-2} \approx 5$ and $\Gamma_{PER-3} \approx 8$ respectively. These accelerations do not depend on the frequency. In the rest of the phase diagram, the trimer can move horizontally and rotate randomly.

The large trimer has been studied for a fixed frequency. The large trimer does not experience too large horizontal excursion compared to the small one. That allows to studied the bouncing modes according to the accelerometer signal. The density of probability of the time delay between successive contacts of any beads with the plate is presented in Fig. 1 (down). The darker area is, the more probable is the time delay. The structure is rather complex but can be reproduced thanks to numerical simulation considering non-smooth contact dynamics. The modes PER-2 and PER-3 are clearly visible at $\Gamma_{PER-2} \approx 5$ and $\Gamma_{PER-3} \approx 8$. These accelerations are particular. For these acceleration, it can be shown that the trimer lands on the plate with a relative speed very close to zero. It results that the trimer sticks on the plate. The information of previous bounce is consequently erased. As the trimer sticks, it takes off when the acceleration of the plate is equal to $-g$. The take-off speed is therefore known. The trimer experiences a parabolic flight and must land with a relative speed equals to zero (that is necessary to ensure the periodicity. That behaviour occurs when $\Gamma = \sqrt{(2n+1)^2\pi^2/4 + 1}$, $n$ is a whole number.

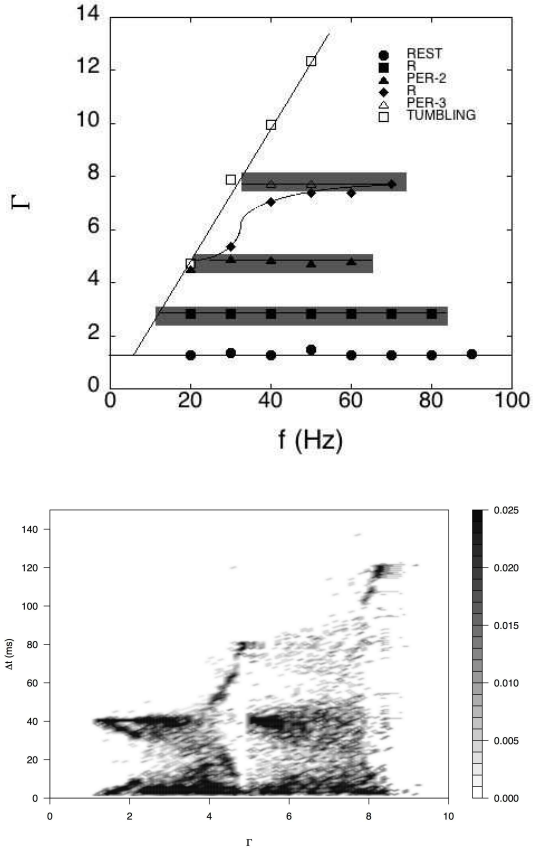


Figure 1: (up) Phase diagram $f - \Gamma$ presenting the different modes encountered for the small trimer. The trimer locks some periodical orbits along the horizontal areas (in grey), namely a rotation mode (black squares), a PER-2 mode (black triangles), a second rotation mode (diamonds) and a PER-3 mode (open triangles). The trimer tumbles when excited above the oblical line passing by open squares. (down) Density of probability of time delay between two successive shocks of any beads with the plate as a function of the reduced acceleration for $f = 25$ Hz

## 4 Conclusion

The bouncing trimer has shown to be a good candidate as a random self-propelled particle. Moreover, very stable modes have been encountered as period-2 and period-3 modes. The particular accelerations for which these modes appear are linked to the sticking of the objet on the plate when it hits the plate with a very low relative speed.

SD would like to thank FNRS for financial support. T. Gilet is acknowledged for fruitful discussions. Part of this work has been financed by "The InterUniversity Attraction Pole INANOMAT" (IAP P6/17).

## References

[1] N. B. Tufillaro, T. Abbot, J. Reilly, *An Experimental Approach to Nonlinear Dynamics and Chaos*, (Addison-Wesley, New-York, 1992).

[2] J. M. Luck and A. Mehta, Phys. Rev. E **48**, 3988 (1993)

[3] J.M. Pastor, D. Maza, I. Zuriguel, A. Garcimartin, and J.F. Boudet, Physica D **232**, 128 (2007)

[4] S. Dorbolo, D. Volfson, L. Tsimring, and A. Kudrolli, Phys. Rev. Lett. **95**, 044101 (2005)

[5] S. Dorbolo, F. Ludewig, and N. Vandewalle, to be published 2009.)

# Self-Excited Oscillations of Drag Bits

Christophe Germay

Epslog SA, Liège, Belgium

The research presented here builds on a model of self-excited axial and torsional vibrations of drag bits first introduced by Richard in 2001. The originality of this model, which we referred to as the RGD model, lays in the coupling between the axial and the torsional modes of vibrations via rate-independent bit/rock interface laws that account for both cutting and frictional processes. On the one hand, the cutting process combined with the quasi-helical motion of the bit leads to a regenerative effect that introduces a coupling of axial and torsional modes of vibrations and a state-dependent delay in the governing equations (see Figure 1). On the other hand, the frictional contact process is associated with discontinuities in the boundary conditions when the bit sticks in its axial and angular motion. In the RGD model, the drillstring is reduced to a two degrees-of-freedom representation consisting of a torsional compliance and a point mass and inertia (see Figure 1). The model was originally motivated by an analysis of downhole field data recorded during drilling operations.

The self-excited vibrations lead sometimes to torsional stick-slip limit cycles, which are accompanied by the formation of a repetitive bottom-hole pattern. Lateral vibrations, which destroy this pattern, inhibit these oscillations and prohibit the occurrence of the stick-slip, as observed in the field when so-called lateral bits are used. A parametric analysis revealed the existence of (i) several stable periodic solutions, such as axial and torsional stick-slip oscillations (see Figure 2), anti-resonance regime of the torsional dynamics, and (ii) a quasi limit cycle or bit bouncing, in the torsional or axial direction, respectively. The complex and diversified numerical simulations motivated a theoretical analysis of the dynamic response of the RGD model, with the aim of identifying the oscillation mechanisms and their parametric dependency. The dimensionless formulation highlights the existence of a large parameter $\psi$ in the model, which enables a two time scales analysis of the fast axial and slow torsional dynamics. An asymptotic analysis decouples the fast axial dynamics (with a frozen constant delay) from the slow torsional dynamics, which is itself only influenced by the averaged behavior of the fast dynamics. When the delay is larger than a critical value $\pi/\sqrt{2n\psi}$, a stable limit cycle in the axial direction is observed over a certain parametric range (see Figure 3). An approximate model of the axial dynamics is proposed to

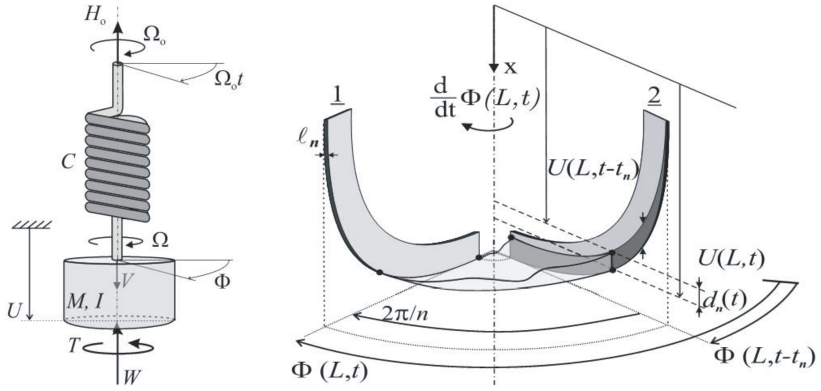


Figure 1: Simplified model of a drilling system (Left) and the illustration of the regenerative effect that couples the axial and torsional modes of vibrations where the bottom-hole profile located between two successive blades of a drill bit, characterized by n identical blades symmetrically distributed around the axis of revolution can be seen (Richard, Germay, and Detournay 2007)).

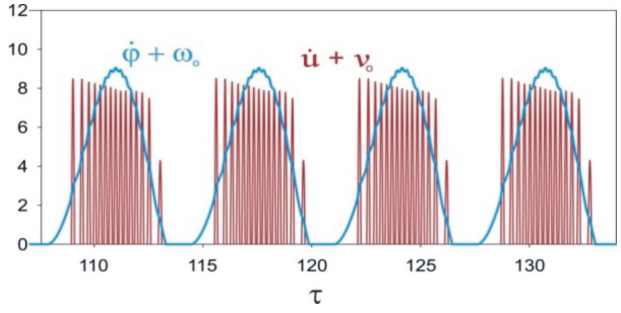


Figure 2: Stick-slip torsional and axial vibrations

provide an analytical characterization of the limit cycle. The resulting analytical predictions match well the numerical observations. They are also useful to characterize the phenomenon of bit bouncing, which originates from the instability of the axial solutions.

The approximate model also provides an analytical expression of the averaged reacting torque-on-bit that influences the torsional dynamics. Its variation in terms of the bit angular velocity recovers the empirical velocity weakening law observed in experiments. The analysis of the slow torsional dynamics predicts the emergence of the different regimes of torsional vibrations (stick-slip vibrations or a quasi-limit cycle) in parametric ranges that agree with the numerical simulations (see Figure 4). The analytical predictions provide useful recommendations for

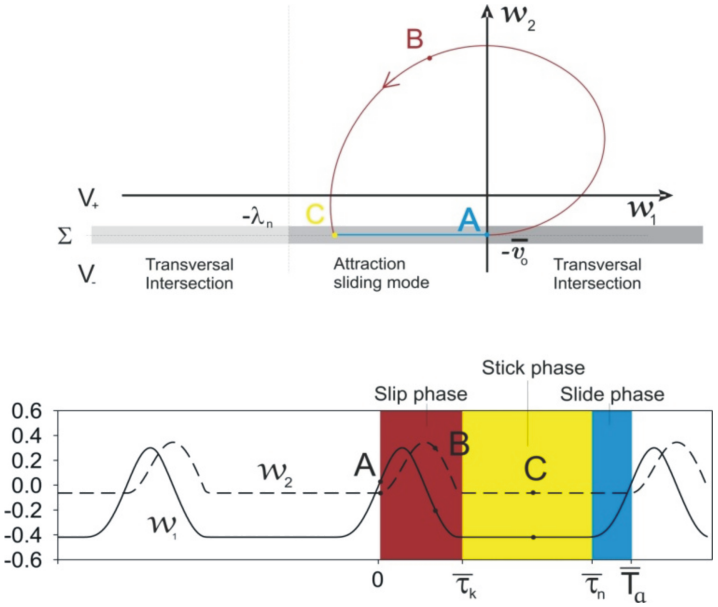


Figure 3: Projection of the axial limit cycle in the perturbed depth of cut axial velocity state space.

the design of drilling structure, the selection of the operating parameters or the control synthesis.

We also discuss some limitations of the two time scales approach to capture phenomena such as the anti-resonance or delayed bifurcations. The anti-resonance regime is characterized by small vibrations of the bit angular velocity around its nominal value although the bit experiences intermittent losses of frictional contact. This regime occurs at low rotational speed, or equivalently at large delay. It is only observable when the axial stick time is large enough to generate a phase locking with the bit angular velocity. An experimental strategy has been proposed to validate the RGD model, using the experimental setup DIVA. Although we conducted some experiments confirming that the so-called velocity weakening of the torque-on-bit is rather a consequence than a cause of the axial vibrations, the results are not entirely conclusive due mostly to the particular behavior of the artificial rock that was used. Moreover, the cutter design was found to be inappropriate for these experiments. The use of stronger natural rocks gave rise to other issues such as strong bit whirling and inadequacy of the hook load control. Finally, the RGD model was extended by basing the formulation of the model on a continuum representation of the drillstring rather than on a characterization of the drilling structure by a two degree-of-freedom

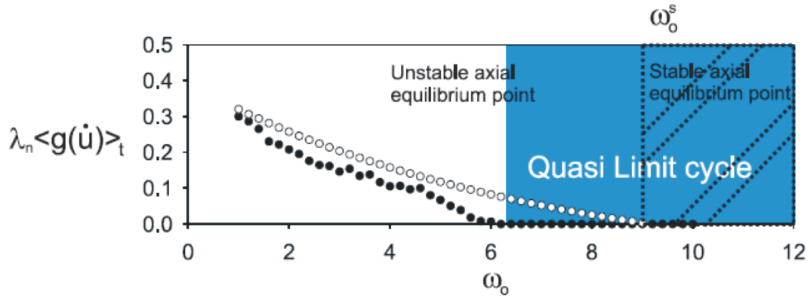


Figure 4: Variation of the averaged response of the friction contact with the rotational speed responsible for the apparent decrease of the mean torque with the RPM. The white dots represent the response of the analytical approximate of the model while the black dots are the results of numerical simulations.

system. The dynamic response of the drillstring is computed using the finite element method. Multiple natural axial and torsional modes of vibrations of the drilling structure can thus be captured by the model, in contrast to the single resonance frequency of a torsional pendulum in the original low dimensional model. It allows the description of a model capable of simulating the vibrations of realistic drilling structures. The general tendencies of the system response that are predicted by the low dimensional model when varying the control parameters, are similarly observed in the FEM model. Namely, occurrence of stick-slip vibrations as well as risk of bit bouncing are enhanced with an increase of the weight-on-bit or a decrease of the rotational speed. Decrease of the torque-on-bit with the bit angular velocity is also observed. All these trends predicted by either model are supported by field measurements. Finally, we should note that further simulations with this computational model indicate that a value larger than 1 of the parameter ß (related to the bit geometry and the friction coefficient) generally prohibits the occurrence of stick-slip vibrations, as in the RGD model. However, new features in the self-excited response of the drillstring are predicted by this computational model. In particular, stick-slip vibrations can be observed at natural frequencies of the drillstring different than the fundamental one, depending on the operating parameters. Interestingly, stick-slip vibrations occurring at a frequency higher than the first natural torsional frequency of the drillstring have been measured with down hole tools in field operations.

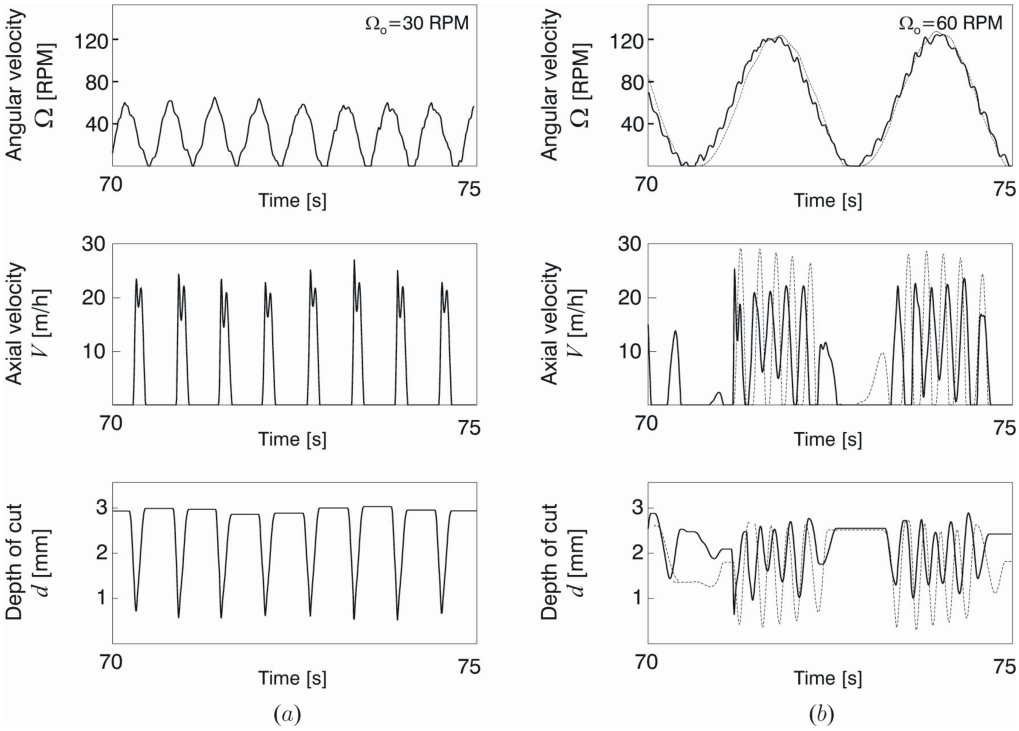


Figure 5: Torsional stick slip vibrations at third natural frequency in torsion (Left) and comparison between the response of the low dimensional and the high dimensional system when vibrating at the first natural frequency of the drillstring (Right).

# Modeling and Experimental Validation of Axial Drillstring Dynamics

Bart Besselink, Nathan van de Wouw

Dynamics & Control, Department of Mechanical Engineering, Eindhoven University of Technology,The Netherlands

## 1 Introduction

In the analysis of torsional stick-slip vibrations in drilling systems using drag bits, the drill string model is generally limited to the torsional dynamics. Herein, the bit-rock interaction is often modeled as a velocity-weakening friction law, which leads to torsional (stick-slip) vibrations. However, bit-rock interaction experiments using single cutters have not revealed any intrinsic velocity-weakening effect, suggesting that this effect is likely to be the result of complex drill string dynamics. This insight led to a different modeling approach, introduced in [3]. Here, the axial and torsional dynamics of the drill string are coupled via a rate-independent bit-rock contact model [1]. Analysis of this model shows that fast self-excited axial vibrations lead to an apparent velocity-weakening effect in the torsional direction [2], causing torsional vibrations and stick-slip.

In this presentation, the focus will be on the experimental validation of the axial dynamics of the model as proposed in [3] and analyzed in [2].

## 2 Experimental validation of the axial dynamics

In [2], it was shown that the fast axial dynamics can be analyzed separately because of the separation of time scales between (fast) axial and (slow) torsional dynamics. Further, self-excited axial vibrations are shown to be the driving force behind an apparent velocity-weakening effect in the torsional dynamics, ultimately leading to torsional stick-slip vibrations. To experimentally validate these results, a test rig involving a mechanical equivalent of the axial dynamics was built at CSIRO, Australia. The experimental setup, named TAZ, is depicted in Figure 1 and consists of a rotating sandstone disk on which a cutter can be lowered. During cutting, both the vertical position and the cutting forces are measured, as well as the rock profile. Experiments under constant weight-on-bit

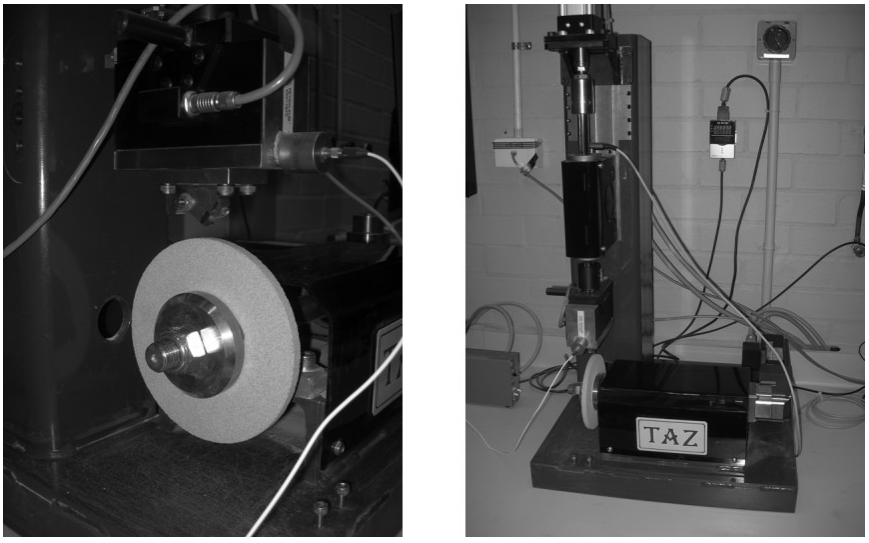


Figure 1: Experimental setup "TAZ", representing axial drill string dynamics (left) and rock sample and cutter detail (right).

reveal discrepancies between the experimental results and the dynamics predicted by the model, suggesting that the bit-rock interaction model is incomplete.

Additional experiments, where the axial position $U$ of the bit is under kinematic control, therefore aim to model the bit-rock contact, focussing on the contact between the rock and the underside of the cutter. This contact area is caused by wear of the cutter and is referred to as the wearflat. In the bit-rock interaction model used in the model of the axial dynamics in [2], a discontinuous behavior of the contact forces with respect to the axial velocity $dU/dt$ is assumed, as depicted in Figure 2. However, a smooth transition between contact and loss of contact is found experimentally. Figure 2 illustrates this experimental fact for the normal forces, whereas the parallel forces show a similar trend. This transition is dependent on the geometry of the contact, as characterized by the approach angle of the cutter. The approach angle is defined as the angle of the velocity vector with respect to the forward motion, as defined in Figure 3. Further, the contact forces are dependent on the depth-of-cut. Based on these results, the bit-rock interaction model is updated, using a piecewise linear approximation for the wearflat forces, as depicted in Figure 2. Simulations using this updated bit-rock interaction model show a significant improvement when comparing the experimental results with the theoretical predictions.

Finally, the updated bit-rock interaction model is implemented in a full drill string model, including the torsional dynamics. Preliminary analyses of this

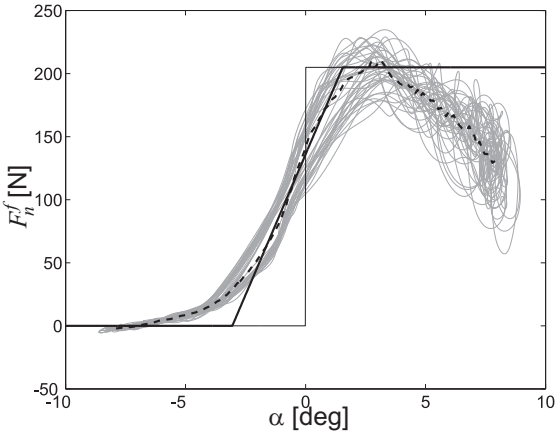


Figure 2: Measured normal wearflat force $F_n^f$ (in gray) for a blunt cutter as a function of the approach angle $\alpha$. The dashed line denotes the averaged result, whereas the bold solid black line denotes the piecewise linear fit. The thin black line denotes the original discontinuous bit-rock interaction model.

model show two distinct regimes. First, for small nominal approach angle, corresponding to a low rate-of-penetration, the axial dynamics is locally asymptotically stable and no torsional vibrations occur. In this regime, the normal bit-rock contact forces are proportional with the approach angle, causing an apparent damping in the axial dynamics that stabilizes the axial equilibrium point, which corresponds to a constant downward velocity of the drill bit. Second, for a higher nominal approach angle, the axial dynamics is unstable, leading to axial limit cycling, which in turn causes an apparent velocity weakening effect in the torsional dynamics. In this regime, the velocity weakening effect causes torsional vibrations and torsional stick-slip, which is similar to the results predicted by the

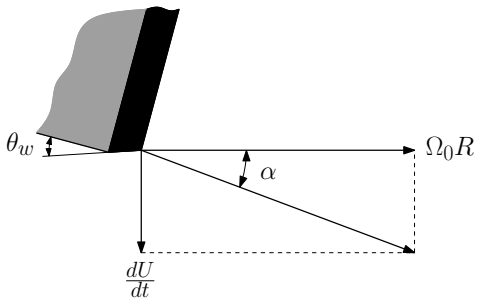


Figure 3: Definition of the approach angle $\alpha$.

original model as in [2].

## 3 Conclusions

The drill string dynamics model analyzed by [2] is validated experimentally. Initial experimental results using a mechanical equivalent of the axial dynamics indicate that the bit-rock interaction model is incomplete. Additional experiments are performed to identify the bit-rock interaction in detail, focussing on the contact forces under the wearflat. Based on these results, the bit-rock interaction model is updated and implemented in a full drill string model. Preliminary analyses of this model show two distinct regions, of which one leads to torsional stick-slip oscillations.

Since the bit-rock interaction is the driving force behind drill string dynamics, future work will focus on additional experiments for the identification of the bit-rock interaction law in more detail.

## Acknowledgements

This work was done in cooperation with Alexandre Depouhon, Thomas Richard (CSIRO, Australia) and Emmanuel Detournay (CSIRO, Australia and University of Minnesota, USA). They are gratefully acknowledged for their contribution.

## References

[1] E. Detournay and P. Defourny. A phenomenological model for the drilling action of drag bits. International Journal of Rock Mechanics and Mining Science & Geomechanics Abstracts, 29:13–23, 1992.

[2] C. Germay, N. van de Wouw, H. Nijmeijer, and R. Sepulchre. Nonlinear drillstring dynamics analysis. SIAM Journal on Applied Dynamical Systems, accepted, 2008.

[3] T. Richard. Self-excited stick-slip oscillations of drag bits. PhD thesis, University of Minnesota, 2001.

# Apparent Coexistence of Multiple Regimes of Self-Excited Vibrations in Drilling Systems

Alexandre Depouhon[1], Emmanuel Detournay[2]

[1] e-Xstream Engineering, Luxembourg
[2] University of Minnesota, USA & CSIRO Petroleum, Australia

## 1 Introduction

The issue of stick-slip oscillations in the rotary drilling systems used to drill deep boreholes for hydrocarbon exploration and production has been explored by Richard *et al.* [1].

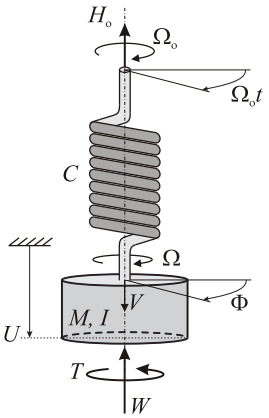


Figure 1: Discrete model.

Their analysis of the dynamics of the drill bit is based on a discrete model of the drillstring (Fig. 1), and rate-independent bit-rock interaction laws. The latter accounting for the regenerative cutting effect taking place at the bit level (Fig. 2) the equations of motion yield a system of discontinuous state-dependent delayed differential equations. Numerical simulations with this model produce self-excited stick-slip oscillations and show the existence of an anti-resonance drilling regime, during which large amplitude axial vibrations of the bit stabilize its angular motion. Further work carried out by Germay *et al.* [2] has formalized the model using the concept of Filippov differential inclusion and brought

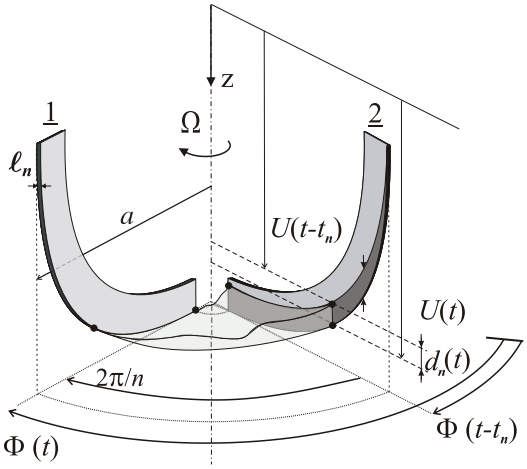


Figure 2: Regenerative cutting.

to light the existence of quasi-periodic solutions for particular parametric configurations of the model. Here, we investigate the slow dynamical behavior that is inherent to particular parametric configurations of this model, and provide, using linear stability analysis, an explanation to the quasi-periodic solutions observed in numerical simulations [1, 2].

## 2 Governing equations

Using the time scale $t_* = \sqrt{I/C}$ and the length scale $L_* = 2C/\varepsilon a^2$, with $\varepsilon$ being the intrinsic specific energy of the rock, $a$ the bit radius, $C$ and $I$ the torsional stiffness and polar mass moment of inertia of the drillstring, Richard *et al.* [1] derived the dimensionless equations of motion for an idealized bit, consisting of $n$ identical radial blades regularly spaced by $2\pi/n$ radians, drilling a homogeneous rock

$$u'' = \psi(\mathcal{W}_0 - \mathcal{W}({}^t_0u, {}^t_0\varphi)), \qquad \varphi'' + \varphi = \mathcal{T}_0 - \mathcal{T}({}^t_0u, {}^t_0\varphi), \tag{1}$$

where $u$ and $\varphi$ are the bit axial displacement and angular position perturbations to the steady-state solution, the prime denotes differentiation with respect to the dimensionless time $\bar{t} = t/t_*$, $\mathcal{W}$ and $\mathcal{T}$ are the dimensionless weight- and torque-on-bit, $\psi$ is the system number and the subscript $_0$ refers to a steady-state quantity. Both $\mathcal{W}$ and $\mathcal{T}$ are functions of the history of $u$ and $\varphi$, denoted by ${}^t_0u$ and ${}^t_0\varphi$, respectively.

In drilling conditions, the scaled efforts $\mathcal{W}$ and $\mathcal{T}$ are given by the bit-rock interaction laws and have experimentally been shown to depend on two distinct

processes, respectively, a cutting and a frictional contact ones, *i.e.* $\mathcal{W} = \mathcal{W}^c + \mathcal{W}^f$ and $\mathcal{T} = \mathcal{T}^c + \mathcal{T}^f$. While the cutting forces are proportional to the bit penetration per revolution, $\delta$, the contact forces are characterized by a threshold following a transition that is function of both $\delta$ and the direction of the relative velocity of the cutters with respect to the rock [3]

$$\mathcal{W} = n\left(\delta_n + \mathcal{W}_n^f\right),\ \mathcal{T} = n\left(\delta_n + \beta\mathcal{W}_n^f\right),$$
$$\mathcal{W}_n^f = \lambda_n \underset{0}{\overset{1}{\mathrm{sat}}}\left(\frac{\alpha + \Theta + \alpha_*}{2\alpha_*}\right) \underset{0}{\overset{1}{\mathrm{sat}}}\left(n\frac{\delta_n}{\delta_*}\right),$$

where $\delta_n({}_0^t u, {}_0^t \varphi)$ is the dimensionless depth of cut per blade, which introduces a delay in the equations of motion as the height of rock ahead of a blade depends on the motion history of the bit, see Figure 2. Also, $\beta$ is the bit geometry number, $\lambda_n$ reflects the wear state of the bit, and $\alpha$ and $\Theta$ characterize the direction of the relative velocity of the bit with respect to the rock and the inclination of the blade wear flat. As $\alpha$ changes along the radius of the bit, the above law is strictly valid for core barrels only. The sat function denotes the saturation operator, while the parameters $\alpha_*$ and $\delta_*$ are rock-dependent parameters that delimit the upper saturation level of the contact force. Whenever the bit sticks and stands still, *i.e.*, $u' + v_0 = \varphi' + \omega_0 = 0$, $v_0$ and $\omega_0$ being the stationary axial and angular velocities of the bit, the boundary condition is given by the equilibrium of the bit, until the torque built up by twisting of the drillstring is large enough to overcome the resistant torque and trigger motion. By further developing the equations, the model reads,

$$\begin{aligned} u'' &= n\psi\left(-[u - \tilde{u} + v_0(\bar{t}_n - \bar{t}_{n,0})] + \mathcal{W}_{n,0}^f - \mathcal{W}_n^f\right), \\ \varphi'' + \varphi &= n\left(-[u - \tilde{u} + v_0(\bar{t}_n - \bar{t}_{n,0})] + \beta(\mathcal{W}_{n,0}^f - \mathcal{W}_n^f)\right), \end{aligned} \tag{2}$$

where $\tilde{u} = u(\bar{t} - \bar{t}_n)$ is the delayed axial perturbation and $\bar{t}_n$ is the state-dependent delay, defined by the threshold condition

$$\int_{\bar{t}-\bar{t}_n}^{\bar{t}} (\varphi'(s) + \omega_0)ds = \frac{2\pi}{n}. \tag{3}$$

## 3 Slow dynamics

Previous works [1, 2] have shown that for the stick-slip or anti-resonance regimes to occur, the steady-state motion of the bit should be unstable. To assess the local stability of the stationary solution of the model, the poles of the linearized

system around that solution are to be located in the complex plane. If any of them has a strictly positive real part, the steady-state is unstable. In case all the poles are located in the left half of the complex plane, the trivial solution is stable. The poles are the roots of the characteristic equation, computed from the linearized system,

$$
\begin{aligned}
&P(s) := s\left[s^4 + n\bar{t}_{n,0}\left(\kappa\psi - \beta\upsilon\right)s^3 + \right. \\
&\left\{1 + n(1 - e^{-s\bar{t}_{n,0}})\left(\psi(1+\chi) - \frac{v_0}{\omega_0}(1+\beta\chi)\right)\right\}s^2 + n\psi(1+\chi)(1 - e^{-s\bar{t}_{n,0}}) \\
&\left. + n\bar{t}_{n,0}\psi\left\{\kappa + n(1 - e^{-s\bar{t}_{n,0}})(1-\beta)\left(\upsilon - \frac{v_0}{\omega_0}\kappa\right)\right\}s\right] = 0, \qquad (4)
\end{aligned}
$$

with the parameters $\kappa$, $\upsilon$ and $\chi$ depending on the steady-state drilling conditions and the bluntness of the bit.

Numerical investigations of the solutions of (4) have shown that for particular parametric configurations, the linearized system has two unstable poles close to $\pm i$, the poles of the torsional pendulum. Although they have a positive real part and thus the stationary solution is unstable, the divergence of the system following any perturbation is very slow due to the smallness of their real part. Accordingly, depending on the external perturbations the system is subject to, the response of the system appears to converge to different periodic solutions and there is apparent coexistence of drilling regimes. Figure 3 exemplifies this feature. The unperturbed system stays at the stationary solution while a small perturbation generates a slow transient regime of quasi-periodic oscillations that will eventually converge to the attractive stick-slip limit cycle. However, this limit cycle is immediately reached after a large perturbation.

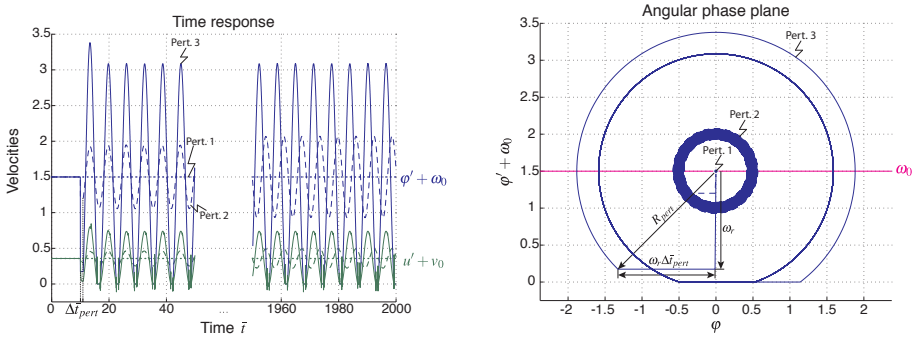


Figure 3: Response of the system to an angular perturbation.

# 4 Conclusion

A physically consistent model, that recovers stick-slip oscillations of deep drilling systems and captures the coexistence of multiple drilling regimes observed in the fields and in lab experiments, has been developed. By performing a linear stability analysis of the delayed differential model, we provide a justification to the coexistence of drilling regimes as we brought to light the slow dynamical nature of such self-excited vibrations.

# References


[1] Richard T., Germay C. and Detournay E.: A simplified model to explore the root cause of stick-slip vibrations in drilling systems with drag bits. *Journal of Sound and Vibration* **307**:432–456, 2007.

[2] Germay C., van de Wouw N., Nijmeijer H. and Sepulchre R.: Nonlinear drillstring dynamics analysis. *SIAM Journal on Applied Dynamical System*. In press. 2009.

[3] Besselink B.: Analysis and validation of self-excited drill string oscillations. MSc Thesis, Technical University Eindhoven. 2008.

# Using Passive Nonlinear Targeted Energy Transfer to Stabilize Drillstring Systems

Régis Viguié, Gaetan Kerschen

Structural Dynamics Research Group, University of Liège, Belgium

## 1 Introduction

Vibration mitigation of the drill-string instabilities could be performed using active of passive methods. In the present study the latter case in investigated. When considering passive techniques, the famous tuned mass damper (TMD) introduced by Frahm [3] and Den Hartog [2] is the most popular device still broadly used nowadays. However besides its amplitude robustness this damper presents a bad frequency robustness as it is designed to perform at a given vibration frequency. To overcome this limitation an essentially nonlinear attachment (i.e., characterized by the absence of a linear term in the force-displacement relation), termed a nonlinear energy sink (NES), has been introduced. As shown in [5, 4, 9] an NES is characterized by two remarkable properties : (i) targeted energy transfer (TET) from a primary structure to an attached NES is achieved and (ii) it has no preferential resonant frequency which makes it capable of resonating with any mode of the primary structure. In the present study, the primary system is nonlinear and therefore characterized by multiple coexisting solution but also by a varying frequency of the LCO with a varying level of the driving voltage $u_c$. This latter feature makes the TMD inadequate to mitigate LCOs whereas the use of an NES seems very well suited.

In this paper, the first section deals with the use of a parametrically designed NES to mitigate limit cycle oscillation of the drill-string system (figure 1). Based on the resulting promising results the following section aims to alleviate the computational cost related to the parametric study by taking advantage of the relevant information associated with the singularities of the bifurcation diagram. Finally the last section presents the conclusions and future works.

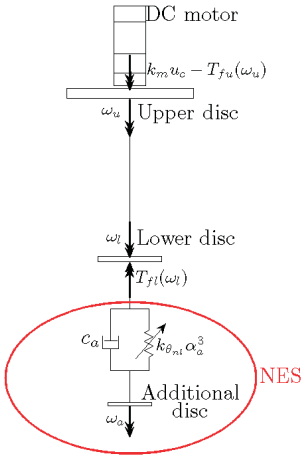


Figure 1: Schematic representation of the drill-string system with an NES.

## 2 Suppression of Friction-Induced Limit Cycling Oscillation by means of a Nonlinear Energy Sink : A Parametric Study

In [11] the assessment of a numerical value for the new parameters introduced has been parametrically performed and the following set of parameter : $J_{add} = 0.025895$ $[kg\ m^2\ /\ rad]$ - $c_a = 0.021$ $[N\ m\ s\ /rad]$ - $k_{nl} = 0.002515$ $[N\ m\ /\ rad^3]$ appears to significantly improve the dynamical behavior of the drill-string system as depicted in figure 2(a). As a proof of the NES performance the new dynamics can be compared with the one related to the drill-string system submitted to active control techniques. A complete analysis of the latter configuration is performed in [1] and figure 2(b) depicts the associated experimentally computed bifurcation diagram. It is well known that active techniques will always exhibit better performances than passive ones. However in the present case, the comparison of both dynamics highlights the very good performance of the NES as active control produces about the same results.

In this context one could wonder whether there is any possibility to find better suited NES parameter values so that its performance could be further increased and overtake the active control ones. This question is the key feature treated in the next section. Finally, for any further details and analyses on the coupling of the drill-string system with an NES, the interested reader may refer to [11].

(a)

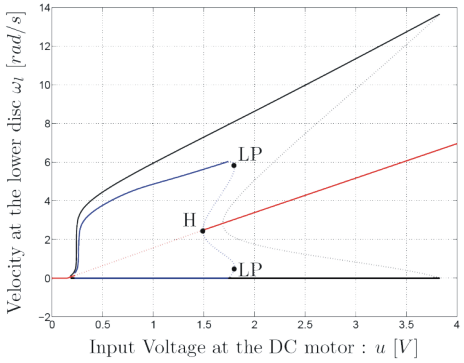


(b)

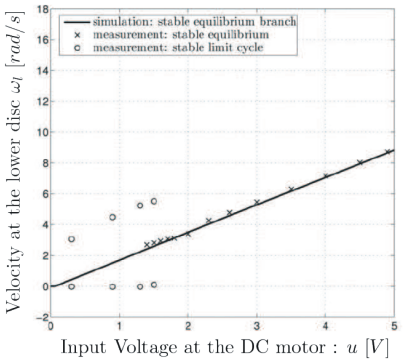


Figure 2: (a) Bifurcation diagram : black lines stand for the uncontrolled drill-string system ; blue and red colors correspond to periodic and equilibrium solutions, respectively; solid and dotted line correspond to stable and unstable solutions, respectively. Finally, H and LP stand for Hopf and Limit Point bifurcation point, respectively / (b) Bifurcation diagram of the drill-string system controlled using active techniques [1].

## 3 Design of an NES Using Bifurcation Analysis

Due to the strongly nonlinear dynamics created by the coupling of an NES to a primary structure, its design is a challenging problem and parametric as well as optimization procedures have been extensively considered so far [6, 11, 12, 7]. Even though these methods generally give good results, they are time demanding which limits their use in some cases. The objective of this section lies in presenting an alternative and complementary procedure based on bifurcation analysis.

Because of their nonlinear character, the system depicted in figure 1 has been characterized through the computation of a bifurcation diagram. This plot has highlighted the presence of bifurcation points that correspond to a singularity in the dynamics expressing a qualitative change of the solution. In the present study the focus is set on the region where LCO exhibit the higher amplitude levels and where Hopf and Limit Point bifurcations occur. The first mentioned corresponds to a loss of stability of an equilibrium point that is transformed into a LCO whereas the second one consists in the creation of an equilibrium through the loss of stability of a LCO. In this context, the localization of these singularities is of high interest as they can divide the bifurcation diagram into several parts related to particular features such as : (i) existence of globally stable equilibrium solution, (ii) coexistence of locally stable equilibrium and LCOs solutions or

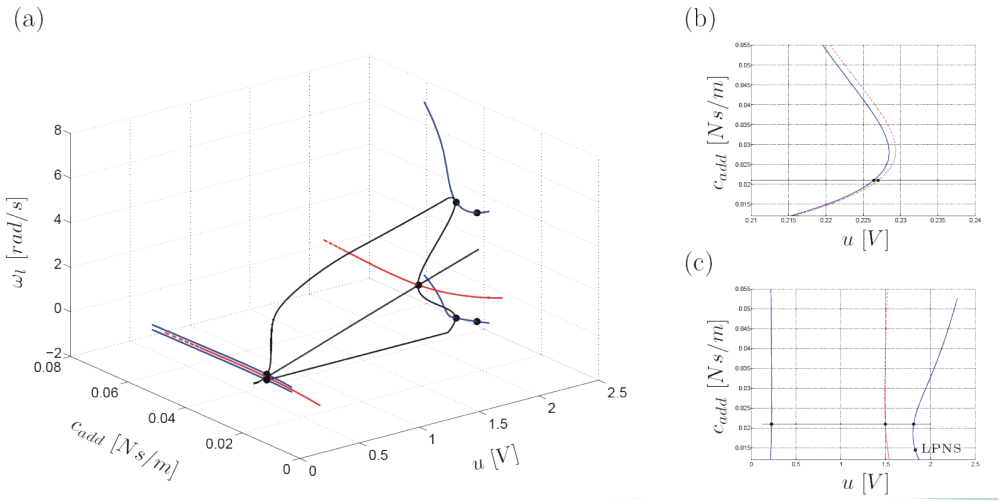


Figure 3: (a) Bifurcation diagram(a) 3D representation of the bifurcation points continuation / (b) Projection in the plane ($c_{add}$,$u$) / (c) Close-up on the low voltage range. The blue solid line, the red dashed line and the black line correspond to the LP continuation, the Hopf continuation and the bifurcation diagram computed depicted in figure 2, respectively.

(iii) existence of stable LCOs. Therefore the bifurcation analysis suggests those bifurcation points to be continued along a third dimension to define boundaries and consequently regions with solutions presenting the same qualitative features. This type of continuation is said to be of codimension 2 as two continuation parameters are considered. Similarly to section 1 and 2 one of them is the driving voltage at the DC motor $u_c$ whereas the second one could be any parameter of the NES.

In this study, the continuation software used is the command line version of MATCONT. Moreover the focus is set on two different objectives :

1. an increase of the input voltage range leading to the global equilibrium solutions.

2. a decrease of the input voltage range leading to unstable equilibrium solution.

These features are related to the localization of the limit point and the Hopf bifurcation, respectively.

The results associated to the analysis on the damping ($c_{add}$) are depicted in figure 3(a-c). Referring to the objectives mentioned above, the first case tends to

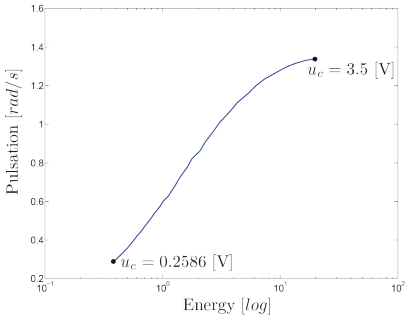


Figure 4: Frequency - Energy dependence of the LCOs for the drill-string system.

be fulfilled when the LP curves get closer from each other whereas for the second case the same property has to be verified for the Hopf curves. The location of the black trace (bifurcation diagram figure 2) is very close from the configurations leading to both the largest range of global equilibrium ($c_{add} = 0.018\ Ns/m$) and the smallest range of unstable equilibrium ($c_{add} = 0.03\ Ns/m$). Moreover, at high damping level, the system progressively tends toward a 2DOF system as the coupling becomes increasingly stiffer and the effects of the essential nonlinearity vanish. At very small energy level, the nonlinear effect is preponderant and a nasty dynamics appears. This latter feature is similar to an increase of the nonlinear stiffness $k_{nl}$ at constant damping which is considered hereafter.

Before going further on this analysis one could wonder whether the nonlinearity law (cubic with positive nonlinear coefficient $k_{nl}$) considered in section 2 ([8]) is well suited to the primary system. In [10] it has been shown the necessity for the nonlinear absorber to get the same frequency-energy dependence as the primary structure. Without going into too many details that are beyond the scope of this paper, it is worth being checked whether, similarly to the NES, the primary system possesses a hardening behavior. Focusing on the LCO, the total energy stored in the system is composed of the potential and kinetic energy. Because the excitation is not appropriated, the evolution of this total energy is cyclic and a mean value is considered as a first approximation. Extracting the frequency of the LCOs and their related energy, a frequency-energy dependence behavior is assessed and depicted in figure 4. Because the frequency of the LCOs increases with the energy injected in the system it can be concluded that the general dynamical behavior is of hardening type. Ideally and according to [10], the nonlinear law of the NES should be such that its frequency-energy dependence would be identical to the one of the primary structure. This will be investigated in subsequent studies.

The bifurcation point continuation is performed with respect to the input

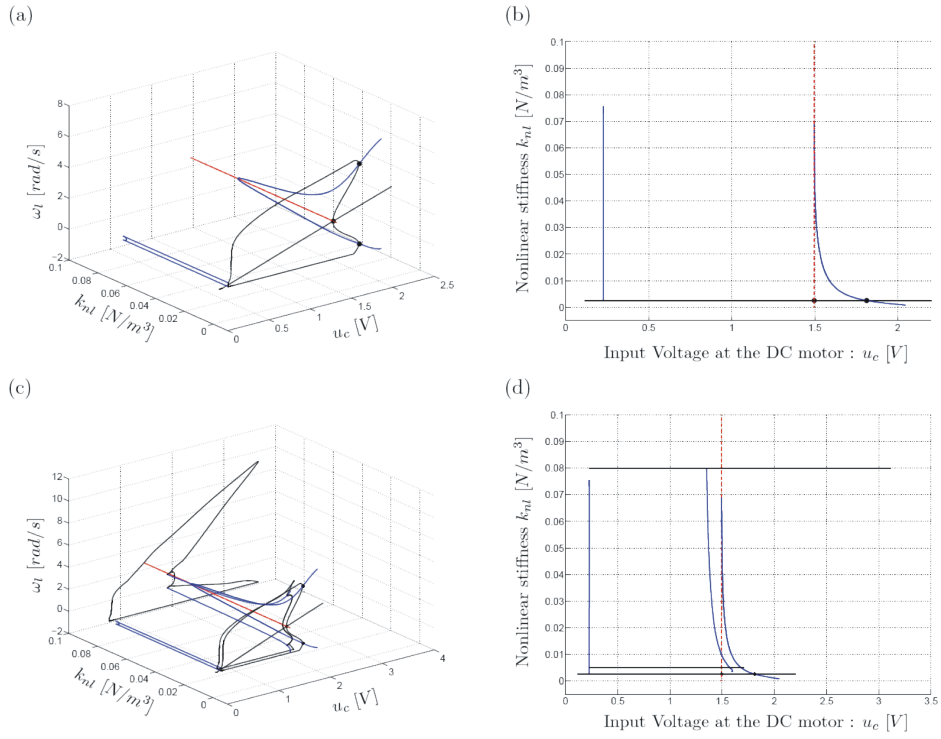


Figure 5: (a-c) 3D representation of the bifurcation points continuation / (b-d) Projection in the plane ($k_{nl}$,$u_c$) / The blue solid line, the red dashed line and the black line correspond to the LP continuation, the Hopf continuation and the bifurcation diagram computed depicted in figure 2, respectively.

voltage $u_c$ and the nonlinear stiffness coefficient $k_{nl}$. Figure 5 (a-b) shows some interesting features :

1. the Hopf bifurcation point does not seem to be influenced by the nonlinear stiffness coefficient $k_{nl}$. Consequently the range of equilibrium solution cannot be increased further more.

2. the limit point continuation exhibit strong changes and beyond $k_{nl} = 0.075$ $[N/m^3]$ additional analyses should be performed to check whether the dynamical behavior is preferable.

Figures 5 (c-d) illustrate the bifurcation diagram for $k_{nl} = 0.08$ $[N/m^3]$. The new dynamics is clearly strongly affected by the nonlinear attachment but is not at all preferable as higher amplitude level of the LCO occur and globally stable equilibrium are changed into locally stable solutions. However the continuation of other limit point bifurcation is of interest to verify the span of this effect at lower nonlinear stiffness coefficient. This continuation affects the dynamics for a nonlinear stiffness coefficient $> 0.0039$ $[N/m^3]$. Therefore the best value of $k_{nl}$ is just below this limit. This confirms the very good quality of the initial set of parameter parametrically determined in section 2.

# 4 Conclusion and Future Work

In this paper, a new design procedure of the NES, based on the analysis of bifurcation points, has been investigated. This latter is devoted to any kind of structure composed of a primary system (SDOF and MDOF linear or nonlinear) coupled to a NES. In the current study the focus has been set on a particular primary structure, namely the drill-string system.

This method relies on the use of reliable continuation softwares such as MATCONT which is used herein.

Considering given objective functions, this method highlights great benefits from a computational cost viewpoint. It directly takes advantage of the relevant information available in the bifurcation diagrams, namely, the bifurcation points. Moreover, unlike asymptotical methods, it is characterized by the independence with respect to any simplifications or restrictive assumptions on the system structure or boundary conditions.

Complementary developments have to be undertaken in subsequent studies such as : (i) the assessment of a nonlinear functional form of the absorber that better fits the frequency-energy dependence of the drill-string structure, (ii) the development and use of the codimension 2 bifurcations (LPNS, R1, ...) into the design procedure.

# References


[1] J.C.A. de Bruin, A. Doris, N. van de Wouw, W.P.M.H. W.P.M.H. Heemels, and H. Nijmeijer. Control of mechanical motion systems with non-collocation of actuation and friction: A popov criterion approach for input-to-state stability and set-valued nonlinearities. Automatica, 45:405415, 2009.

[2] J. P. Den Hartog. Mechanical Vibrations. Dover Books on Engineering, 4th edition, 1985.

[3] H. Frahm. A Device for Damping Vibrations of Bodies. US Patent 989958, 1911.

[4] G. Kerschen, Y. S. Lee, A. F. Vakakis, D. M. McFarland, and L. A. Bergman. Irreversible passive energy transfer in coupled oscillators with essential nonlinearity. SIAM Journal of Applied Mathematics, 66(2):648679, 2006.

[5] Y. S. Lee, G. Kerschen, A. F. Vakakis, P. N. Panagopoulos, L. A. Bergman, and D. M. McFarland. Complicated dynamics of a linear oscillator with a light, essentially nonlinear attachment. Physica D, 204:4169, 2005.

[6] Y. S. Lee, A. F. Vakakis, L. A. Bergman, D. M. McFarland, and G. Kerschen. Suppression of aeroelastic instability by means of broadband passive targeted energy transfers, part i : Theory. AIAA Journal, 45(3):693711, 2007.

[7] L. I. Manevitch, E. Gourdon, and C. H. Lamarque. Parameters optimization for energy pumping in strongly nonhomogeneous 2 dof system. Chaos, Solitons and Fractals, 31(4):900911, 2007.

[8] A. I. Musienko, C. H. Lamarque, and L. I. Manevitch. Design of mechanical energy pumping devices. Journal of Vibration and Control, 12:355371, |2006|. article.

[9] A.F. Vakakis, O.V. Gendelman, L.A. Bergman, D.M. McFarland, G. Kerschen, and Y.S. Lee. Nonlinear Targeted Energy Transfer in Mechanical and Structural Systems. Springer, Dordrecht, 2009.

[10] R. Viguié and G. Kerschen. Nonlinear vibration absorber coupled to a nonlinear primary system : a tuning methodology. Journal of sound and Vibration (Submitted), 2009.

[11] R. Viguié, G. Kerschen, J.-C. Golinval, D. M. McFarland, L. A. Bergman, and N. van de Wouw. Using passive nonlinear targeted energy transfer to stabilize drill-string system. Mechanical Systems and Signal Processing, 23:148169, 2009.

[12] R. Viguié, M. Peeters, G. Kerschen, and J.-C. Golinval. Energy transfer and dissipation in a duffing oscillator coupled to a nonlinear attachment. Journal of Computational and Nonlinear Dynamics (Accepted for publication), 2008.

# Influence of Friction Characteristics on Stick-slip Vibration of Drillstrings

Marcos Silveira, Marian Wiercigroch

Centre for Applied Dynamics Research, School of Engineering, University of Aberdeen, Aberdeen, AB24 3UE, UK.

## 1 Introduction

Traditionally, drilling a borehole for oil and gas extraction is done by means of rotary motion of a drill-bit against the rock. The rotary motion is transmitted to the bit from a motor, usually at the surface of the well, by a drill-string. This drill-string is made of tube sections with threaded connections. It can reach lengths of various kilometers, making it a very slender structure. Torsional vibration is one of the most important vibration modes in drill-string, and the main phenomenon related to it is stick-slip vibrations. The friction laws representing the friction at the drill-bit can be defined in various ways. A comparison of three such friction laws will be presented in this study in order to establish the influence of these models in the response of the system.

## 2 Modelling stick-slip vibrations

*Friction models for bit-rock interaction*

The torque-on-bit ($T_b$) is a friction law, a function that defines the resistive torque on the bit and models the interactions between the drill-bit and the rock, often a function of the relative drill-bit velocity, $\dot{\phi}_1$. It can be defined in various ways, following the form:

$$T_{b_1} = \begin{cases} T_{st} & \text{if } \dot{\phi}_1 = 0, \\ T_{sl} & \text{if } \dot{\phi}_1 \neq 0. \end{cases} \tag{1}$$

The simplest model for $T_{sl}$ is a piece-wise Coulomb-like friction law (Friction Model 1), with a value for static friction and another, lower, value for sliding (or dynamic) friction, which in this case is independant of the velocity. More realistic friction laws account for dependancy on the velocity and weight-on-bit

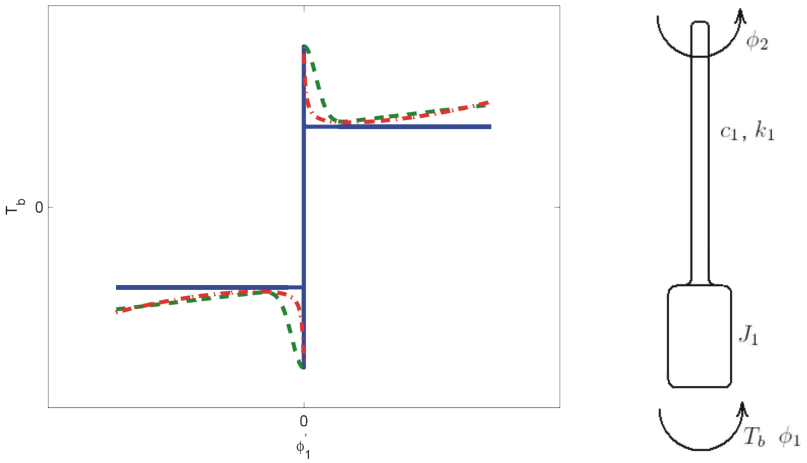


(a) (b)

Figure 1: (a) Friction models showing dependency of friction torque on rotary velocity (Tb1 -blue, Tb2 - -green, Tb3 -.red); (b) Physical model of 1DOF system.

(WOB), and are usually discontinuous at null velocity. A comprehensive survey of various friction models is given by Wojewoda et al. [1].

A more complex friction model (Friction Model 2) accounts for dependency of the static and dynamic coefficients, $\mu_0$ and $\mu_1$, on the contact velocity, and is given by [2]:

$$T_{b_2} = \operatorname{sgn}\left(\dot{\phi}_1\right) W_b \left( \frac{\mu_0 - \mu_1}{1 + \lambda_1 \left|\dot{\phi}_1\right|} + \mu_1 + \lambda_2 \dot{\phi}_1^2 \right), \tag{2}$$

where $\lambda_1$ and $\lambda_2$ are dry friction constants and $W_b$ is the weight-on-bit. A third friction model (Friction Model 3) incorporates an exponential dependency on the contact velocity, allowing better accuracy near null velocity, and is given by [3]:

$$T_{b_3} = T_{sl} + (T_{st} - T_{sl})\, e^{-\left|\dot{\phi}_1/\omega_{sl}\right|^{\delta_{sl}}} + b_l \left|\dot{\phi}_1\right|, \tag{3}$$

where $T_{st}$ and $T_{sl}$ are the static and dynamic friction torques and $\omega_{sl}$, $\delta_{sl}$ and $b_l$ are dry friction constants.

*1-DOF torsional pendulum model - Model 1*

As a first approximation, the drill-string can be modelled as a 1-DOF torsional pendulum [4–6]. The interest is in the relative displacement between the top and the bottom, as the torque stored in the drill-string depends on this quantity.

With this in mind, the relative angular displacement between the rotary table and the bit is defined as:

$$\phi = \phi_2 - \phi_1 \tag{4}$$

then the equation of motion can be written as:

$$J_1\ddot{\phi} + c_1\dot{\phi} + k_1\phi - T_b = 0, \tag{5}$$

where $J_1$ is the equivalent mass moment of inertia of the drill-string, $c_1$ is the equivalent damping coefficient along the drill-string, $k_1$ is the equivalent torsional stiffness of the drill-pipes,$\phi_1$ is the angular position of the bit at the bottom of the drill-string,$\phi_2$ is the angular position of the rotary table at the top of the drill-string and $T_b$ is the torque-on-bit.

*1-DOF torsional pendulum with parametric excitation of the angular velocity – Model 2*

As observed in field data [4–6], the velocity of the rotary table oscillates around the nominal velocity when the bit is experiencing stick-slip oscillations. The oscillations of the rotary table have smaller amplitude and higher frequency than the stick-slip oscillations. This oscillation is introduced in the model by applying a parametric excitation in the velocity of the rotary table, in the form of:

$$\phi_2 = \Omega_2 t + A\cos(\omega t), \tag{6}$$

where $A$ is the amplitude of oscillations and $\omega$ is the frequency of oscillations. It is possible then to tune the values of $A$ and $\omega$ to emulate the behaviour of the velocity of the rotary table. It is clear that nulling these two parameters makes this model similar to Model 1.

*Simulating discontinuous systems*

The models considered are highly non-linear, exhibiting relaxation vibrations, and also because of the friction models used. Therefore, the investigations were performed with numerical simulations of the differential equations, using a $4^{th}$ order Runge-Kutta solver in conjunction with the bisection method to improve accuracy. Extensive studies have been undertaken in simulation of discontinuous systems undergoing stick-slip vibrations [2, 7–10]. These simulations have to tackle the problem by separating the discontinuous phase space into a series of adjacent continous regions. In the present case, two regions are necessary, one for the stick mode and one for the slip mode, with the stick region being a straight line. A switch function is used to perform the transitions from stick to slip modes.

*Sliding surface*

The limits of the sliding surface, which determine the conditions for stick mode, are given in this system by the torque in the drill-string, which is the result of the twist. Expressing the torque in terms of $\phi$ results in the upper and

lower limits of this state variable that represent the sliding surface [11, 12]. It is possible to demonstrate that the sliding surface does not depend on the state of the system while this is at stick mode. The upper and lower limits are calculated by:

$$\phi_{upper} = \frac{-c_1\dot{\phi}_1 + T_{f_{\max}}}{k_1} \quad , \quad \phi_{lower} = \frac{-c_1\dot{\phi}_1 - T_{f_{\max}}}{k_1}. \tag{7}$$

While at stick mode, $\phi_1 = 0$. Moreover, $T_{f_{\max}}$ and $k_1$ do not depend on the state of the system, and $\phi_2$ depends only on $A$ and $\omega$. It follows that $\phi_{lower}$ and $\phi_{upper}$ will not change for varying $\Omega_2$, while the dependency on $A$ and $\omega$ clearly comes through the excitation present in $\phi_2$ in Model 2.

## 3 Comparison between the friction models

The comparison between friction models is carried out by selecting five representative points along the stick-slip limit-cycle, these being the first five points chosen on the stick-slip limit-cycle. Model 2 was used for this comparison, varying the parameters $A$, $\omega$ and $\Omega_2$.

Results of the comparison between the three friction models show small difference between a more simple friction model and a more complex one, confirming that the main aspect of the system in order to exhibit stick-slip vibrations is the difference between the static and dynamic friction characteristics. Figure 2 shows that the phase-planes of stick-slip vibrations for all three models are very similar. The small oscillations on the velocity of the top (Model 2) introduces quasi-periodicity to the system. The point on the limit-cycle most affected by this is the transition between the slip mode into stick mode. The charateristic shape of the Friciton Model 3 near zero velocities causes the trajectories in the phase-plane to vary slightly at each cicle. Bifurcation diagrams confirm that there is a region in parameter space that allows the system to operate without stick-slip vibrations.

## 4 Experimental set-up

A small scale experimental set-up has been designed to gain additonal insight and validate some of the models and the data from the numerical simulations. Axial and lateral forces are present, as there is an axial force applied on the bit and frictional forces along the drill-string due to the torsional buckling of the shaft, resulting in contact with the borehole wall. There are no fluid forces along the drill string. The borehole is a long glass tube. Rotating inside the borehole is the drill-string, which is a long and flexible shaft with low torsional stiffness.

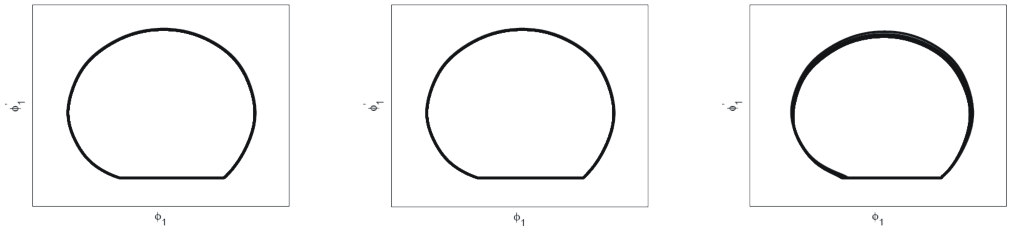

Figure 2: Phase-plane of stick-slip vibrations (a) Friction Model 1, (b) Friction Model 2, (c) Friction Model 3.

The load applied to the bit (WOB) is taken by means of a load cell and a linear amplifier. A sample of rock is fixed in one end of the load cell. This load cell is pushed against the bit by means of a screw and a spring, generating frictional torque.

The inputs introduced to the experimental set-up are the nominal voltage supplied to the motor and the WOB given by adjusting the spring on the load cell. The outputs of interest are the velocity of the motor, the velocity of the bit and the axial force on the load cell. The aim is to measure how the two velocities oscillates as the drill-string experiences stick-slip oscillations during drilling. Fluctuations of the axial load will also be measured and will be related to the behaviour of the drill-bit. The transparent borehole enables the clear visualisation of the torsional buckling experienced by the drill-string when operating under high torsional loads.

## 5 Conclusions

The comparison between the three friction models used shows small difference between more simple and more complex models, which confirms that the main aspect responsible for a system to exhibit stickslip vibrations is the difference between the static and dynamic friction characteristics. The point on the limit-cycle most affected by oscillations of the velocity of the rotary table is the transition between the slip mode into stick mode. The bifurcation analysis allowed to determine the velocity 2 above which the system operates without stick-slip vibrations. More importantly, this velocity does not change substantially with different friction models. Also, the sliding surface does not change for different friction models, as the maximum value for friction does not depend on the contact velocity. A combination of angular velocities and damping on the system can also avoid stick-slip vibrations. For further analysis, a small scale experimental

setup is being constructed, which will enable the investigations of correlating the numerical simulations to experimental data.

## References


[1] Wojewoda J, Stefanski A, Wiercigroch M, Kapitaniak T. Hysteretiv effects of dry friction: modelling and experimental studies. Phil Trans R Soc A. 2008;366:747–765.

[2] Wiercigroch M. A note on the switch function for the stick-slip phenomenon. Journal of Sound and Vibration. 1994;175(5):700–704.

[3] Wouw N, Nijmeijer H, Mihajlovic N. Friction-induced limit cycling in flexible rotor systems: an experimental drill-string system. In: Proceedings of IDETC/CIE; 2005. p. 200–300.

[4] Jansen JD, Steen L. Active damping of self-excited torsional vibrations in oil well drillstrings. Journal of Sound and Vibration. 1995;179(4):257–279.

[5] Steen L. Suppressing stick-slip induced drill-string oscillations: a hyperstability approach [PhD Thesis]. University of Twente; 1997.

[6] Payne M. Drilling bottom-hole assembly dynamics [PhD Thesis]. Rice University; 1992.

[7] Galvanetto U. Bifurcations and chaos in a four-dimensional mechanical system with dry friction. Journal of Sound and Vibration. 1997;204(4):690–695.

[8] Galvanetto U. Some discontinuous bifurcations in a two-block stick-slip system. Journal of Sound and Vibration. 2001;248(4):653–669.

[9] Galvanetto U. Non-linear dynamics of multiple friction oscillators. Computer Methods in Applied Mechanics and Engineering. 1998;178:291–306.

[10] Galvanetto U, Bishop SR. Computational techniques for nonlinear dynamics in multiple friction oscillators. Computer Methods in Applied Mechanics and Engineering. 1998;163:373–382.

[11] di Bernardo M, Kowalczyk P, Nordmark A. Bifurcations of dynamical systems with sliding: derivation of normal-form mappings. Physica D. 2002;170:175–205.

[12] Kowalczyk P, di Bernardo M. Two-parameter degenerate sliding bifurcations in Filippov systems. Physica D. 2005;204:204–229.

# Modeling Transient Vibrations while Drilling using a Finite Rigid Body Approach

Jahir Pabon[1], Nathaniel Wicks[1], Yong Chang[2], Richard Harmer[3]

[1] Schlumberger Doll Research Center, Cambridge, MA, USA
[2] Schlumberger Sugar Land Product Center, Sugar Land, TX, USA
[3] Schlumberger Technologies, Beijing, China

## 1 Introduction

Downhole vibrations while drilling are a complex phenomenon, sensitive to a wide range of factors, many of which change as the drilling process takes place or are hard to quantify within a typical drilling environment. Examples of these factors are rock properties (strength, elasticity, and attenuation), wellbore friction factor, hole washout, tool imbalance, component wear or damage, mud damping, etc. Field experience has shown that it is not sufficient to simply identify resonant conditions using modal analysis [1] (although, this approach can provide value, [2] especially if used in a relative sense). The reasons above have driven the implementation of real-time downhole drilling mechanics measurements [3] over the past 20 years. As drilling costs and the cost associated with equipment failures increase, there is increasing pressure to provide more reliable solutions, and a high-tier drilling mechanics analysis service has evolved involving the application of advanced dynamics models ([4], [5], [6]).

Given that there are a number of important unknown factors that impact drillstring vibrations, it should not be expected that an advanced dynamics model will ever be able to fully capture reality. However, an advanced model may capture enough of the physics to provide valuable insight into specific questions such as:

- What is the impact of an increased friction factor around the BHA contact points?
- How sensitive is a specific BHA to imbalance at different wellbore inclinations?
- How does a reamer react to washout around the body area?

- What is the risk of running a flexible collar section below a mud motor to improve steering performance?

## 2 Approach

A transient BHA vibrations modeling tool is under development that typically simulates 10 to 60 seconds of drilling with the following aims:

- Enhancing our understanding of the dynamic behavior of the drillstring/BHA while drilling.
- Helping us make better comparisons between different BHA designs and evaluate drilling parameters from a best drilling practice perspective.
- Aiding the design of BHAs and tools more resistant to shock and vibration.

We have chosen a finite rigid body (FRB) approach as a careful compromise among modeling simplicity, computational cost, and physical relevance of the computed results. The drillstring is split into segments typically 1 to 5 diameters long. The segments are assumingly connected through axial, shear, bending, and torsional springs with spring constants appropriately determined based on material and geometric properties of the tool. The segments need not be azimuthally symmetric (mass imbalance and bending anisotropy can be accounted for). Additionally, appropriately encapsulated physical models are used to simulate the interaction of the BHA with its environment, as described below.

The borehole wall is modeled as a viscoelastic boundary with friction. Different models have been tried to account for the elastic part of the restoring force. We have opted for a modified form of the Hertzian contact formulation, which takes into account the compliance due to the hollow geometry of the tool cross section. The effects of the drilling fluid are accounted for, including buoyancy, effective added inertia, and lateral, torsional, and lateral drag (although, the drag computation uses simplified linear assumptions based on a centered tool configuration).

The drillbit interaction with the rock is modeled using an extension of the formulation proposed by Detournay,7 in which reaction forces and torques are mainly dependent on the depth of cut (thickness of rock layer cut per revolution). The extension is aimed at characterizing all six degrees of freedom of the bit movement. For instance, natural bit imbalance, sideways cutting action, and rock reactions to changes in bit axis direction are included in the formulation.

A model of an electric motor is used at the other end of the model to represent the topdrive, with the user asked to prescribe a target surface ROP and rpm.

Torques and hook loads are applied at the top of the model, and the drillstring response is monitored. Different feedback control strategies can be tried to continuously adjust the input torque and hook load in order to achieve (or stay close enough) to the desired ROP and rpm.

The modeling tool also includes simplified but physically meaningful models of special drilling modules such as stabilizers, mud motors, adjustable bends, reamers, and rotary steerable tools. In the case of mud motors, in addition to modeling the transmission of torque between collar and rotor, we also take account of axial and lateral effects such as the whirling of the rotor inside the collar as it turns.

## 3 Example of simulated results

A software prototype incorporating the modeling technology described above is under development. Figure 1 illustrates a typical simulation run. In this case, a short 900-ft drillstring is being simulated. The lower right panel shows a color-coded picture of the tool in its actual 3D configuration. The tool diameter has been appropriately scaled for ease of visualization. The color in this case is chosen to represent instantaneous torsional strain (blue indicates low strain while yellow indicates high strain). There is a mud motor near the bit. The upper panel is a clearance gap display showing the centerline of the tool as it lies inside the wellbore (the apparent protrusions in the wellbore correspond to drillpipe joint locations where the annular gap between the tool and the wellbore is narrower). The middle left panel shows the time history of the torque as measured at the bit (green) and at the surface (red). Notice that there is appreciably more "noise" near the bit, which in this case corresponds to torsional waves traveling between the bit and the mud motor. The lower left panels show cross sections at different specified locations, illustrating the lateral movement of the tool.

A validation exercise is also taking place. On one side, we have been able to check against problems with known analytical or semi-analytical solutions such as predicting the onset of sinusoidal buckling of a smooth pipe in a horizontal well and the not-so-gradual transition to helical buckling as compression increases. On the other side, we have obtained qualitative agreement with particular field cases on the vibration reduction effects due to modifications made to drilling tools such as removing asymmetric tool features typically introduced by adjustable bend subs. However, we realize that there are important limitations introduced by the simplifying assumptions used in the modeling, and we are in the process of exploring reasonable uses of this technology.

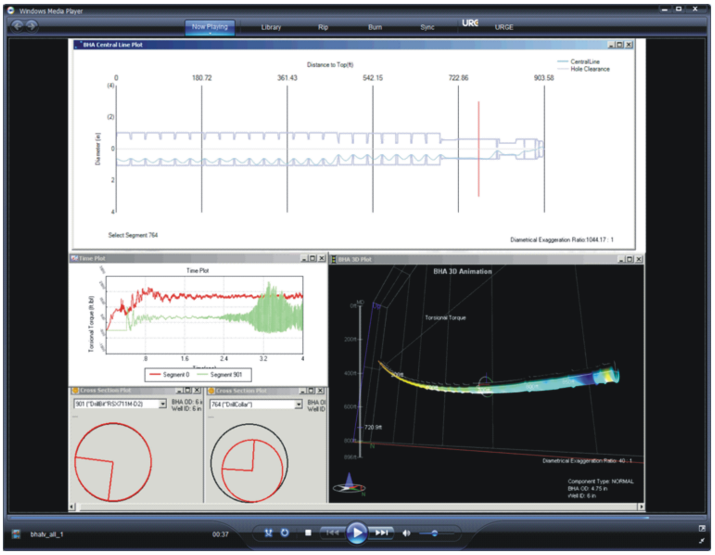


Figure 1: Sample simulation run.

# 4 Conclusions

We have described a modeling effort aimed at studying the transient dynamics of drilling tools. A prototype simulation tool has been developed using an FRB approach in the time domain. A validation effort is under way to explore the limits in the usability of the technology.

# Acknowledgments

This effort would not have been started without the continuous support from Geoff Downton. Additionally, valuable feedback has been provided by Richard Meehan, Simon Griffin, Kevin Gray, and Martin Hayes. Field data has been provided by Ashley Johnson and Frank Espinosa. Also, support with validation efforts have been provided by Ian Robson and Maja Ignova. All of the people mentioned here are members of the Schlumberger organization.

# References

[1] Burgess, T.M., McDaniel, G.L., and Das, P.K.: "Improving BHA Tool Reliability With Drillstring Vibration Models: Field Experience and Lim-

itations," paper SPE/IDAC 16109 presented at the SPE/IADC Drilling Conference, New Orleans, Louisiana, USA (March 15-18, 1987).

[2] Jardine, S., Malone, D., and Sheppard, M.: "Putting a Damper on Drillings Bad Vibrations," Oilfield Review (January 1994), 15-20.

[3] Rewcastle, S.C., and Burgess, T.M.: "Realtime Downhole Shock Measurements Increase Drilling Efficiency and Improve MWD Reliability," paper IADC/SPE 23890 presented at the IADC/SPE Drilling Conference, New Orleans, Louisiana, USA (February 18-21, 1992).

[4] Dykstra, M.W., Neubert, M., Janson J.M., Meiners, M.J.: "Improving Drilling Performance by Applying Advanced Dynamics Models," paper SPE/IADC 67697 presented at the SPE/IADC Drilling Conference, Amsterdam, The Netherlands (February 27 – March 1, 2001).

[5] http://www.smithbits.com/DrillSol/iDrill.aspx.

[6] http://www.worldoil.com/MAGAZINE/MAGAZINE_DETAIL.asp?ART_ID=3342&MONTH_YEAR=Nov-2007.

[7] Richard, T., Germay, C., and Detournay, E.: "A simplified model to explore the root cause of stick-slip vibrations in drilling systems with drag bits," JSV (2007) 305, 432–456.

# The Problem of a Drillstring Inside a Curved Borehole: a Perturbed Eulerian Approach

Vincent Denoël[1], Emmanuel Detournay[2]

[1] National Fund for Scientic Research & University of Liège, Belgium
[2] University of Minnesota, USA & CSIRO Petroleum, Australia

## 1 Introduction

This paper is concerned with the calculation of the deformed configuration of a drillstring during drilling, which critically hinges on accurately identifying the contacts between the drillstring and the borehole walls. For this study, we assume that the position of the bit relative to rig is fixed and that a known axial force is imposed at the rig. A mathematically related problem is the insertion (or the pulling) of the drillstring into (or out of) the borehole, as the nature of the axial boundary conditions at both ends of the drillstring is exchanged.

This subject matter is part of a larger class of problems involving *a priori* unknown contacts between an elastica and a rigid boundary. These problems are computationally challenging, especially in the context of the drilling applications. Indeed, the large deflections of the drillstring from a stress-free configuration require consideration of a geometrically non-linear model. Furthermore, application of standard numerical tools to this problem results in an ill-conditioned system of equations, owing mainly to the narrowness of the borehole compared to its length, but also to the large flexibility of the drillstring and the assumed rigid nature of the borehole walls.

We propose here a novel mathematical formulation of this problem, which takes advantage of the extreme slenderness of the borehole and which is based on expressing the deformed configuration of the drillstring as a perturbation of the borehole axis.

## 2 Problem Definition

We consider a borehole of length $L$ and radius $A$, assumed to be contained in a vertical plane. Its *known* geometry is completely defined by the inclination $\Theta(S)$ of the borehole on the vertical axis $\mathbf{e}_1$, where $S$ $(0 \leq S \leq L)$ is the

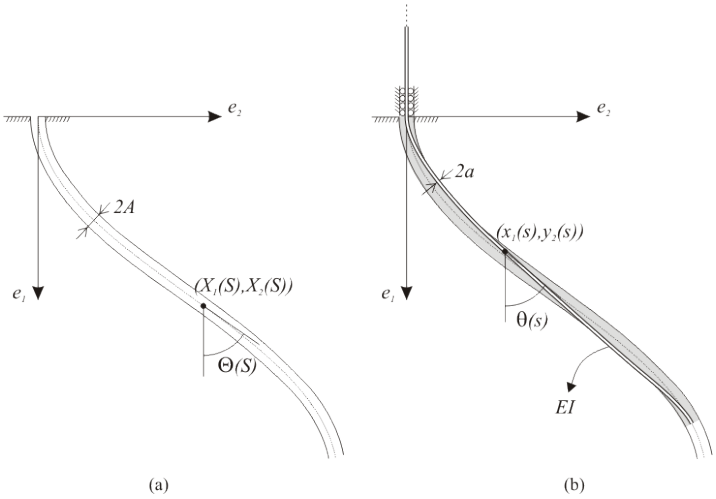


Figure 1: Problem definition.

borehole curvilinear coordinate with origin on the ground surface, see Fig. 1. A drillstring of external radius $a$, bending stiffness $EI$, and weight per unit length $w$ is contained within the wellbore, with the bit at the hole bottom. Assuming that the position of the bit is fixed, we seek to determine the length $\ell$ and the deformed configuration of the drillstring, defined by its inclination $\theta_*(s)$ on $\mathbf{e}_1$, where $s$ $(0 \leq s \leq \ell)$ is the drillstring curvilinear coordinate. For simplicity, we refer to $S$ as the Eulerian coordinate and to $s$ as the Lagrangian coordinate. The constraint on the drillstring to deform inside the borehole leads to the appearance of contacts between the borehole and the drillstring, either discrete or continuous. The contacts, which can be assumed to be frictionless as the drillstring is rotating, impose conditions on the distance $\Delta$ between the borehole and the drillstring axes, on the inclination $\theta_*$ and also on the curvature for continuous contacts, namely $\Delta = A - a$, $\theta_* = \Theta$, and $\theta_*' = \Theta'$.

The deformation of the drillstring (assumed to be inextensible) is governed by the classical geometrically nonlinear beam equations, which outside the contacts read

$$\begin{aligned} F_{1*}\theta_*' + F_{2*}' - w\sin\theta_* &= 0, \\ F_{2*}\theta_*' - F_{1*}' - w\cos\theta_* &= 0, \\ M_*' + F_{2*} &= 0, \\ EI\theta_*' &= M_*, \end{aligned} \tag{1}$$

where $F_{1*}(s)$, $F_{2*}(s)$ and $M_*(s)$ denote the axial force, transverse force and bending moment, respectively. This system of equations can be reduced to a 4th

order nonlinear differential equation

$$EI\left(\theta'_*\theta''''_* - \theta''_*\theta'''_* + \theta'^3_*\theta''_*\right) = w\left(\theta''_*\sin\theta_* - 2\theta'^2_*\cos\theta_*\right). \qquad (2)$$

The formulation of this problem is closed, with the imposition of the boundary conditions at the rig ($s = S = 0$) and at the bit ($s = \ell$, $S = L$), besides the conditions at the *a priori* unknown contacts. At the rig, the boundary conditions take the form $F_{1*} = H$, $\Delta = 0$, and $\theta_* = \Theta$ , while at the bit, $\Delta = 0$, $\theta_* = \Theta$ (for example) in addition to an integral constraint on $\sin\theta_*$ and on $\cos\theta_*$ that express that bit is positioned at the hole bottom. The problem of determining $\theta_*(s)$, $\ell$, and the contacts is thus well posed, in principle [1]. However, semi-analytical or numerical methods that are directly based on solving the non-linear differential equation (2) result in ill-conditionned sets of equations that fail to converge when the dimensionless parameter $EI/wl^3$, where $l$ is the distance between two contacts, becomes too small ( $\simeq 0.2$).

## 3 Perturbed Eulerian Formulation

The approach proposed in this paper overcomes the above issues by expressing the drillstring configuration as a perturbation from the geometry of the borehole using the variable $\Delta$, rather than in terms of $\theta_*$, and by reformulating the problem in terms of the Eulerian coordinate $S$. Furthermore, as already proposed in [1], both the drillstring and the borehole are divided into segments limited by contacts and the global problem is expressed as a connected set of elementary problems. The number of elementary problems is *a priori* unknown, however. The critical aspect of these computations involve the determination of the positions of the contact points, which are used to segment the original problem into elementary ones. Each elementary problem is solved by assuming the positions of the contacts to be given; these positions are then recalculated at the reconnection stage in order to satisfy some continuity conditions at the contacts. The solution of the global problem requires therefore iterations to solve for the positions of the contacts, and each iteration requires the solution of a succession of elementary problems.

Evidently, all the elementary problems can be treated similary, by means of what we refer to as the auxiliary problem, namely the problem of finding the deformed configuration of the drillstring in a segment of the borehole between two contact points. First, we introduce the following dimensionless quantities: $\xi = (S - S_{i-1})/L_i$ where $L_i = S_i - S_{i-1}$ is the length of the borehole segment situated between contacts $i-1$ and $i$, $\alpha = (A-a)/L_i$, $\epsilon^2 = EI/wL_i^3$, and the scaled distance $\delta(\xi) = \Delta\left[S\left(\xi\right)\right]/(A-a)$. With the introduction of $\delta(\xi)$ as the fundamental unknown, we have expressed the drillstring deformed configuration

as a perturbation of the borehole geometry. We also introduce the borehole inclination $\vartheta(\xi) = \Theta[S(\xi)]$, which is readily deduced from $\Theta(S)$.

Formulated in terms of $\delta(\xi)$, the differential equation (2) becomes after dropping terms of order $O(\alpha^2)$ and above

$$\alpha D[\delta(\xi); \vartheta(\xi); \epsilon] + F[\vartheta(\xi); \epsilon] = 0 \tag{3}$$

where $D$ is a 5th order linear differential operator on $\delta(\xi)$ and $F$ is a functional of $\vartheta(\xi)$ given by

$$F = \epsilon^2 \left(\vartheta'\vartheta'''' - \vartheta''\vartheta''' + \vartheta'^3\vartheta''\right) - \vartheta'' \sin\vartheta + 2\vartheta'^2 \cos\vartheta. \tag{4}$$

It can readily be seen by setting $\delta(\xi) = 0$ in (3), that $F$ is actually a measure of the out-of-balance forces that need to be applied on the drillstring so that it is espouses exactly the borehole geometry. Because (3) results from the consideration that $\theta$ is a small perturbation of $\vartheta$, the function $\alpha D(\delta)$ is necessarily of the same order as $F(\vartheta)$, as otherwise the deviation of $\theta$ from $\vartheta$ would be too large and there would be an intermediate contact between the two ends $\xi = 0$ and $\xi = 1$. This is an application of the so-called method of dominant balance [2]. The boundary conditions for the differential equation (3) are that $\delta = \delta' = 0$ at both ends. Furthermore the axial force at one end is known, which provides a supplementary condition on a linear combination of $\delta''$ and $\delta''''$ .

With the perturbed Eulerian formulation, the integro-restrained nonlinear boundary value problem in $\theta_*$ (2) has been transformed into a classical linear boundary value problem in $\delta$ (3). The advantages of the new formulation are therefore obvious but are further clarified next by solving (2) and (3) with a similar shooting method.

## 4 Examples

The shooting method consists in transforming the 2-point boundary value problem into an initial value one by collecting the boundary conditions at the second end and, eventually, the restraining conditions in the form of objective functions $G(\boldsymbol{\Upsilon})$, where $\Upsilon$ represents the assumed initial conditions. Enforcement of the conditions that have been discarded in the formulation of the initial value problem is done by imposing that $G(\boldsymbol{\Upsilon}) = 0$. This method is used to solve the auxiliary problem expressed in Lagrangean coordinates (2) and in Eulerian coordinates with the perturbed formulation (3).

As an example, let us consider the auxiliary problem with $\Theta(S) = S/R$, $S_0 = 0$, $S_1 = L = R\pi/2$, which corresponds to a quadrant of a circular borehole.

Since there are only two contact points, we dispense of the subscript 1, when referring to the borehole or beam segment; i.e., $\ell = \ell_1$ and $L = L_1$.

In the Lagrangean formulation (2), the problem is solved with the following boundary conditions

$$\theta_*(0) = 0 \quad ; \quad \theta_*(L) = \frac{\pi}{2}$$
$$\int_0^\ell \sin\theta_*(s)\, ds = R \quad ; \quad \int_0^\ell \cos\theta_*(s)\, ds = R \tag{5}$$

expressing the compliance of inclination between the drillstring and the borehole at both ends as well as the constraints related to the offset between both beam ends. Conditions (5) are expressed as functions of the unknown beam length $\ell$. A supplementary condition, related to the axial force $F_{1*} = \pi_1 wL$ (with a given number $\pi_1$) at $s = 0$, or equivalently to $\theta_*'''(0)$, is therefore added to obtain a closed set of equations. With this approach, the augmented initial conditions vector $\boldsymbol{\Upsilon}_*$ collects $\theta_*'(0)$ and $\theta_*''(0)$, as well as the unknown beam length $\ell$, while the objective function $G_*(\boldsymbol{\Upsilon}_*)$ gathers the second end condition and both constraints in (5).

In the perturbed Eulerian formulation, these boundary conditions are simply

$$\delta(0) = \delta(L) = \delta'(0) = \delta'(L) = 0. \tag{6}$$

They need also to be complemented, in order to close the system of equations, by a fifth condition on the axial force at $S = 0$, which is equivalently written as a function of $\delta''''(0)$ . In this case, the augmented initial condition vector $\boldsymbol{\Upsilon}$ contains $\delta''(0)$ and $\delta'''(0)$, whereas the objective function expresses both second end conditions in (6).

Figure 2 shows contour levels of functions $G_*(\boldsymbol{\Upsilon}_*)$ and $G(\boldsymbol{\Upsilon})$ for $\pi_1 = 1$, $\varepsilon = 1$ and $\alpha = 0.001$. The solution of the problems with the shooting method is geometrically illustrated as the computation of the intersections of zero level curves of $G_*(\boldsymbol{\Upsilon}_*)$ and $G(\boldsymbol{\Upsilon})$. This is typically performed with a non-linear solver. The complexity of the level curves is a reflection of the convergence rate. Figure 2 illustrates therefore the advantages of the Eulerian approach of the problem, combined with a perturbation formulation.

## 5 Outlook

The Eulerian view of the drillstring flow into the borehole is especially advantageous within the context of a propagating borehole, when this model is used

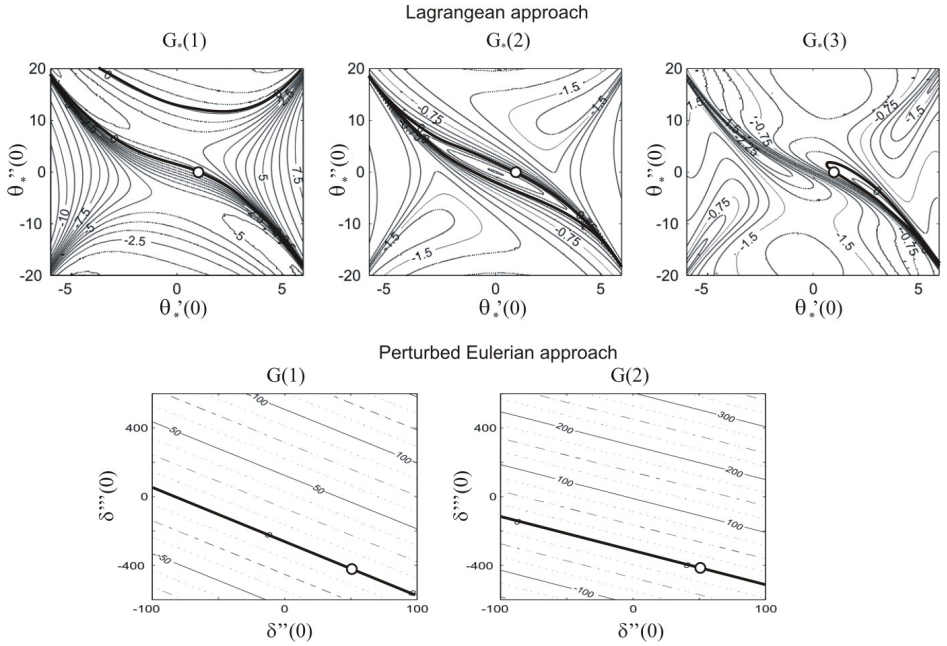


Figure 2: Level curves of $\mathbf{G}_*(\boldsymbol{\Upsilon}_*)$ for $\Upsilon_*(1) = \ell = 1.5697$ (the solution) and level curves of $\mathbf{G}(\boldsymbol{\Upsilon})$ for $\pi_1 = 1$, $\varepsilon = 1$ and $\alpha = 0.001$. Thick lines represent zero level curves. They intersect at the white dots, the solution of the shooting method.

to calculate successive equilibrium configurations of the drillstring. Indeed, the position of any contact becomes stationary in reference to the borehole with increasing distance between this contact and the bit, whilst it continues to slide along the moving drillstring.

The motivation to analyze this particular problem is multifold. First, there is the question of determining the transmission of forces between the rig and the bit (known as the *torque-and-drag* problem in the Petroleum Industry [3]), which is essentially controlled by the contacts between the drillstring and the borehole. Second, modeling the evolution of the borehole during drilling requires determination of the forces acting on the bit, which themselves depend on the deformed configuration of the drillstring. Finally, any analysis of the surface vibrations of the drillstring would benefit from *a priori* knowledge of the positions of the contacts along the string.

## References


[1] V. Denoël, Advantages of a semi-analytical approach for the analysis of an evolving structure with contacts, *Communications in Numerical Methods in Engineering*, vol. 24, pp. 1667-1683, 2008.

[2] C. M. Bender and S. A. Orszag, Advanced Mathematical Methods for Scientists and Engineers: Asymptotic Methods and Perturbation Theory 1999.

[3] S. Menand, H. Sellami, M. Tijani, D.C. Dupuis, C. Simon, Advancements in 3D Drillstring mechanics: From the Bit to the Topdrive (IADC/SPE 98965)

# A Quasi-Polynomial Expression for Borehole Propagation Incorporating both Spatial and Temporal Effects

Geoff Downton

Schlumberger, Drilling and Measurements, Houston, TX, USA

To a first order, it is possible to mathematically model the way a drilling tool propagates the centre line of a borehole by using delay differential equations. The delay terms come about because the forces present on the bit (and thus its direction of drilling) are a consequence of the shape of the bore hole just drilled. In this analysis we allow ourselves the simplifying step that the drilling tool's touch-point's are discrete contact points and finite in number. With some care we can model the borehole propagation of most drilling systems by considering just 4 touch-points in a plane. The expression for borehole propagation can be derived in a linear form and thus easily converted to Laplace Transfer functions allowing their incorporation into larger scale system using standard loop design techniques e.g. Nyquist. The independent variable used is distance-drilled rather than the more conventional time.

This has been reasonably successful in providing a closed form expression to capture the drilling response and stability of drilling tools and compares well to the prediction obtained by the full finite element models of the drilling process.

However, drilling dynamics is the cause of many drilling issues that are cumbersome to include in a quasi-static force approach. Consequently one of the next steps in the progression of this analytical technique is to include some aspect of the drilling tool's dynamics into the expression for borehole propagation.

After covering the above preamble, the paper to be presented will show a very simple case where both a drilling tool's dynamics of motion and borehole propagation (kinematics) are combined into one linear expression.

# Mathematical Model of the Near-Bit Region of an Advancing Drilling System

Emmanuel Detournay

University of Minnesota, USA & CSIRO Petroleum, Australia

## 1 Introduction

Starting in the 1950's with the seminal contribution of Lubinski and Woods [1], substantial efforts have been invested in the formulation of a borehole propagation model that could in principle predict the trajectory of a borehole, given the loads and kinematic constraints acting on the drillstring and the characteristics of the rock formation and of the drilling system, see for example [2, 3, 4, 5, 6, 7, 8, 9]. These efforts are mainly motivated by engineering issues, such as designing a bottom-hole assembly (BHA) including the location of the stabilizers, interpreting downhole data, and controlling rotary steerable systems (RSS) [9]. The development of such a mathematical model is challenging, however, in part because of the nature of the boundary conditions at the bit, but also because of the delayed effect of the borehole geometry on the forces transmitted to the bit through the constraints on the deformed configuration of the BHA imposed by the stabilizers sliding along the borehole.

This paper discusses some aspects of a borehole propagation model, by focusing on the near-bit region of an advancing drilling system. We restrict considerations to a borehole contained in a vertical plane. Let $\boldsymbol{e}_1$ and $\boldsymbol{e}_2$ denote the axes of a fixed system of coordinates, $L$ the current length of the borehole, and $S$ the borehole curvilinear coordinate ($0 \le S \le L$) with $S = 0$ corresponding to the borehole entry (see Fig. 1). At lengthscale $L$, the borehole is a 1D object and thus its geometry can be completely defined by the inclination angle $\Theta(S)$, see Fig. 1. This 1D characterization of the borehole geometry needs to be complemented, however, by a description at the bit length scale. Indeed, the main borehole feature affecting the interaction between the bit and the rock, besides the geometrical properties that are embodied in the function $\Theta(S)$, is the clearance between the bit and the borehole, as it constraints the bit tilt. This additional description of the borehole geometry is done with the overgauge factor $\Xi(S)$ defined as $\Xi = A/a - 1$, with $A(S)$ denoting the mean borehole radius and

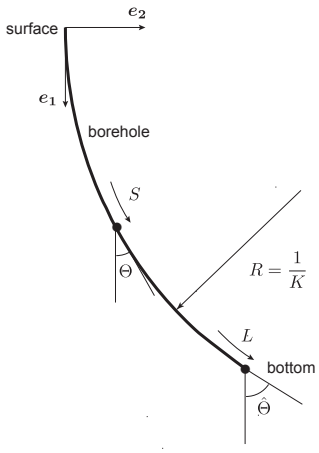


Figure 1: Borehole geometry: coordinate $S$, length $L$, inclination angle $\Theta$, curvature $K$.

$a$ the bit radius. Although $\Xi(S) \geq 0$ by definition, the overgauge factor cannot be smaller than $\Xi_o \ll 1$, for a variety of technological and practical reasons. Formulation of a borehole propagation implies therefore writing the equations governing the evolution of both $\Theta$ and $\Xi$.

## 2 Elements of a Model of Borehole Propagation

Formulating a relationship between the geometrical evolution of the borehole and the mechanical forces acting on the drillstring requires a sequence of steps: first, the link between the incremental propagation of the borehole and the penetration of the bit in the rock; then, the connection between penetration and forces at the bit-rock interface; finally, the relationship between the forces on the bit and the forces acting on the drillstring. Each component of the model is addressed next.

The state variables that characterize the bit penetration are naturally expressed in the director basis $(\hat{\boldsymbol{\imath}}_1, \hat{\boldsymbol{\imath}}_2)$ associated with the bit, see Fig. 2(a). For planar trajectories, three quantities are needed to describe the penetration of the bit per revolution: the axial penetration $d_1$, the lateral penetration $d_2$, and the angular penetration $\varphi$. The inclination $\beta$ of the penetration vector $\boldsymbol{d}$ on the axis of revolution of the bit is given by $\beta = \arctan(d_2/d_1)$. Figure 2 illustrates the three modes of penetration of the bit into rock.

The inclination $\hat{\Theta}$, the curvature $\hat{K}$, and over-gauge factor $\hat{\Xi}$ of the borehole at $S = L$ are in fact related to the penetration variables $d_1$, $d_2$, and $\varphi$, as well as

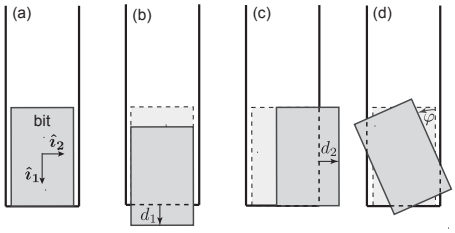


Figure 2: Bit penetration into rock after one revolution: (a) initial configuration with director axes $\boldsymbol{i_1}$ and $\boldsymbol{i_2}$, (b) axial penetration $d_1$, (c) lateral penetration $d_2$, (d) angular penetration $\varphi$.

to the inclination $\hat{\theta}$ and tilt $\psi = \hat{\theta} - \hat{\Theta}$ of the bit, according to

$$\hat{\Theta} = \hat{\theta} + \beta, \quad \hat{K} = \frac{\varphi + \delta\beta}{d}, \quad \hat{\Xi} = \Xi_o + \frac{2}{\pi}\nu|\beta| \tag{1}$$

where $\delta$ denotes the variation of a quantity over a revolution of the bit, and a "hat" the value of a field quantity at the bit. In particular, $\delta\hat{\theta}$ represents the variation of the absolute bit inclination and $\delta L$ the increment of the borehole length after one bit revolution; hence, $\delta\hat{\theta} = \varphi$ and $\delta L = d$. The first equation in (1) expresses that $\psi + \beta = 0$, since the penetration vector $\boldsymbol{d}$ is tangent to the borehole axis. The expression for the borehole curvature at the bit is then deduced from $\hat{K} = \delta\hat{\Theta}/d$. The equation for $\hat{\Xi}$ is obtained from simple geometrical considerations involving a cylindrical bit with slenderness $\nu$.

The penetration variables represent the fundamental state variables for the bit-rock interface laws. The dynamical quantities that are conjugated to the penetration variables are the force on bit $\hat{\boldsymbol{F}}$ and the moment on bit $\hat{\boldsymbol{M}}$, with $\hat{\boldsymbol{M}}$ contained in the plane orthogonal to $\hat{\boldsymbol{\imath}}_1$. For plane trajectories, only the weight on bit $\hat{F}_1$, the transverse force $\hat{F}_2$ and the moment $\hat{M} = \hat{M}_3$ (where the subscript 3 has been dropped for simplicity) are relevant, since the "directional" dissipation per revolution of the bit, $D = -\hat{F}_1 d_1 - \hat{F}_2 d_2 - \hat{M}\varphi$.

The bit-rock interface law is simply the relationship $\mathcal{F} = \mathcal{H}(\mathcal{D})$ between the "force" $\mathcal{F} = \{\hat{F}_1, \hat{F}_2, \hat{F}_3, \hat{M}_2, \hat{M}_3\}^T$ and the "penetration" $\mathcal{D} = \{d_1, d_2, d_3, \varphi_2, \varphi_3\}^T$. It can be argued on the basis of single cutter experiments that the two basic processes that are taking place when the bit is interacting with the rock, contact and penetration, lead to a bi-linear relationship between $\mathcal{F}$ and $\mathcal{D}$ [10].

The last component of the problem is the drillstring. For a plane curve, its geometry is completely defined by the inclination $\theta(s)$. As the drillstring is moving along the borehole, its geometrical configuration is changing. Since the problem

is rate-independent, it is convenient to use $L$ as the evolution variable. Hence, the evolving geometry of the drillstring is described by the function $\theta(s, L)$ during drilling. Through the classical Euler-Bernoulli beam equations, the moment $M$ and the axial force $F_1$ and the transverse force $F_2$ can readily be derived from $\theta(s, L)$ and from the external forces acting on the drillstring.

# 3 Equilibrium Curvature for a BHA with Finite Rigidity

The system of equations, consisting of (i) the kinematical relationship between the penetration variables and the borehole geometry, (ii) the bit-rock interface laws, and (iii) the drillstring mechanics, is closed. To show that the problem is indeed well-posed, we calculate the equilibrium curvature of a borehole for the simple case of a flexible BHA with one stabilizer and one RSS pad that applies a known transverse force $\breve{F}$ on the BHA at distance $\breve{s}$ from the bit. The axial force $\bar{F}_1$ on the stabilizer is assumed known, see Fig. 3.

The system of equations that governs the equilibrium curvature of the borehole can be simplified on account that the deformed configuration of the BHA remains invariant in this case.

- Bit-rock interaction:

$$\hat{F}_1 = G_1 + H_1 d_1, \quad \hat{F}_2 = -G_2 - \eta H_1 d_2, \quad \hat{M} = -G_0 - \chi \lambda^2 H_1 \varphi \tag{2}$$

  where $G_0$, $G_1$, $G_2$, and $H_1$ are coefficients of the bit-rock interaction laws.

- Relationship between bit penetration and borehole geometry:

$$\kappa = \frac{\varphi \lambda}{d}, \quad \Xi = \Xi_o + \frac{2}{\pi} \nu |\beta| \tag{3}$$

- Drillstring mechanics:

$$\frac{\hat{F}_2}{w\lambda} = \frac{1}{2}\mathcal{F}_b \Upsilon (\kappa - 2\beta) - \frac{1}{2}\mathcal{F}_s \Upsilon \kappa + \mathcal{F}_w \sin\theta_m + \mathcal{F}_r(\Lambda)\Phi \tag{4}$$

$$\frac{\hat{M}}{w\lambda^2} = \frac{1}{2}\mathcal{M}_b \Upsilon (\kappa - 2\beta) - \frac{1}{2}\mathcal{M}_s \Upsilon \kappa + \mathcal{M}_w \sin\theta_m + \mathcal{M}_r(\Lambda)\Phi \tag{5}$$

  where the coefficients $\mathcal{F}$'s and $\mathcal{M}$'s are given in Table 3 for the two limiting cases of a blocked stabilizer ($\bar{\theta} = \bar{\Theta}$) and a freely rotating stabilizer ($\bar{M} = 0$). It is worth mentioning that the consideration of additional stabilizers will only be reflected in the particular expressions of the coefficients $\mathcal{F}$'s and $\mathcal{M}$'s.

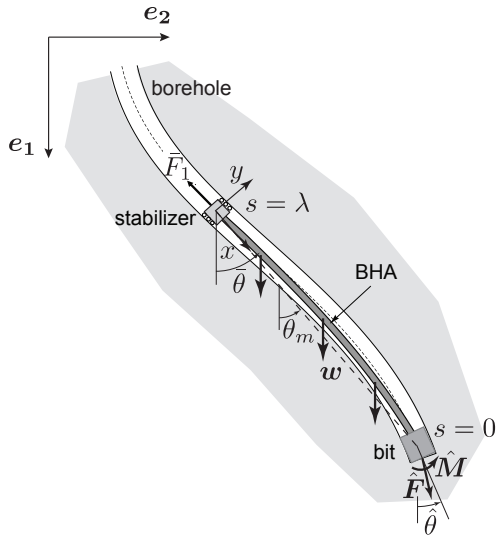


Figure 3: Segment of BHA between the bit and the first stabilizer.

In the above, $\theta_m$, $\nu$, $\beta$, $\eta$, $\chi$, $\kappa$, $\Xi$ $\Lambda$, $\Upsilon$, $\Phi$ are dimensionless quantities: $\theta_m$ is the inclination of the BHA on the gravity, while $\eta$ and $\chi$ denote the lateral and angular steering resistance, respectively. The borehole curvature $\kappa$, the distance $\Lambda$ between the RSS pad and the first stabiliser, the BHA rigidity $\Upsilon$, and the force on the RSS pad $\Phi$ are respectively defined as

$$\kappa = K\lambda, \quad \Lambda = \frac{\lambda - \breve{s}}{\lambda}, \quad \Upsilon = \frac{EI}{w\lambda^3}, \quad \Phi = \frac{\breve{F}}{w\lambda}. \tag{6}$$

The expected orders of magnitude of these numbers are: $\nu = O(1)$, $\eta = O(10)$, $\chi = O(10^{-1} \sim 1)$, $\beta = O(10^{-2})$, $\kappa = O(10^{-2} \sim 10^{-1})$, $\Xi = O(10^{-2})$, $\Lambda = O(10^{-1} \sim 1)$, $\Upsilon = O(1 \sim 10^3)$, $\Phi = O(1 \sim 10)$; also $|\theta_m| \leq \pi/2$.

Table 3: Coefficients $\mathcal{F}$'s and $\mathcal{M}$'s.

| BC at $s = \lambda$ | $\mathcal{F}_b$ | $\mathcal{F}_s$ | $\mathcal{F}_w$ | $\mathcal{F}_r$ | $\mathcal{M}_b$ | $\mathcal{M}_s$ | $\mathcal{M}_w$ | $\mathcal{M}_r$ |
|---|---|---|---|---|---|---|---|---|
| $\bar{\theta} = \bar{\Theta}$ | -6 | -6 | $\frac{1}{2}$ | $-(3-2\Lambda)\Lambda^2$ | 4 | 2 | $-\frac{1}{12}$ | $(1-\Lambda)\Lambda^2$ |
| $[\bar{M}] = 0$ | -3 | 0 | $\frac{5}{8}$ | $-\frac{1}{2}\Lambda\left(3-\Lambda^2\right)$ | 3 | 0 | $-\frac{1}{8}$ | $\frac{1}{2}\Lambda\left(1-\Lambda^2\right)$ |

The system of equations (2)-(5) can be reduced to a linear system in $\beta$ and $\kappa$. For example, the following asymptotic expressions for $\beta$ and $\kappa$ hold for $\bar{M} = 0$, if the BHA is rigid enough ($\Upsilon \gtrsim 50$)

$$\beta = \beta_\infty - \frac{\chi \mathcal{G}}{\Upsilon} + O\left(\frac{1}{\Upsilon^2}\right), \quad \kappa = \kappa_\infty + \frac{\eta \mathcal{G}}{\Upsilon} + O\left(\frac{1}{\Upsilon^2}\right) \tag{7}$$

where

$$\beta_\infty = \frac{2(\Lambda\Phi - \Gamma_0 - \Gamma_2) - \sin\theta_m}{2(\eta + 2\chi)(\Pi - \Gamma_1)}, \quad \kappa_\infty = 2\beta_\infty \tag{8}$$

$$\mathcal{G} = \frac{-8\Gamma_0\eta + 16\Gamma_2\chi + \left[8\chi\left(\Lambda^2 - 3\right) + 4\eta\left(\Lambda^2 - 1\right)\right]\Lambda\Phi + (\eta + 10\chi)\sin\theta_m}{12(\eta + 2\chi)^2}. \tag{9}$$

The simple result that $\kappa_\infty = 2\beta_\infty$ (for an infinitely rigid BHA) can readily be interpreted geometrically.

Consider the following numerical values: $a = 0.1$ m, $\nu = 2$, $\theta_m = 1$, $w = 10^3$ N/m, $\lambda = 10$ m, $EI = 10^7$ N·m$^2$, $\breve{s} = 1$ m, $G_0 = G_2 = 0$, $G_1 = 10^4$ N, $H_0 = 10^9$ N·m, $H_1 = 10^7$ N/m, $H_2 = 10^8$ N/m, $\hat{F}_1 = 10^5$ N, $\breve{F} = -10^4$ N. Then, the values of the control numbers are: $\eta = 10$, $\chi = 1$, $\Upsilon = 10$, $\Lambda = 0.9$, $\Gamma_0 = 0$, $\Gamma_1 = 1$, $\Gamma_2 = 0$, and the loading parameters are $\Pi = 10$, $\Phi = -1$. Hence, $\kappa \simeq -1.16 \cdot 10^{-2}$ and $\beta \simeq -9.28 \cdot 10^{-3}$ if $\bar{\theta} = \bar{\Theta}$ and $\kappa \simeq -9.24 \cdot 10^{-3}$ and $\beta \simeq -1.37 \cdot 10^{-2}$ if $[\bar{M}] = 0$. These values translate into a radius of curvature $R$ and borehole radius $A$ given by $R \simeq 863$ m and $A = 0.1029$ m for the case $\bar{\theta} = \bar{\Theta}$ and by $R \simeq 1082$ m and $A = 0.1038$ m for the case $[\bar{M}] = 0$, assuming $\Xi_o = 0.01$.

# 4 Conclusions

In this paper, we have discussed aspects of a borehole propagation model, namely the kinematical relationships governing the geometrical evolution of the borehole, (ii) the laws that link the bit/rock penetration variables to the forces on the bit, and (iii) the relationships between the forces on the bit and the loads on the drillstring. We have demonstrated that this system of equations is closed by computing the equilibrium points of the dynamical system, which correspond to borehole segments with constant curvature. The consideration of an angular bit penetration and its link to the borehole curvature are among the novelties introduced in this formulation. The complete evolution problem remain to be formulated, however, so as to enable the prediction of borehole trajectories characterized by change in curvature, either sudden or progressive.

## References


[1] A. Lubinski and H. B. Woods. Factors affecting the angle of inclination and dog-legging in rotary bore holes. In Mid-Continent District, pages 222-250, Tulsa, U.S.A., 1953. American Petroleum Institute.

[2] C. E. Murphey and J. B. Cheatham. Hole deviation and drill string behavior. Society of Petroleum Engineers Journal, 6(1):44-54, March 1965. SPE 1259.

[3] K. Millheim. The effect of hole curvature on the trajectory of a borehole. In 52nd Annual Fall Technical Conference and Exhibition of the Society of Petroleum Engineers of AIME, volume SPE 6779, pages 1-8, Denver, Colorado, U.S.A., October 1977.

[4] E. T. Brown, S. J. Green, and K. P. Sinha. The influence of rock anisotropy on hole deviation in rotary drilling - a review. International Journal of Rock Mechanics and Mining Sciences, 18(5):387-401, 1981.

[5] H.-S. Ho. Prediction of drilling trajectory in directional wells via a new rock-bit interaction model. In Proc. SPE Annual Technical Conference and Exhibition, number SPE 16658, 1987.

[6] M. Neubert and G. Heisig. Mathematical description of the directional drilling process and simulation of directional control algorithm. Zeitschrift für angewandte Mathematik und Mechanik, 76:361-362, 1996.

[7] S. Menand, H. Sellami, M. Tijani, O. Stab, and C. Simon. Advancements in 3d drillstring mechanics: From the bit to the topdrive. In IADC/SPE Drilling Conference, volume IADC/SPE 98965, pages 1-12, Miami, Florida, U.S.A., February 2006.

[8] R. Boualleg, H. Sellami, S. Menand, and C. Simon. Effect of formations anisotropy on directional tendencies of drilling systems. In IADC/SPE Drilling Conference, volume IADC/SPE 98865, pages 1-10, Miami, Florida, U.S.A., February 2006.

[9] G. C. Downton. Directional drilling system response and stability (paper 724). In IEEE Multi-conference on Systems and Control. IEEE Control Systems Society, 2007.

[10] E. Detournay, T. Richard, and M. Shepherd. Drilling response of drag bits: theory and experiment. International Journal Rock Mechanics & Mining Sciences, 45(8):1347-1360, 2008.

# Theoretical Determination of the Bit-Rock Interaction Coefficients£

Luc Perneder[1], Emmanuel Detournay[1,2]

[1]University of Minnesota, USA
[2] CSIRO Petroleum, Australia

## 1 Introduction

The bit-rock interaction laws characterize the relationship between the penetration variables and the generalized forces on the bit. Based on single cutter experiments, we first postulate that the bit-rock interaction can be captured by bilinear laws between the penetration variables and the generalized forces. We then focus on the determination of the "bitmetrics" coefficients, the parameters of the bit-rock interaction laws, for a cylindrical PDC bit; in particular we show that some of these coefficients depend on the bit tilt.

## 2 Bilinear Single Cutter Law

Consider a blunt rectangular cutter of width $w$, removing rock over a constant depth $d$ (Fig 1). The scratching process consists generally of two independent processes: pure cutting and frictional contact. Assuming that cutting takes place in the ductile mode [1], single cutter experiments indicate that the relationship between the cutting force and the depth of cut $d$ is bilinear. This bilinearity reflects the existence of two regimes: Regime I where the forces on the cutter are proportional to the depth of cut $d$, and Regime II where the forces on the wearflat are constant but the forces on the cutting face remain proportional to the depth of cut. The transition from Regime I to II is characterized by a threshold depth of cut $d_*$ and force $F_*$. In Regime I ($d \lesssim d_*$), the forces in the directions $n$ and $s$ (perpendicular and parallel to the cutter velocity, respectively) are given by

$$F_n^I = \zeta' \varepsilon w d, \quad F_s^I = \zeta'' \varepsilon w d$$

while in the Regime II ($d \gtrsim d_*$), they are given by

$$F_n^{II} = \sigma w l + \zeta \varepsilon w d, \quad F_s^{II} = \mu \sigma w l + \varepsilon w d$$

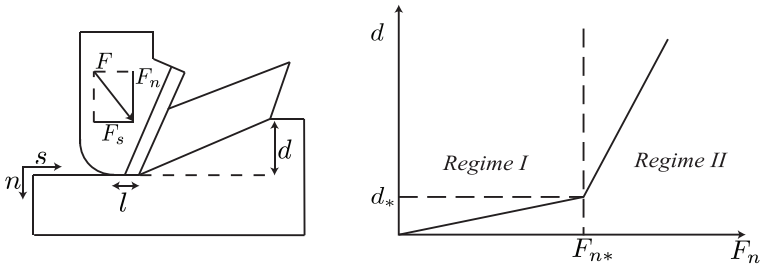


Figure 1: Single cutter test. Bilinear law for the normal force $F_n$.

where $\varepsilon$ is the intrinsic specific energy of the rock, $w$ is the width of the cutter, $\sigma$ is the maximum contact pressure on the interface wearflat/rock, $\mu$ is a coefficient of friction and $\zeta$, $\zeta'$, $\zeta''$ are dimensionless coefficients.

# 3 Penetration Variables and Generalized Forces

Let the axis $\hat{\mathbf{i}}_1$ of a director basis coincide with the bit axis of symmetry while pointing ahead of the bit and let the axes $\hat{\mathbf{i}}_2$ and $\hat{\mathbf{i}}_3$ be perpendicular to $\hat{\mathbf{i}}_1$ (Fig. 2). The origin of the director basis is fixed at the center of the bit face.

The penetration of the bit is characterized by a penetration vector $\mathbf{d}$ per revolution and an angular penetration vector $\varphi$ per revolution, which is orthogonal to the bit axis of revolution. The trajectory of the bit is assumed to be in the plane $(\hat{\mathbf{i}}_1, \hat{\mathbf{i}}_2)$ and the penetration of the bit is characterized by three penetration variables in the basis $(\hat{\mathbf{i}}_1, \hat{\mathbf{i}}_2, \hat{\mathbf{i}}_3)$: the axial penetration $d_1$, the lateral penetration $d_2$ and the angular penetration $\varphi_3$. Moreover, the trajectory radius $R$ and the penetration variables are assumed to be constant with time.

The penetration vector $\mathbf{d}$ is tangent to the borehole so that it is aligned with the borehole axis. The axis of revolution of the drill bit $\hat{\mathbf{i}}_1$ is not necessarily aligned with the borehole axis. The inclination of the bit with the borehole trajectory is called the bit tilt $\psi$ and is related to the penetration variables by

$$\psi = -\arctan\left(\frac{d_2}{d_1}\right). \tag{1}$$

The dynamical quantities that are conjugated to the penetration variables are the force on bit $\mathbf{F}$ and the moment on bit $\mathbf{M}$. The moment $\mathbf{M}$ acting on the bit is perpendicular to the axis of revolution of the bit and does not include the torque. In the director basis $(\hat{\mathbf{i}}_1, \hat{\mathbf{i}}_2, \hat{\mathbf{i}}_3)$, the force $\mathbf{F}$ and moment $\mathbf{M}$ acting on the bit have components $F_1$, $F_2$, $F_3$, $M_2$, $M_3$.

# 4 Mathematical Formulation

We consider a cylindrical bit of radius $a$ and height $2b$. In the following, we assume that $a/R \ll 1$, $a/b = O(1)$, $d_2/d_1 \ll 1$. The cutters of the bit face and gauge can be conceptualized as two equivalent blades, one for the bit face and another one for the gauge. The characteristics of these equivalent blades are fixed in such way that the forces on the blades are the same as those on all the cutters when averaged over one revolution and they can be deduced from the emplacement and geometry of the cutters.

The expected magnitude of the penetration variables are such that the bit-rock interaction is assumed to occur in Regime II on the bit face and in Regime I on the bit gauge.

The first step is to determine the bit-rock interaction surface and calculate the penetration of a point $P$ on this surface. The relation between the local penetration $d$ at a point $P$ and the penetration variables $d_1$, $d_2$, $\varphi_3$ is a function of the position of P and on the relative orientation of the normal $n$ to the bit profile at $P$ with respect to the axis $\hat{\mathbf{i}}_1$.

If the bit face fully interacts with the rock, the penetration of a point $P$ of the bit face is given by

$$d = d_1 - \varphi_3 r \cos\omega_1. \tag{2}$$

For the gauge, the interaction surface depends on the geometrical configuration of the bit in the borehole, which is expressed in terms of the bit tilt $\psi$ and the parameter $\psi_*$ defined as

$$\psi_* = \frac{2b}{R}. \tag{3}$$

The penetration of a point of the bit gauge is the projection of the lateral displacement onto the normal of the gauge surface

$$d = (d_2 - 2\varsigma b\varphi_3)\cos\omega_1 \tag{4}$$

where the variable $\varsigma \in [0,1]$ is the dimensionless coordinate running from the bottom to the top of the gauge. The penetration given by (4) can be negative, which shows that not all the gauge interacts with the rock. Thus, the gauge-rock interaction surface is defined by positive penetrations $d$ and can take four different configurations depending on the ratio $\psi/\psi_*$.

- If $\psi \geq 0$, the contact is located on the outer side of the gauge. Outer and inner sides of the gauge denote the sides of the gauge facing respectively the inside or outside of the circular trajectory of the bit.

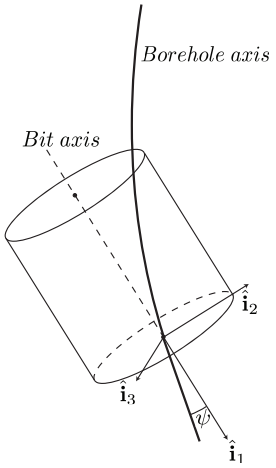


Figure 2: Definition of the director basis centered on the bit face and the tilt angle $\psi$.

- If $\psi \in \left[-\frac{\psi_*}{2}, 0\right]$, both sides of the gauge are in partial contact with the rock.
- If $\psi \in \left[-\psi_*, -\frac{\psi_*}{2}\right]$, the inner side is partially in contact with the rock.
- If $\psi \leq -\psi_*$, the inner side is in full contact with the rock.

The forces acting at a point $P$ of the bit are deduced from the penetration $p$ at $P$. The last step is to integrate these forces on the length of the equivalent blade and then to average the result on a rotation of the bit. This leads to the expressions of the general forces acting on the bit.

# 5 Results

The dimensionless general form of the interface laws is

$$\begin{bmatrix} F_1/\varepsilon a^2 \\ F_2/\varepsilon a^2 \\ F_3/\varepsilon a^2 \\ M_2/\varepsilon a^3 \\ M_3/\varepsilon a^3 \end{bmatrix} = - \begin{bmatrix} \frac{\sigma}{\varepsilon}\frac{l_e}{a} \\ 0 \\ 0 \\ 0 \\ 0 \end{bmatrix} - \begin{bmatrix} \zeta & 0 & 0 \\ 0 & \frac{1}{2}\zeta'\nu\Psi_1 & -\frac{1}{2}\zeta'\nu^2\Psi_2 \\ 0 & \frac{1}{2}\zeta''\nu\Psi_1 & \frac{1}{4}\zeta - \frac{1}{2}\zeta''\nu^2\Psi_2 \\ 0 & \frac{1}{2}\zeta''\nu^2\Psi_2 & -\frac{2}{3}\zeta''\nu^3\Psi_3 \\ 0 & -\frac{1}{2}\zeta'\nu^2\Psi_2 & \frac{1}{6}\zeta + \frac{2}{3}\zeta'\nu^3\Psi_3 \end{bmatrix} \begin{bmatrix} d_1/a \\ d_2/a \\ \varphi_3 \end{bmatrix} \quad (5)$$

where $l_e$ is the equivalent wearflat length of the cutting face of the bit, $\nu = b/a$ defines the slenderness of the bit and $\Psi_1$, $\Psi_2$, $\Psi_3$ are functions of the ratio $\psi/\psi_*$

and depend on the gauge/rock interaction surface configuration. For the first and fourth configurations (when one side of the gauge is in full contact with the rock), $\Psi_1 = \Psi_2 = \Psi_3 = 1$ and the bit-rock interaction laws are bilinear relashionships. But, for the second and third configurations, $\Psi_1$, $\Psi_2$, $\Psi_3$ depend on the bit tilt $\psi$ and the bit/rock interaction laws are no longer bilinear relashionships of the penetration variables.

This analysis indicates that the axial penetration $d_1$ generates only an axial force. In contrast, the lateral and angular penetration $d_2$, $\varphi_3$ both generate lateral forces and moments on the bit due mainly to the interaction of the gauge of the bit with the rock.

## References

[1] Richard T. *Determination of Rock Strength from Cutting Tests*. M.S. thesis, University of Minnesota, Minneapolis, U.S.A., (1999).

# Experimental Determination of the Bit-Rock Interaction Coefficients

Thomas Richard

Drilling Mechanics Group, CSRIO Petroleum, Perth, Australia

## 1 Introduction

This talk presents results of drilling tests performed to estimate the bitmetrics coefficients that relates the penetrations variables (axial, $d_1$; lateral, $d_2$ and angular $\varphi_3$ penetrations per revolution of the bit) to the conjugated force $\boldsymbol{F}$ and moment $\boldsymbol{M}$ acting on a drag bit. A series of straight and curved in plane boreholes were drilled under precise kinematic control while the force and moment were continuously recorded just above the drill bit.

The analytical formulation of the bitmetric coefficients stems from interactions laws derived for a single blunt cutter, see Figure 1. The components (tangential and normal) of the force acting on a cutter with a width $w$ and contact length $\ell$ read:

$$F_s = \zeta' \varepsilon w d, \quad F_n = \zeta" \varepsilon w d \qquad d < d_* \tag{1}$$

$$F_s = \mu \sigma w \ell + \varepsilon w d, \quad F_n = \sigma w \ell + \zeta \varepsilon w d \qquad d \geq d_* \tag{2}$$

where the intrinsic specific energy $\varepsilon$ and contact stress $\sigma$ are related to the rock strength. It is well documented [1, 2] that the coefficents $\mu$, $\zeta$ that characterize the friction mobilized on the wear flat and cutting face, respectively, are both of order $O(0.1 \sim 1)$. Based on a few experimental evidences [2, 3], the coefficients $\zeta,'$ $\zeta"$ are expected to be of order $O(10 \sim 100)$.

The concepts applied to a single cutter can be extended to full drill bit of radius $a$ and gauge height $2b$, see Figure 2. The components of the force and moment acting on the bit can be derived explicitly for simple bit geometry assimilated to a pseudo-cylinder with straight blades orthogonal to the bit axis of revolution and longitudinal blunt blades located on the gauge of the bit. For the particular case of interest here characterized by no bit tilt ($\psi = 0$) and with $\varphi$

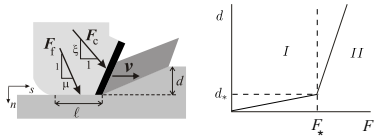


Figure 1: Single cutter and single cutter response

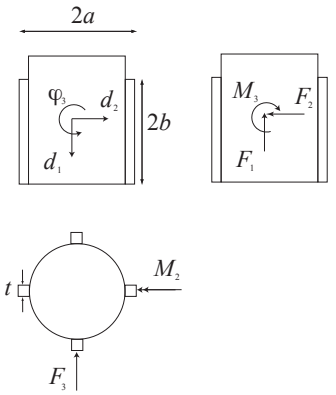


Figure 2: Penetration variables applied on bit and resulting force and moments acting on the bit.

passing through the bit geometric centre, they read [4, 5]:

$$\begin{Bmatrix} F_1 \\ F_2 \\ F_3 \\ M_2 \\ M_3 \end{Bmatrix} = - \begin{Bmatrix} \sigma \ell a \\ 0 \\ 0 \\ 0 \\ 0 \end{Bmatrix} - \varepsilon \begin{bmatrix} \zeta a & 0 & 0 \\ 0 & \frac{1}{2}\zeta' b & 0 \\ 0 & \frac{1}{2}\zeta" b & -\frac{1}{4}a^2 \\ 0 & 0 & \frac{1}{4}a^2 b - \frac{1}{6}\zeta" b^3 \\ 0 & 0 & \frac{1}{6}\zeta a^3 + \frac{1}{6}\zeta' b^3 \end{bmatrix} \begin{Bmatrix} d_1 \\ d_2 \\ \varphi_3 \end{Bmatrix} \tag{3}$$

## 2 Experimental Setup

A device dubbed Ibis was designed in order to drill under kinematic control straight and curved boreholes. The axial, $v_1$, lateral, $v_2$, rotational $\Omega$, and angular $\varphi$ velocities of the bit (with respect to the rock sample) are imposed via servo

motors, while the three components of the force and moment acting on the bit are measured. The machine (Figure 3) consists of a metallic welded frame with two vertical ball rails along which travels ($v_1$) a plate hosting a brace, which itself hosts a rotating module that carries the motor ($\Omega$), drilling shaft and the drill bit. The angular rotation $\varphi$ of the module is controlled by an actuator. The rock sample sits at the base of the machine on a plate whose lateral motion ($v_2$) is also controlled by an actuator. It is critical to ensure that the cutting process mobilized at the bit rock interface is similar to the process mobilized on a real bit. Practically, it means penetration variables of the order of $O$ (0.1 mm) for $d_1$, $O$ ($10^{-4} - 10^{-3}$ mm) for $d_2$, and $O$ ($10^{-6} - 10^{-4}$ rad) for $\varphi$. Also, geometrical aspect ratios of the bit ($\frac{b}{a}$ of order $O(1)$) but also of the bit radius with the borehole radius of curvature $R$ ($\frac{R}{a}$ of order $O(10^2 - 10^4)$) were kept similar to field conditions.

Detailed attention was given in the design, machining and setup of the equipment to ensure precise angular adjustement between axes; in particular precise alignment between the bit axis of revolution and its axis of rotation (within $10^{-4}$ rad) and ability to finely adjust the vertical axis of travelling with the bit axis (again within $10^{-4}$ rad). This precision is critical as the bit tilt (angle between the bit axis and the borehole tangent) is expected to be of the order $O(10^{-3}$-$10^{-2})$ in field conditions. The drill bit is made of 4 blades evenly spaced with a radius $a = 27$ mm, and gage height $2b = 48$ mm and thickness $t = 5$ mm. And, the selected rock material is Tuffeau, a fine grain homogeneous limestone with the following mechanical properties estimated from single cutter scratch tests: $\varepsilon = 10$ MPa $\sigma = 9$ MPa, $\zeta = 0.54$ and $\mu = 0.68$.

## 3 Preliminary results

First a series of lateral drilling tests were conducted. From a straight vertical prehole, the bit was moved laterally with respect to the rock ($d_1 = 0$; $\varphi = 0$; $d_2 > 0$). The evolution of the mean side force component $F_2$ with respect to the imposed lateral displacement $d_2$ is shown in Figure 4. The results suggest that the force increases non-linearly with the depth of cut. If we simply calculate $\zeta'$ as $\zeta' = \frac{2F_2}{b\varepsilon d_2}$ , we obtain a $\zeta'$ varying between about 800 and 200. Results of the experiments suggest also that $\zeta'' \sim 0.7\zeta'$. These results are in accordance with results obtained on full bit [6].

Second a curved borehole with a radius of curvature $R$ equal to 5 m was drilled. The following drilling parameters were imposed $d_1 = 0.1$ mm, $d_2 = 0$,$\varphi = 2.10^{-5}$rad, and $\Omega = 2\pi$ rad/s. Some results are displayed in Figure 5. The side force component $F_2$ and moment $M_{3s}$ measured at the sensor and the moment $M_3$ estimated at the bit according to $M_3 = M_{3s} - F_2 h$ where $h$ is the axial

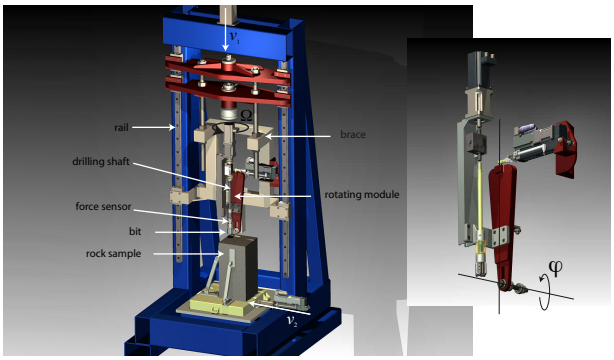


Figure 3: 3D sketch of Ibis and zoom on the rotating module.

distance between the sensor reference point and the point of application of the side force. It was assumed that the force is applied close to the bit centre. It is possible that the measure side force is not found equal to zero because the center of rotation is not passing exactly at the gauge mid-height. However, interestingly, the moment estimated at the bit is found close to the model prediction $M_3 = (\frac{1}{6}\zeta a^3 + \frac{1}{6}\zeta' b^3)\varphi_3 \simeq \frac{1}{6}\zeta' b^3 \varphi_3 = 0.37$ N.m where $\zeta'$ was taken equal to 800 based on the results shown in Figure 4, as the "local depth of cut" along the gauge for a angular rotation $\varphi_3 = 2\,10^{-5}$ ranges from 0 to $5\,10^{-4}$ mm.

# 4 Conclusions

We have presented results of preliminary drilling tests performed with a novel machine, Ibis. Results of lateral drilling tests are in accordance with results published in the literature on full scale bit. To our knowledge, the first curved borehole in rock was drilled under control conditions in a laboratory. The results are encouraging, and the order of magnitude of the force and moment recorded during the test are in accordance with the model prediction. Few modifications are being applied on the machine in order to increase its stiffness and limit the deformation (in particular out of plane). Then, additional tests will be conducted to explore the relation between the moment and the angular penetration, and investigate the effect of the gauge height and width. Also tests are programmed to estimate the effect of the axial penetration $d_1$ on the lateral force and moment,

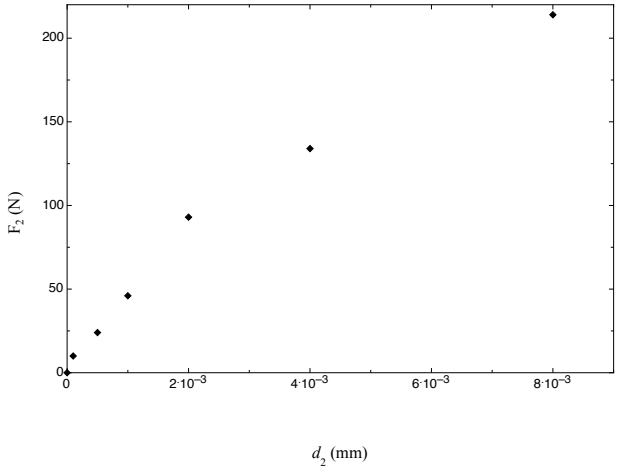


Figure 4: Evolution of the side force with the lateral penetration.

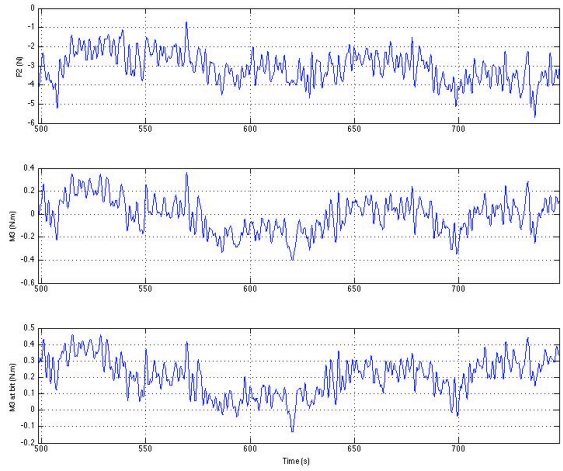


Figure 5: Evolution of the side force with the lateral penetration.

as well as the effect of the lateral penetration on the moment and axial force. This study will require drilling curved borehole with a non zero tilt angle.

## Acknowledgements

The author would like to thank for their support Emmanuel Detournay, Gregory Lupton (who designed Ibis), Luiz Franca and Luis Mariano.

## References

[1] T. Richard. Determination of rock strength from cutting tests. Master of science, University of Minnesota, December 1999.

[2] J. I. Adachi. Frictional contact in rock cutting with blunt tools. Master of science, University Of Minnesota, May 1996.

[3] F. Dagrain. Etude des Mecanismes de Coupe des Roches avec Couteaux Uses - Approche des mécanismes de frottement sous les couteaux par le concept du troisième corps. Thèse de doctorat en sciences appliquées, Faculté Polytechnique de Mons, June 2006.

[4] E. Detournay. Mathematical model of the near-bit region of an advancing drilling system. Technical Report SLB-BM-07-1, Geoff Downton Schlumberger Stonehouse, April 2007.

[5] L. Perneder. Theoretical determination of the bit-rock interactiin coefficients. Technical report, CSIRO Petroleum, 2008.

[6] S. Menand, H. Sellami, and C. Simon. Classification of pdc bits according to their steerability. In SPE/IADC Drilling Conference, number SPE/IADC 79795, pages 1–13, Amsterdam, Netherlands, February 2003.

# List of Participants

**BESSELINK Bart**
Eindhoven University of Technology
Dynamics & Control, Department of Mechanical Engineering
P.O. Box 513, 5600 MB, Eindhoven, The Netherlands
b.besselink@tue.nl

**BOUALLEG Riadh**
Schlumberger
Schlumberger Cambridge Rsearch Center
High Cross Madingley Road Cambridge, CB3 0EL UK
rboualleg@slb.com

**BROGLIATO Bernard**
INRIA, BIPOP team-project, ZIRST Montbonnot
655 avenue de l'Europe
38334 Saint Ismier, France
bernard.brogliato@inrialpes.fr

**DENOEL Vincent**
University of Liège
Structural Engineering Division, ArGEnCo Department
Chemin des Chevreuils, 1, B52/3, B-4000 Liège 1, Belgium
v.denoel@ulg.ac.be

**DETOURNAY Emmanuel**
University of Minnesota
Department of Civil Engineering
Minneapolis, MN 55455, USA
detou001@umn.edu

**DORBOLO Stéphane**
University of Liège
Statistical Physics, Department of Physics
Allée du 6 Août, 17, B5, B-4000 Liège 1, Belgique
s.dorbolo@ulg.ac.be

**DOWNTON Geoff**
Schlumberger
Drilling and Measurements
300 Schlumberger Drive, Sugar Land, TX 77478 USA
GDownton1@sugar-land.oilfield.slb.com

**ERNEUX Thomas**
Université Libre de Bruxelles
Theoretical Nonlinear Optics
Campus Plaine, C.P. 231 Boulevard du Triomphe B-1050 Bruxelles, Belgium
terneux@ulb.ac.be

**FRANCA Luiz**
Commonwealth Scientific and Industrial Research Organisation
CSIRO Petroleum, Drilling Mechanics
26 Dick Perry Avenue, Technology Park, WA 6151 Kensington, Australia
luiz.franca@csiro.au

**GERMAY Christophe**
Epslog S.A.
Rue Hors-Château, 37, B-4000 Liège 1, Belgium
christophe.germay@epslog.com

**GUZINA Bojan**
University of Minnesota
Department of Civil Engineering
Minneapolis, MN 55455, USA
bojan7@gmail.com

**INSPERGER Tamas**
Budapest University of Technology and Economics
Department of Applied Mechanics
Mûegyetem rkp. 3-9. H-1111 Budapest, Hungary
inspi@mm.bme.hu

**JEFFRYES Benjamin**
Schlumberger
Schlumberger Cambridge Rsearch Center
High Cross Madingley Road Cambridge, CB3 0EL UK
jeffryes@cambridge.oilfield.slb.com

**KERSCHEN Gaetan**
University of Liège
Space Structures and Systems Lab, Department of Aerospace and Mechanical Engineering
Chemin des Chevreuils, 1, B52/3, B-4000 Liège 1, Belgium
g.kerschen@ulg.ac.be

**KOVALYSHEN Yevhen**
University of Minnesota
Department of Civil Engineering Department
Minneapolis, MN 55455, USA
kova0132@umn.edu

**PERNEDER Luc**
University of Minnesota
Department of Civil Engineering Department
Minneapolis, MN 55455, USA
luc.perneder@hotmail.com

**RICHARD Thomas**
Commonwealth Scientific and Industrial Research Organisation
CSIRO Petroleum, Drilling Mechanics
26 Dick Perry Avenue, Technology Park, WA 6151 Kensington, Australia
thomas.richard@csiro.au

**SEPULCHRE Rodolphe**
University of Liège
Systems and Modelling, Department of Electricity, Electronics and Informatics
Grande Traverse, 10, B28, B-4000 Liège 1, Belgique
r.sepulchre@ulg.ac.be

**SILVEIRA Marcos**
Aberdeen University
Centre for Applied Dynamics Research, School of Engineering, King's College
AB24 3UE, Aberdeen, UK
m.silveira@abdn.ac.uk

**STEPAN Gabor**
Budapest University of Technology and Economics
Department of Applied Mechanics
Mûegyetem rkp. 3-9. H-1111 Budapest, Hungary
stepan@mm.bme.hu

**van de WOUW Nathan**
Eindhoven University of Technology
Dynamics & Control, Department of Mechanical Engineering
P.O. Box 513, 5600 MB, Eindhoven, The Netherlands
n.v.d.wouw@tue.nl

**WICKS Nathan**
Schlumberger
Doll Research Center 1
Hampshire St. Cambridge, MA 02139-1578 USA
nwicks@slb.com

**WIERCIGROCH Marian**
Aberdeen University
Centre for Applied Dynamics Research, School of Engineering, King's College
AB24 3UE, Aberdeen, UK
m.wiercigroch@abdn.ac.uk

# Notes